COMPUTATIONAL DESIGN OF BIO-INSPIRED VESICLES AND THEIR

INTERACTIONS WITH NANOPARTICLES USING COARSE-GRAINED MODELS

by

FIKRET AYDIN

A dissertation submitted to the

Graduate School – New Brunswick

Rutgers, The State University of New Jersey

In partial fulfillment of the requirements

For the degree of

Doctor of Philosophy

Graduate Program in Chemical and Biochemical Engineering

Written under the direction of

Dr. Meenakshi Dutt

And approved by

_____

_____

_____

_____

_____

New Brunswick, New Jersey

October 2015

ABSTRACT OF THE DISSERTATION

Computational Design of Bio-Inspired Vesicles and Their Interactions with Nanoparticles

using Coarse-Grained Models

By Fikret Aydin

Dissertation Director:

Dr. Meenakshi Dutt

One of the key challenges in the design of self-assembled nanostructured materials as delivery vehicles is the prediction of their resultant shape and size as well as controlling their interactions with various nanoparticles and macromolecules while optimizing their circulation time and biodistribution profile. In order to overcome the challenges behind the optimal design of such nanostructured soft materials, the mesoscopic properties of soft biomaterials such as cell membranes or liposomes need to be investigated. Fundamental insight into the morphology and dynamics of these materials will require the development and utilization of a suite of modeling tools with each class of tools tuned to address physical phenomena over a specific spatio-temporal scale. These multiple modeling techniques have to be interfaced at the juncture of two scales to enable a multiscale resolution of the system behavior over large length (from 1 nm up to 1 μm) and time scales (nano-seconds to micro-seconds). The aim of this work

to understand the underlying mechanisms that affect the organization, shape, stiffness and interfacial stability of biomaterials, and furthermore investigate the cooperative relations among them which dictate their final structural and functional state. Understanding these fundamental processes can help developing simple models of stable bio-inspired membranes and vesicles with tunable phase segregation properties as well as desirable stiffness and shape characteristics for various applications such as the design and prediction of novel hybrid soft materials for encapsulation and delivery of therapeutic agents, cellular sensing and sustainability. It will also contribute to understanding the underlying mechanisms of the interactions between micelles, proteins or synthetic particles with bio-inspired multi-component membranes, or liposomal drug delivery vehicles.

Acknowledgements

I feel extremely honored to be trained by my advisor Dr. Meenakshi Dutt and would like to express my deepest gratitude to her for the continuous support, patience, valuable knowledge and encouragement during my Ph.D study. Dr. Dutt taught me everything from scratch in a very enthusiastic way and never let me feel inadequate in my studies. She always found a way to motivate me towards my goals, and she pushed me farther than I thought I could go. "Tell me and I forget, teach me and I may remember, involve me and I learn." This quote by Benjamin Franklin reflects the mentality I learnt from her. She encouraged me to involve in various departmental activities, attend conferences, workshops, and develop my mentorship skills, which led me to learn knowledge that I will never forget. I would like to thank my advisor once again for all the effort she put into our training and helping us to become future scientists!

I also would like to thank the rest of my thesis committee: Dr. Jha, Dr. Roth, Dr. Shapley and Dr. Sofou for their critical comments and giving me new insights into my Ph.D thesis project, which help me to improve it from various perspectives. I would like to thank Dr. Jha for teaching me how to approach various problems by considering their time complexity and ability to identify the best algorithmic way to tackle these problems. I also would like to thank him for sharing his high performance computing resources with us and for teaching us the computational tools to maximize our use of these resources. I would like to thank Dr. Roth for sharing his valuable experiences in the experimental design of biological products and the drug delivery systems with me. He helped me to get a better understanding of my thesis project by suggesting methods to relate our computational model with the experimental systems. I would like to thank Dr. Shapley

iv

for her insightful questions related to the practicality and applicability of our computational models to real systems. She helped me to have a general picture of my project and see different aspects of it, which I didn't realize before. I would like to thank Dr. Sofou for increasing my understanding of biomembranes and drug delivery systems from the experimental point of view, and also helped me to improve our model by her fruitful suggestions for making connections between our computational model and experimental systems. I would also like to thank her for sharing her detailed notes with me after proposal exam, which helped me to organize my plans for the next phase.

I would like to thank my fellow colleagues in Dr. Dutt's research group for their support to help me complete this dissertation, and also for all the fun we have had in the last a few years. I would like to show my gratitude to my fellow PhD colleague, Leebyn Chong, for making the research more interesting and also for being a great friend. He is a perfect person to ask for a discussion about a research topic as he has a very good critical thinking and communication skills. I would like to send my special thanks to Geetartha Uppaladadium and Paul Ludford for their active contribution in this dissertation. I would have not been able to complete this work successfully without their efforts and support. I would also like to thank Xiaolei Chu. Although he is not included in the work presented here, we have several other projects together and he is an excellent fellow to work with. We learn from each other while working on these projects.

I gratefully acknowledge the funding received towards my PhD from Chemical & Biochemical Engineering (CBE) departmental fellowship and School of Engineering (SOE) fellowship at Rutgers University. I would also like to acknowledge the Graduate

Table of Contents

List of Tables

List of Figures

Chapter 1

Introduction and Objectives

Biological cell membranes are dynamic, responsive multi-component soft materials which separate and protect the cellular contents from the external environment, and participate in vital functions, such as intracellular and extracellular traffic, sensing and cell signaling.[1-4] These membranes are composed of a variety of amphiphatic molecules which can self-organize to modulate the membrane tension and thereby, its mechanical properties to facilitate various physiological processes, or promote binding or catalytic events at the membrane interface.[2,3,5] Earlier studies[2] have shown phospholipid molecules to be the primary component of cell membranes; these amphiphilic entities have a hydrophilic head group and two hydrocarbon tail chains. The head and tail groups of the phospholipid species can have distinct chemistries which endows a characteristic molecular geometry[6,7] and transition temperature[8-10], and drives the self-organization of the various species into domains or rafts.[4,11-24] The active nature of the cell membranes allows it to modulate its tension via the reorganization of its molecular constituents, thereby facilitating a multitude of cellular functionalities such as interfacial binding,[2,25] fusion, budding and vesiculation events.[26,27] For example, cells can maintain their mechanical properties under a range of thermal conditions by adjusting the molecular composition of their membrane.[28,29] Investigations have shown domain and raft formation in cell membranes to be critical for interfacial binding events on the cell surface,[30,31] responsible for promoting intra- and extracellular communication. A fundamental understanding of the physico-chemical mechanisms driving the formation of domains and

rafts in membranes will enhance the development of novel therapeutic approaches targeting these processes.

In addition to the organization of the molecular species in the membrane, their stiffness is also critical for the physiological functions of the cell membranes as well as the design of lipid based drug delivery vehicles. The stiffness of the hydrocarbon tails of lipid molecules is dependent upon their length and saturation.[32-34] Lipid molecules with shorter hydrocarbon tails have lower stiffness and viscosity as they are more susceptible to changes in kinetic energy.[32-34] Unsaturated lipid molecules are unable to pack as tightly as saturated lipid molecules due to the kinks in their hydrocarbon tails, and are therefore more susceptible to changes in kinetic energy. The stiffness of the lipid molecules is known to affect the stability and bending rigidity of the lipid bilayers.[33,35] It has also effects on the dynamical properties of the membranes such as mechanical rupture strength and water permeability.[33,36] The living cell membranes must be strong enough to regulate the permeation of the small molecules across the cell and also flexible enough to allow them move and change shape easily.[32] For example, the red blood cells are able to flow through the capillaries whose diameter is three times smaller than that of the red blood cells.[32] Similarly, the drug loading capability and circulation time of the drug delivery vehicles in the blood stream depend on the elasticity of the membranes.[32,37]

The shape of the drug delivery vehicles play important role in determining their behavior in the living systems. The shape is considered to be one of the most effective factors influencing the circulation time and biodistribution profile of the drug delivery vehicles. For example, it has been shown that filamentous worm-like micelles (filomicelles) have longer circulation times than the spherical micelles due to their

improved transport and trafficking characteristics.[38] There are also attempts to design deformable particles which are similar in their size and shape to the red blood cells so that they will have longer circulation time and improved biodistribution profile.[37] The improved delivery characteristics mentioned in these examples are also considered to be affected by the elastic modulus of the vehicles.[37,38] The molecular stiffness of the species can affect the local curvature of the lipid aggregates via controlling the packing of the molecules in the bilayer. Dobereiner et al.[39] demonstrated that vesicles composed of two lipid species which have different hydrocarbon tail lengths adopt more elongated shape upon an increase in the temperature. In this case, lipid molecules with shorter hydrocarbon tails will be more susceptible to changes in temperature, and thus have lower chain stiffness. Nieh et al.[40] studied ellipsoidal unilamellar vesicles composed of ternary lipid mixtures, and speculated that the ellipsoidal morphology might be a result of the lateral heterogeneities due to the presence of saturated and unsaturated lipid species with different hydrocarbon chain lengths. Another study by Sandstrom et al.[41] demonstrated a mixture of phospholipids and PEGylated lipids with different hydrocarbon chain melting temperatures to form cylindrical micellar structures at high temperatures, which transform to circular discoidal structures upon decreasing the temperature. They also reported long threadlike micelles to transform into more circular shapes with the addition of molecular components that increase the chain order of the lipids in the bilayer, such as cholesterol. These findings show that the chain stiffness of molecules in the bilayer has an impact on the resulting shapes of the aggregates.

The carbohydrate chains on the surface of cell membranes can inspire the design of biocompatible therapeutic targeted delivery vehicles with longer circulation times via

the use of end-functionalized phospholipids.[42-46] Earlier investigations[42-46] have demonstrated liposomes composed of end-functionalized lipids to have extended circulation due to enhanced stability promoted by its steric hindrance. Sterically stable biocompatible materials can be designed so as to completely eliminate or significantly reduce the interactions with untargeted cells and adsorption of proteins onto their surface. A common route to designing sterically stable liposomes is via the grafting of Poly ethylene glycol (PEG) chains to the lipid head groups[47-49] PEG chains have been shown to control the size,[49-51] morphology,[41,51,52] compressibility,[50,53,54] encapsulation efficiency[49,55,56] and permeability of liposomes.[49,55] The shape of the sterically stabilized lipid aggregates can be influenced by the spatial distribution of curvature-inducing functional groups present in the bilayer.[57-59]

In addition to intrinsic factors such as molecular interactions, architecture and composition, extrinsic factors such as the volume of the confinement can be also used for controlling the shape of aggregate structures.[35,60] Earlier studies have shown the size and geometry of the confining region to control the morphology of self-assembled materials on account of the increased local concentration, configurational frustration of the molecules and interactions with the confining surfaces.[61,62] The dimensions, geometry and surface selectivity of the confining environment have been found to strongly affect the self-assembled morphologies of block copolymers.[61,63-67] On the other hand, the role of the relative concentration of the molecular species, their molecular geometry and the height of a slit-like confining volume on the structure and morphology of the lipid aggregates is still not well understood. Confinement induced microfluidic self-assembly can be used to produce lipid-polymeric nanoparticles for drug encapsulation or lipid-

quantum dot nanoparticles for imaging purposes. This technique is advantageous compared to the conventional methods for the synthesis of multicomponent nanoparticles since there are no additional steps like heating, vortexing and long incubation times and the reproducibility of the particle size distribution is much higher by using microfluidic directed self-assembly.[68] The impact of confinement can also be used to study shape transformations of red blood cells due to entropic contributions.[69]

The aim of this work to understand the underlying mechanisms that affect the organization, shape, stiffness and interfacial stability of biomaterials for various applications such as the design and prediction of novel hybrid soft materials for encapsulation and delivery of therapeutic agents, cellular sensing and sustainability by using modeling techniques which enable a multiscale resolution of the system behavior over large length (from 1 nm up to 1 µm) and time scales (nano-seconds to micro-seconds).

All-atom simulations of lipid bilayers that resolve the dynamics of the lipid and water molecules are computationally expensive and limit the investigation to small spatio-temporal scales.[70-76] These tools are not suitable for addressing phenomena occurring on the mesoscale, such as membrane fusion and rupture, and domain formation in the multicomponent membranes.[77] Dynamics spanning large length and time scales can be resolved via coarse-graining[3,35,60,78-96], implicit solvent approaches[70,71,77,79-81,97-100] or mean field theoretical approaches.[101-109] Numerical studies have adopted implicit solvent models to investigate phase segregation dynamics via Monte Carlo[110] and coarse-grained Molecular Dynamics (MD)[23] techniques. Other studies have used a MD-based approach entitled Dissipative Particle Dynamics (DPD),[1,3,4,14,15,35,60,82-86,111-116] which

simultaneously resolves both the molecular and continuum scales, and reproduces the hydrodynamic behavior, to examine phase segregation in multi-component lipid vesicles.[4,14,15,111,112,117,118] Continuum approaches[17,18,119] have also been used to investigate the phase separation dynamics in mixed membranes. In this dissertation, two different coarse-grained MD based simulation methods will be used. One of them is DPD method which is capable of capturing the hydrodynamic effects and the other one is the coarse-grained implicit solvent MD which does not have any solvent molecules but it is capable of capturing larger length and time scales due to the fact that most of the time in explicit-solvent simulations has been spent on the solvent molecules. The coarse-grained implicit solvent MD enables studying the system sizes of around ~ 1 micron and time scales of around ~1 – 10 microseconds.

This dissertation is composed of 3 chapters which focus on understanding the factors affecting the organization, stiffness, shape and stability of the multicomponent lipid based systems and the underlying mechanisms of the interactions between biological particles or synthetic particles with them. The specific objectives of each chapter are described as follow:

Chapter 2 - Designing Bio-Inspired Multi-component Vesicles via Dissipative Particle Dynamics and Implicit Solvent Molecular Dynamics Simulation Methods: Investigating the role of chemical dissimilarity in the head and tail groups of the lipid species on the phase segregation and structural properties of binary vesicles by using DPD method. Identifying the effect of the molecular stiffness on the phase segregation process and the vesicle shape. Obtaining the relation between the phase segregation and

thermodynamic variables such as interfacial line tension and surface tension, and correspondence between existing theory and experiments, and the simulation results.

Investigation of the self-assembly of single and binary component vesicles composed of two-tail phospholipid molecules, and the phase segregation in a binary vesicle by using implicit solvent coarse-grained molecular dynamics technique. Demonstrating the formation of fluid lipid bilayer in the absence of solvent by using broad attractive potentials between the hydrocarbon tail beads. The measurement of the scaling exponents for the coarsening dynamics in a binary system and comparison of the results with previous theoretical and simulation studies. Characterization of the physical properties of binary vesicles such as area per lipid and bilayer thickness as a function of temperature and degree of dissimilarity between the tail groups of two lipid species.

Chapter 3 - The Design of Shape-Tunable Hairy Vesicles: Demonstrating the formation of sterically stable biocompatible vehicles aka 'hairy vesicles' via self-assembly of phospholipids and pegylated lipid molecules by using DPD simulation method. Determination of the growth dynamics and size distribution of hairy vesicles during self-assembly process. Determination of the optimum distribution of hairy lipids in the self-assembled vesicles. Identifying the factors such as phase separation, molecular stiffness and relative concentration of the species, and hair length that can control the shape of the vesicles.

Demonstrating the formation of self-assembled hairy vesicles under volumetric confinement and investigating the effect of confinement on the shape changes and aggregation dynamics of hybrid aggregates at different relative concentrations of the hairy lipids and hair lengths.

Chapter 4 - Modeling Interactions between Patchy Nanoparticles and Multi-component Nanostructured Soft Biomaterials: Investigating the effects of the relative size of the NPs to the hair length, and the relative concentration of the hairy lipids on adsorption behavior of nanoparticles on to the surface of hairy vesicles. Identifying the effects of the relative affinity of the nanoparticles for the tethers and phospholipid head groups on their adsorption behavior. Determination of the diffusive behavior of nanoparticles on the surface of hairy vesicle.

Implementation of long range screened electrostatic interactions in the implicit solvent model developed for two-tail phospholipid molecules as demonstrated in Chapter 2. Application of this model on studying the interactions between charged nanoparticles and multicomponent vesicles. Investigating the effects of nanoparticle adsorption on the reorganization of molecular species in the vesicle bilayer.

Chapter 2

Designing Bio-Inspired Multi-component Vesicles via Dissipative Particle Dynamics and Implicit Solvent Molecular Dynamics Simulation Methods

The publications relevant to details of the discussions provided in this section:

- Aydin, F., Ludford, P., Dutt, M., 2014, Phase segregation in bio-inspired multi-component vesicles encompassing double tail phospholipid species. Soft Matter 10 (32), 6096-6108.

- Aydin, F., Dutt, M., 2014, Bioinspired Vesicles Encompassing Two-Tail Phospholipids: Self-Assembly and Phase Segregation via Implicit Solvent Coarse-Grained Molecular Dynamics. J. Phys. Chem. B 118 (29), 8614-8623.

Contributions to this work:

- Implementing modified potentials for the implicit solvent CG MD model into the open source code called Large-scale Atomic/Molecular Massively Parallel Simulator (LAMMPS).

- Running the simulations

- Writing the computer programs which are used to characterize the system

- Performing the analysis and visualization of the system

- Writing the manuscript

2.1 General overview on coarsening dynamics in multi-component bilayers

Phospholipid molecules are the primary component of cell membranes and they are composed of a hydrophilic head group and two hydrocarbon tail chains which can have distinct chemistries. This will give phospholipid molecules a characteristic molecular geometry[6,7] and transition temperature[8-10], and result in the formation of domains or rafts via self-organization of various molecular species.[4,11-24] Earlier experimental investigations have demonstrated phase segregation in two-component phospholipid membranes[120,121] and vesicles.[122] These investigations were performed using lipid species with dissimilar polar head groups (and identical hydrocarbon tail groups), or identical polar head groups (and hydrocarbon tail groups of different

lengths).[123-126] Macroscopic sized domains have been also shown to form in ternary mixtures composed of a lipid with low melting temperature, a lipid with high melting temperature and cholesterol.[11,16,127,128] The relative concentrations of the lipids and the temperature determine the area fraction of each phase. For temperatures corresponding to a two-phase region: the early stages of the coarsening dynamics is accompanied by the nucleation of small domains due to the lateral diffusion and collision between the lipid molecules followed by their coalescence, or the Ostwald ripening mechanism.[16] At latter times, the growth of the domains occurs via their diffusion, collision and coalescence, with the kinetics determined by the membrane and the bulk fluid.[16,119]

The existing particle-based numerical studies on the coarsening dynamics in multi-component bilayers have modeled the lipid molecules with a single hydrocarbon chain.[4,14,15,23,111] Investigations on binary vesicles composed of two-tail lipids of different chain length have explored the effect of the relative concentration of one of the lipid species on the mechanical properties of the vesicles.[112] This work focuses on a bilayer vesicle composed of two types of phospholipid molecules (each species has two hydrocarbon tails) which are the major component of biological cell membranes. Studies on multi-component vesicles have identified four key length scales which determine the phase segregation process: the hydrodynamic diameter, the domain size, the correlation length for domains in the vicinity of a critical miscibility limit and the vesicle diameter.[16] Numerical studies of coarsening dynamics in multi-component bilayers must be able to resolve the relevant spatio-temporal scale to capture all stages of the phase segregation process. This work considers these key length scales by adopting a mesoscopic particle-based computational approaches entitled Dissipative Particle Dynamics (DPD) and

implicit solvent coarse-grained MD, which can simultaneously resolve both the molecular and continuum scales.

2.2 Dissipative Particle Dynamics (DPD)

2.2.1 Technical background

DPD is a mesoscopic MD-based simulation technique that uses soft-sphere coarse-grained (CG) models to capture both the molecular details of the system components and their supramolecular organization while simultaneously resolving the hydrodynamics of the system over extended time scales.[35,60,82,83,113,129] The dynamics of the soft spheres in the DPD technique is captured through integrating Newton's equation of motion via the use of similar numerical integrators used in other deterministic particle-based simulation methods.[113,130] The force acting on a soft sphere i due to its interactions with a neighboring soft sphere j (j ≠ i) has three components: a conservative force, a dissipative force and a random force, which operate within a certain cut-off distance r_c from the reference particle i. These forces are pairwise additive and yield the total force acting of particle i, which is given by

$$\mathbf{F}_i = \sum_{j \neq i} \mathbf{F}_{c,ij} + \mathbf{F}_{d,ij} + \mathbf{F}_{r,ij} \tag{2.1}$$

The soft spheres interact via a soft-repulsive force

$$\mathbf{F}_{c,ij} = a_{ij}(1 - {r_{ij}}/{r_c})\hat{\mathbf{r}}_{ij} \quad (\text{for } r_{ij} < r_c) \tag{2.2}$$

$$\mathbf{F}_{c,ij} = 0 \quad (\text{for } r_{ij} \geq r_c) \tag{2.3}$$

a dissipative force

$$\mathbf{F}_{d,ij} = -\gamma \omega^d(r_{ij})(\hat{\mathbf{r}}_{ij} \bullet \mathbf{v}_{ij})\hat{\mathbf{r}}_{ij} \tag{2.4}$$

and a random force

$$\mathbf{F}_{r,ij} = -\sigma\omega^r(r_{ij})\theta_{ij}\hat{\mathbf{r}}_{ij} \tag{2.5}$$

where

$$\omega^d(r) = [w^r(r)]^2 = (1-r)^2 \qquad (\text{for } r < 1) \tag{2.6}$$

$$\omega^d(r) = [w^r(r)]^2 = 0 \qquad (\text{for } r \geq 1) \tag{2.7}$$

$$\sigma^2 = 2\gamma k_B T \tag{2.8}$$

a_{ij} is the maximum repulsion between spheres i and j, $\mathbf{v}_{ij} = \mathbf{v}_i - \mathbf{v}_j$ is the relative velocity of the two spheres, $\mathbf{r}_{ij} = \mathbf{r}_i - \mathbf{r}_j$, $r_{ij} = |\mathbf{r}_i - \mathbf{r}_j|$, $\hat{\mathbf{r}}_{ij} = \mathbf{r}_{ij}/r_{ij}$, $r = r_{ij}/r_c$, γ is viscosity related parameter used in the simulations, σ is the noise amplitude, $\theta_{ij}(t)$ is a randomly fluctuating variable from Gaussian statistics, ω^d and ω^r are the separation dependent weight functions which become zero at distances greater than or equal to the cutoff distance r_c. Each force conserves linear and angular momentum. Since the local momentum is conserved by all of these three forces, even the small systems exhibit hydrodynamic behavior.[113] The constraints imposed on the random and dissipative forces by certain relations ensure that the statistical mechanics of the system conforms to the canonical ensemble.[113,130] The relation between the pair repulsion parameter a_{ij} and the Flory interaction parameter χ for a bead number density $\rho = 3r_c^{-3}$ is given by[113]

$$\chi = (0.286 \pm 0.002)(a_{ij} - a_{ii}) \tag{2.9}$$

2.2.2 Modeling and parameterization of system components

The individual lipid molecules are represented by bead-spring models, and are modeled by a head group comprised of three hydrophilic beads and two hydrocarbon tails represented by three hydrophobic beads each, as shown in Figure 2.1 (a). Two

consecutive beads in a chain are connected via a bond that is described by the harmonic

spring potential

$$E_{bond} = K_{bond}((r-b)/r_c)^2 \qquad (2.10)$$

where K_{bond} is the bond constant and b is the equilibrium bond length. The constants,

K_{bond} and b are assigned to the values of 64ε and 0.5r_c, respectively.[35,60,82,83,86,129] The

three-body stiffness potential along the lipid tails has the form

$$E_{angle} = K_{angle}(1+\cos\theta) \qquad (2.11)$$

where θ is the angle formed by three adjacent beads. The coefficient K_{angle} is set to be

20ε in our simulations. This stiffness term increases the stability and bending rigidity of

the bilayers.[35]
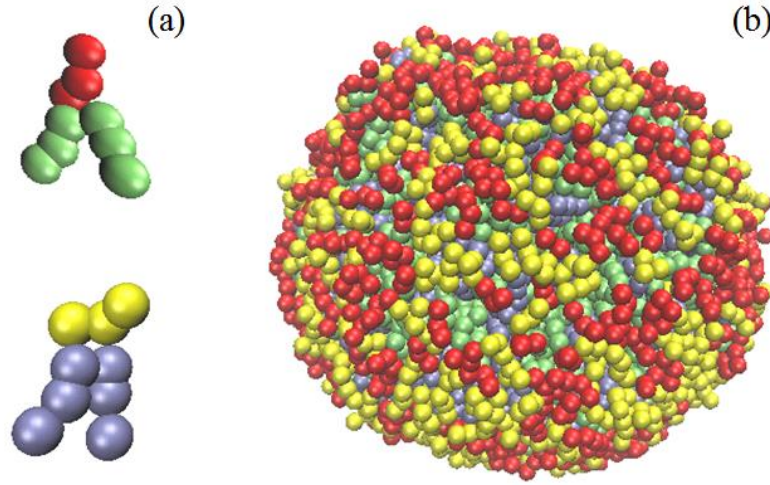
Figure 2.1: (a) The amphiphilic lipid molecules, (b) completely mixed binary component lipid vesicle at t = 10,000τ.

The dissimilarity in the amphiphilic lipid species can arise due to differences in

the chemistry of the head or tail groups, which can be modeled effectively through a soft

repulsive interaction parameter a_{ij}. Differences in the tail groups can also arise due to molecular chain stiffness that is captured in our model by suitably tuning the hydrophobic tail stiffness parameter K_{angle}.

The soft repulsive pair potential parameters for the lipid molecule head and tail beads were selected to capture its amphiphilic nature. The interaction parameters between the like components, a_{ij}, are based on the property of water.[113] The repulsion parameter between two beads of the same type is set at $a_{ii} = 25$ (measured in units of $k_B T / r_c$) which is based upon the compressibility of water at room temperature[113] for a bead density of $\rho = 3r_c^{-3}$. The soft repulsive interaction parameter a_{ij} between hydrophobic and hydrophilic beads is set at $a_{ij} = 100 \, k_b T / r_c$, and is determined by using the Flory-Huggins interaction parameters, χ, as[113]

$$a_{ij} = a_{ii} + 3.496\chi \quad \text{(for } \rho = 3r_c^{-3}\text{)} \tag{2.12}$$

The soft repulsive interaction parameters between the head (h), tail (t) beads of lipid types 1 and 2, and the solvent (s) beads are assigned the following values (in units of $k_B T / r_c$): $a_{ss} = 25$, $a_{h1h1} = 25$, $a_{t1t1} = 25$, $a_{h2h2} = 25$, $a_{t2t2} = 25$, $a_{h1t1} = 100$, $a_{h1s} = 25$, $a_{t1s} = 100$, $a_{h2t2} = 100$, $a_{h2s} = 25$, $a_{t2s} = 100$, $a_{h1t2} = 100$ and $a_{h2t1} = 100$. The values of the inter-lipid species head-head a_{h1h2} and tail-tail a_{t1t2} soft repulsive interaction parameters will span values ranging from 26 to 50, to mimic mixtures of lipid species with different head or tail group properties. The soft repulsive interaction parameters are summarized in Table 2.1. These parameters are selected to model the effective distinct chemistry of the molecular species, thereby capturing the differences in the melting temperature of the

individual species.[4,14,15,23,111,112,131-133] This approach enables us to develop a simple representation of mixtures composed of lipids with two hydrocarbon tails.

In our simulations, the respective characteristic length scale and energy scale are r_c and $k_B T$. As a result, our characteristic time scale can be described as

$$\tau = \sqrt{m r_c^2 / k_B T} \tag{2.13}$$

Finally, $\sigma = 3$ and $\Delta t = 0.02\tau$ are used in the simulations along with the total bead number density of $\rho = 3r_c^{-3}$ and a dimensionless value of $r_c = 1$.[86] The mass of all the beads is set to unity.[1,3,35,60,82,83,86,88,89,112,113,129]

Aij ($k_b T/r_c$)	Head 1	Tail 1	Head 2	Tail 2	Solvent
Head 1	25	100	—	100	25
Tail 1	100	25	100	—	100
Head 2	—	100	25	100	25
Tail 2	100	—	100	25	100
Solvent	25	100	25	100	25

Table 2.1:   The soft repulsive interaction parameters, a_{ij} between head, tail beads of lipid type 1 and 2 and the solvent beads. The boxes with "—" represent the interaction parameters that can be varied for the mixture of lipids with different chemical properties.

We used a constant volume simulation box of dimensions 40x40x40 r_c^3 with the periodic boundary conditions in all three directions. In our simulations, we have 1178 lipid molecules, or 5.6% bead concentration of amphiphilic species, with 10602 head and tail beads. The total number of beads in the system (including solvent molecules) is 192,000.

2.2.3 Length, time and energy scales of the system

We draw a correspondence between our model and physical systems via the experimental properties of biological lipid bilayers. We obtain the characteristic length scale for our model through the comparison of experimental measurements of the

interfacial area per lipid of a DPPC bilayer with similar measurements from our simulations. Experimental measurements of the area per lipid of DPPC bilayers were found to be 64 A^2 at 50 $^{\circ}$C.[134] To compute the average area per lipid, the vesicle is divided into 128 rectangular patches with an average area of 10.5 r_c^2 so that each patch can be treated as a bilayer membrane. The average area per lipid for the vesicle bilayer is computed by summing the areas of all the patches, and averaging over the total number of lipid molecules in all the patches. Using the value for the area per lipid (1.12 r_c^2) computed for a stable self-assembled single component lipid vesicle, the length scale for our model is r_c = 0.76 nm.

The time scale τ was calculated to be 6.0 ns by comparing the experimental measurement of the diffusion coefficient of dipalmitoylphosphatidylcholine (DPPC) bilayer, which is given by 5x10^{-12} m^2/s,[86] with that obtained from the simulations. The diffusion coefficient of the lipid molecule in the simulations can be found by tracking the mean squared displacements of 10 lipid molecules in a vesicle bilayer. We use the relation

$$\frac{\partial \left\langle r^2(t) \right\rangle}{\partial t} = 2dD \qquad (2.14)$$

to relate the diffusion coefficient D to the mean square displacement of a particle in a time interval t.[135] The variable d is the dimensionality of the system that is given to be 3 for our system. We calculate the diffusion coefficient D to be 0.052 r_c^2 / τ, using the slope of the time evolution of the mean square displacement. Using a temperature of 50 $^{\circ}$C, the energy scale is calculated to be $\varepsilon = k_B T = 4.5$x10^{-21} J.

2.3   Results and discussion (DPD)

2.3.1 Formation of multi-component vesicles

We begin by verifying the suitability of the soft repulsive interaction parameters for generating stable binary lipid vesicles. Via self-assembly of amphiphilic phospholipids in a hydrophilic solvent, we generate a binary lipid vesicle.[84] Two types of amphiphilic lipid molecules and hydrophilic solvent beads are randomly dispersed in a 30 r_c x 30 r_c x 30 r_c simulation box composed of 5.6 % bead concentration of amphiphilic species, or 504 lipid molecules.[60,90] To enable the formation of a stable mixed vesicle, the pair interaction potentials are tuned to effectively treat both types of lipid molecules as a single specie. The unfavorable enthalpic interactions between the hydrophilic and hydrophobic components drives the system to minimize its free energy through the self-assembly of the lipid molecules to form a lipid bilayer vesicle.[84]

We use a stable pre-assembled mixed vesicle composed of two chemically dissimilar amphiphilic lipid molecules in a 40 r_c x 40 r_c x 40 r_c simulation box composed of 1178 lipid molecules with 589 molecules of specie 1 and the remaining 589 molecules belonging to specie 2. An analogous protocol detailed earlier is adopted to generate a mixed binary vesicle by treating both the lipid types as a single specie, as shown in Figure 2.1 (b).

2.3.2 Coarsening-dynamics in multi-component vesicles

We investigate the self-organization of the lipid species for values of the head-head and tail-tail interaction parameters, respectively a_{h1h2} and a_{t1t2}, ranging from 26 to 50 for a time interval of 10000 τ. The coarsening dynamics for bilayers composed of lipid species with chemically distinct head groups (and identical tail groups, for example 1-Palmitoyl-2-oleoylphosphatidylcholine and 1-Palmitoyl-2-oleoyl-sn-glycero-3-phosphoethanolamine) is shown in Figure 2.2. The interfacial tension arising from the

unfavorable enthalpic interactions between the distinct head groups drives chemically identical lipids to organize into small domains or clusters, via their diffusion and collision in the vesicle bilayer. Therefore, the self-organization among the lipid species is limited by the lateral diffusion of the different lipid species. Our calculations show the unfavorable enthalpic interactions between the head groups of the distinct lipid species to be small compared to the favorable enthalpic interactions between the hydrocarbon tail groups.

For bilayers composed of lipid species with dissimilar tail groups (and identical head groups, for example 1,2-distearoyl-sn-glycero-3-phosphocholine and 1,2-Dipalmitoyl-sn-glycero-3-phosphocholine), the highly unfavorable enthalpic interactions between the hydrocarbon groups results in a large interfacial energy. The system minimizes its free energy via the interfacial energy through the self-organization of the two molecular species into small domains in the bilayer, mediated by the diffusion and collision of the lipid molecules. For sufficiently high interfacial tension between the distinct lipid species, as the domains grow in the system the coarsening dynamics progresses through the diffusion and collision of the domains, or the evaporation-condensation mechanism. In the latter, individual lipid molecules are observed to evaporate from the boundaries of small domains and condense into the larger domains.[4,14,15,22,128] We observe these processes for binary vesicles comprising of lipid species with greater dissimilarity between the tail groups.

The coarsening dynamics of the binary vesicles is determined by the degree of dissimilarity that is effectively captured by the soft repulsive interaction parameters a_{h1h2}, a_{t1t2}, as shown in Figure 2.2 (a) – (c) and Figure 2.3 (a) – (c). We have selected the range

for the parameters a_{h1h2}, and a_{t1t2} to induce phase segregation of the lipid species while avoiding budding and vesiculation processes on the vesicle bilayer.[15] All the results have been averaged using particle trajectories from four simulations that begin from the same initial conditions but have different random seeds.

The coarsening dynamics in a two-component lipid bilayer is characterized by measuring the number of clusters or domains composed of a given lipid specie, as a function of time (beginning from the mixed state, as shown in Figure 2.1 (b)). A cluster is defined to be composed of lipids from a given species whose head group beads are within interaction range from each other. This definition of a cluster enables us to distinguish between the clusters formed in the two monolayers. The lipid molecules in the inner monolayer are more closely packed as the inner monolayer occupies a spherical shell of smaller volume than the outer monolayer.[136] The difference in the occupied volumes is reflected in the asymmetry in the number of clusters in the two monolayers, as we observe fewer clusters in the inner monolayer. Our measurements of the time evolution of the cluster count show the cluster growth to be influenced by the degree of dissimilarity between the lipid species, as shown in Figures 2.2 (d) and 2.3 (d). We observe the interfacial tension to increase with the dissimilarity between the lipid species, thereby inducing the phase segregation process to minimize the interfacial tension by forming fewer clusters of a given lipid species. Given the higher number of tail beads per lipid molecule, the interfacial tension for systems containing lipid molecules with distinct hydrocarbon tail groups is greater than those with different head groups. Hence, for identical values of the soft repulsion parameters a_{h1h2} and a_{t1t2}, we report fewer clusters for lipid mixtures with distinct tail groups.[131,137]
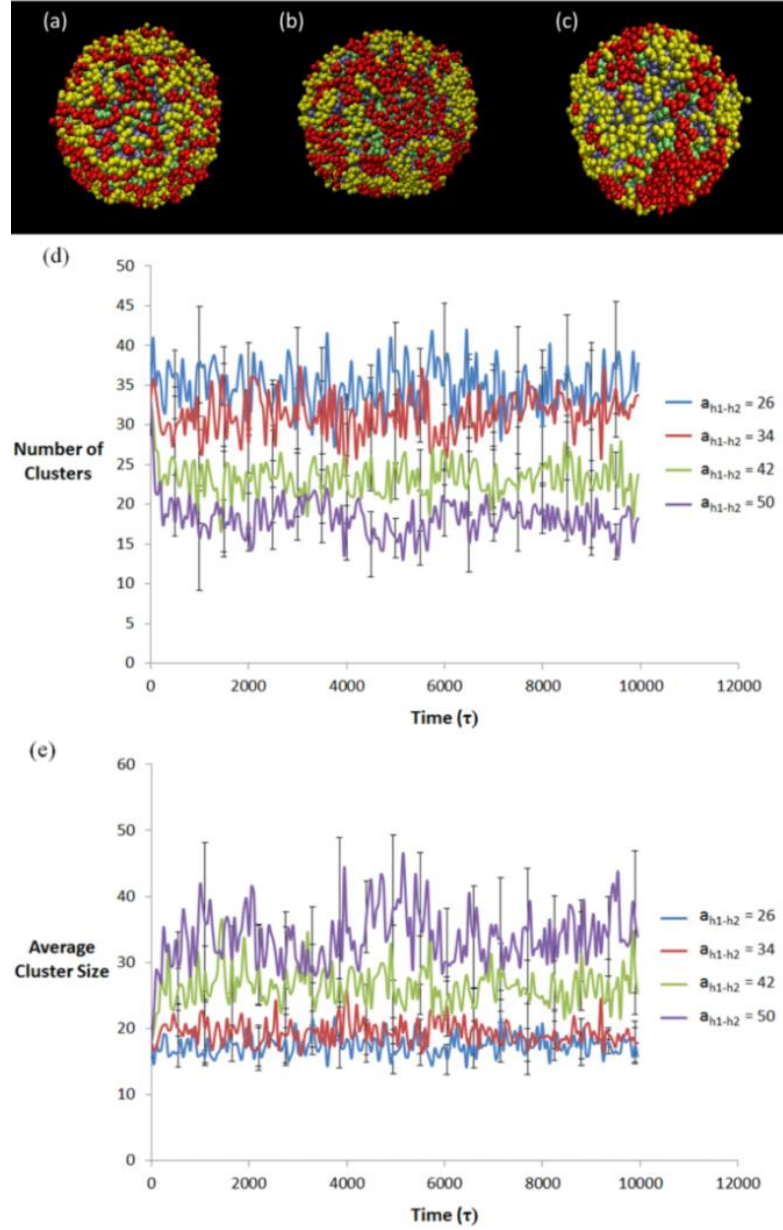
Figure 2.2: Snapshots from the final configurations of the binary component lipid vesicle at t = 5,000τ for different soft repulsive interaction parameters between the head groups of the two lipid species (a) a_{h1-h2} = 26, (b) a_{h1-h2} = 42, (c) a_{h1-h2} = 50. All the simulations start from the completely mixed state. (d) A plot of the time evolution of the total number of clusters of one type of lipid after a single stable vesicle has formed for the head-head soft repulsive interaction parameters of a_{h1-h2} = 26, 34, 42, and 50. (e) A plot of the time evolution for the average cluster size of one type of lipid after a single stable vesicle has formed for the head-head soft repulsive interaction parameters of a_{h1-h2} = 26, 34, 42, and 50. The simulations have been run for a total time of 10,000τ from the mixed state and each data point has been averaged over four simulation runs using different random seeds.
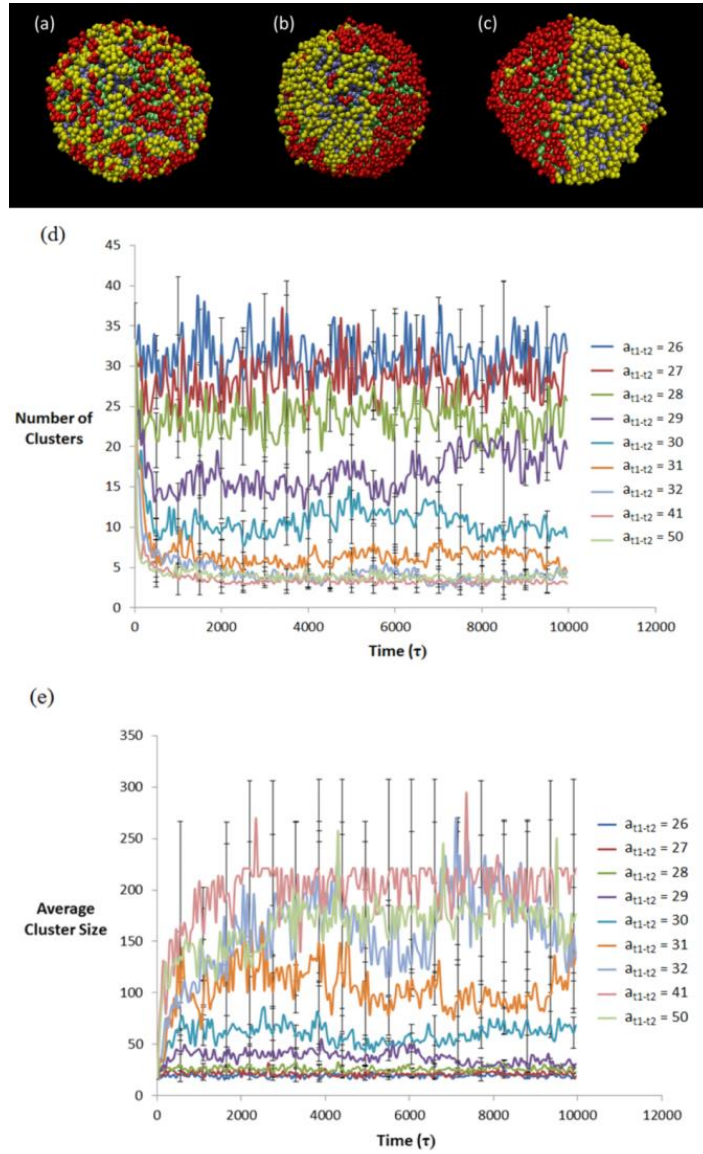
Figure 2.3: Snapshots from the final configurations of the binary component lipid vesicle at t = 5,000τ for different soft repulsive interaction parameters between the tail groups of the two lipid species (a) a_{t1-t2} = 26, (b) a_{t1-t2} = 29, (c) a_{t1-t2} = 31. All the simulations start from the completely mixed state. (d) A plot of the time evolution of the total number of clusters of one type of lipid after a single stable vesicle has formed for the tail-tail soft repulsive interaction parameters of a_{t1-t2} = 26, 27, 28, 29, 30, 31, 32, 41, and 50. (e) A plot of the time evolution for the average cluster size of one type of lipid after a single stable vesicle has formed for the tail-tail soft repulsive interaction parameters of a_{t1-t2} = 26, 27, 28, 29, 30, 31, 32, 41, and 50. The simulations have been run for a total time of 10,000τ from the mixed state and each data point has been averaged over four simulation runs using different random seeds.

For sufficiently low interfacial tensions, the thermal fluctuations of the bilayer can dominate the energetically favorable interactions between the like lipid species to cause fragmentation of the clusters. Variations in the cluster count are observed to occur due to the high mobility of the lipid molecules between two successive time steps. Figure 2.4 demonstrates the rapid changes in the positions of the lipid head beads for four consecutive time steps. Therefore, the coalescence or fragmentation of clusters can be induced by factors such as thermal fluctuations of the bilayer and lipid mobility.
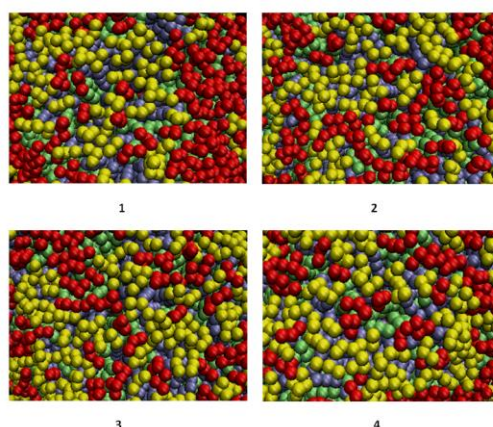
Figure 2.4: The distribution of the head beads in the two-component system as a function of four consecutive time steps. The exact same region of the vesicle is shown in all the snapshots.

For temperature dependent phase segregation in multicomponent bilayers, studies[13,128,128] have shown the coarsening dynamics to be determined by the characteristic correlation length of the fluctuations of the domain boundaries and the hydrodynamic radius, for temperatures below the critical demixing value.

The coarsening dynamics process can be also characterized through the time evolution of the average size of the clusters, as shown in Figures 2.2 (e) and 2.3 (e). The size of a cluster is defined as the total number of molecules of a given lipid species that comprises a cluster. Higher values of the line tension between the dissimilar components

are expected to result in the rapid formation of fewer but larger-sized clusters. We find the measurements to support our expectations and report the trends in the time evolution of the average cluster size to be inverse to those for the number of clusters.[16,138,139] We have summarized our observed trends of the aggregate size as a function of the distinction between the head and the tail groups in Figure 2.5.

The error bars are calculated based on the standard deviation of the results over four different random seeds. Large error bars are found for the higher values of the soft repulsive interaction parameters between the tail beads of the two lipid species (see Figure 2.3 (e)). A plausible explanation for the large error bars is the presence of very few clusters (corresponding to the very large average cluster sizes) at the high soft repulsive interaction parameters of the tail beads. For example, when we use very high soft repulsive interaction parameter such as $a_{t1t2} = 50$, we observe a highly segregated vesicle which has, on the average, two to four clusters of a specific lipid type. Our measurements for the number of clusters, average cluster size and the corresponding standard deviations are computed using smaller number of samples.

The time evolution of the coarsening dynamics can be used to compute the scaling exponent of the clustering process by using the following relation

$$N(t) \sim C\, t^{-\alpha} \tag{2.15}$$

where $N(t)$ is the number of clusters, C is a constant, t is time, and α is the scaling exponent. Similarly, the growth in the average size of a cluster can be characterized by using the following relation

$$<S(t)> \sim D\, t^{\beta} \tag{2.16}$$
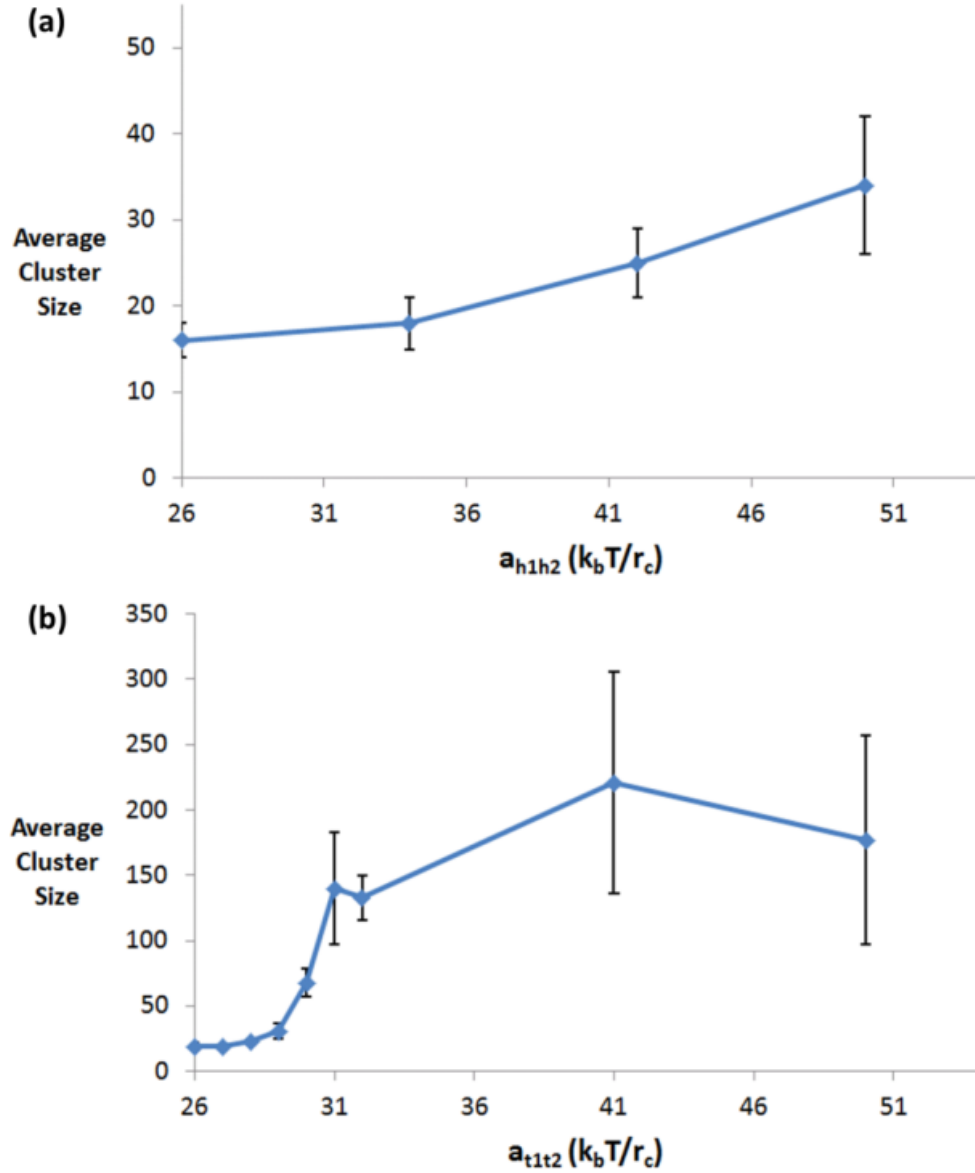
Figure 2.5: A plot of the aggregate size as a function of the soft repulsion interaction parameters between (a) the head groups (a_{h1h2}) and (b) the tail groups (a_{t1t2}). The simulations have been run for a total time of $10,000\tau$ from the mixed state and each data point has been averaged over four simulation runs using different random seeds.

where $< S(t) >$ is the average size of the clusters, D is a constant, t is time, and β is the scaling exponent. Table 2.2 provides the scaling exponents α and β for the values of the soft repulsive interaction parameters a_{t1t2} which result in macroscopic phase segregation.

$a_{t1\text{-}t2}$ (k_bT/r_c)	α	β
31	-0.57	0.61
32	-0.54	0.55
41	-0.51	0.56
50	-0.53	0.52

Table 2.2: Table of the scaling exponents α (obtained from the measurements of number of clusters) and β (obtained from the measurements of the average cluster size) for different soft repulsive interaction parameters of the tail groups of the two lipid species, $a_{t1\text{-}t2}$ = 31, 32, 41, and 50. The simulations used to obtain the scaling exponents have been run for a total time of 10,000τ and averaged over four different random seeds.

The cluster number and the average cluster size scaling exponents demonstrate inverse trends with increasing dissimilarity of the lipid species. The average cluster size measurements can be used to calculate the time evolution of the average area of the clusters $< A(t) >$ through the average area per lipid a_{lipid}, corresponding to a given soft repulsion interaction parameter (as shown Table 2.3). The average area of the clusters $A(t)$ can be demonstrated to have a similar scaling behavior as the average cluster size using the following approximations

$$< A(t) > \sim a_{lipid} < S(t) > \sim a_{lipid} D\, t^{\beta} \propto t^{\beta} \qquad (2.17)$$

If we assume the clusters to be a circle with an average radius $R(t)$, then

$$< A(t) > \propto R(t)^{2} \qquad (2.18)$$

and

$a_{t1\text{-}t2}$ ($k_b T/r_c$)	Bilayer Thickness (σ)	Area per lipid (σ^2)
31	6.24±0.04	1.13±0.02
32	6.24±0.04	1.13±0.02
41	6.25±0.05	1.16±0.03
50	6.28±0.04	1.18±0.04

Table 2.3: The bilayer thickness and area per lipid of the binary component vesicle as a function of different soft repulsive interaction parameters between the tail groups of the two lipid species, $a_{t1\text{-}t2}$ = 31, 32, 41, and 50. The simulations have been run for a total time of 10,000 τ and each data point has been averaged over four simulation runs using different random seeds.

$$R(t) \propto t^{\beta/2} \tag{2.19}$$

If the total interface length $L(t)$ of the clusters is given by

$$N(t) \, 2 \, \Pi R(t) \tag{2.20}$$

and the A_{total} is the total area occupied by the clusters of a given species, the following relation can be obtained: [4,14]

$$R(t) \sim A_{total}/L(t) \tag{2.21}$$

Our measurements of the scaling exponents, as detailed in Table 2.2, are in agreement with earlier numerical and experimental results[4,14-17,22] showing $N(t) \propto t^{-2/3}$, $L(t) \propto t^{-1/3}$ and $R(t) \propto t^{1/3}$. A growth exponent for the average radius of 1/3 is usually attributed to the evaporation-condensation effect.[4,14,16,140] Our simulations have also demonstrated the domain dynamics at the latter stages to be determined by the diffusion and collisions of the clusters. We have provided the plots of the time evolution of the number of clusters and the average cluster size used to compute the scaling exponents in Figures 2.6 and 2.7.
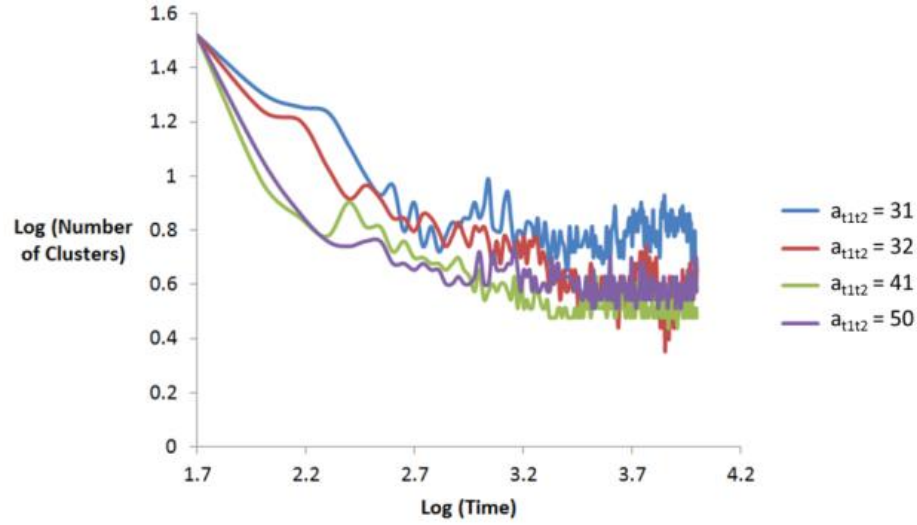
Figure 2.6: A plot of time scale behavior for the number of clusters used to obtain the scaling exponent (α) for the tail-tail soft repulsive interaction parameters of a_{t1-t2} = 31, 32, 41, and 50. The simulations have been run for a total time of 10,000τ from the mixed state and each data point has been averaged over four simulation runs using different random seeds.
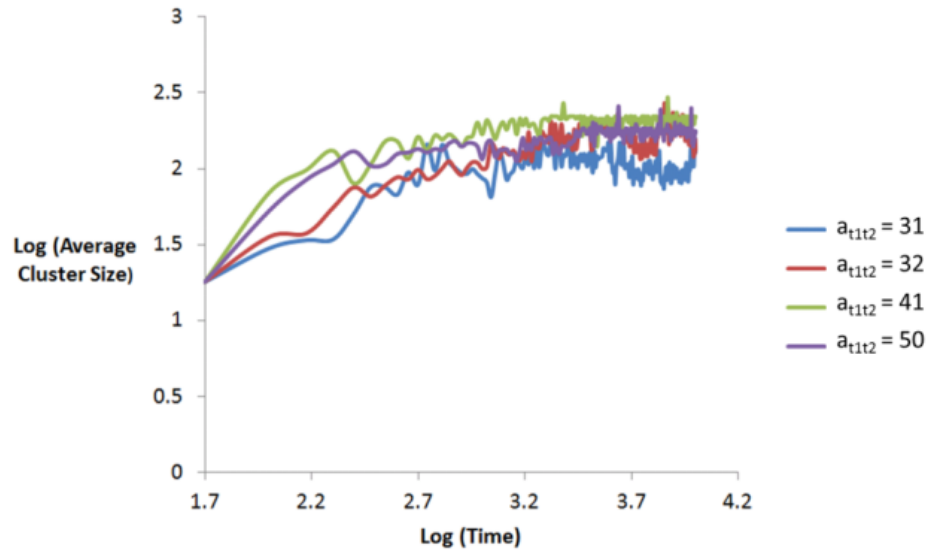
Figure 2.7: A plot of time scale behavior for the average cluster size used to obtain the scaling exponent (β) for the tail-tail soft repulsive interaction parameters of a_{t1-t2} = 31, 32, 41, and 50. The simulations have been run for a total time of 10,000τ from the mixed state and each data point has been averaged over four simulation runs using different random seeds.

2.3.3 Packing properties of multi-component vesicles

The packing of the lipid molecules in the vesicle bilayer is found to be not very sensitive to differences in the head or tail groups , and can be characterized by the bilayer thickness and the area per lipid, as shown in Table 2.3. To calculate the bilayer thickness, the vesicle is divided into 128 patches so that each patch can be treated effectively as a bilayer membrane. The bilayer thickness is computed by measuring the distance between the lipid head groups in the opposing monolayers, in a given patch. These measurements were computed using the particle configurational data obtained from four simulations using identical initial conditions but different random seeds. The bilayer distance was measured for each patch and was averaged over all the patches, the particle configurational snapshots and the different random seeds. The area per lipid was measured using the approach detailed in Section *2.2.3*.

2.3.4 The relation between thermodynamics and coarsening-dynamics in multicomponent vesicles

The phase segregation on the vesicle bilayer is driven by the thermodynamics of the system. We draw correspondence between the degree of phase segregation and thermodynamic properties by measuring the interfacial line tension and surface tension of the lipid vesicles, for the different tail-tail interaction parameters. The measurements are performed on equilibrium configurations of the binary mixtures, for a range of dissimilarities between the tail groups of the two lipid species. The line tension of an interface separating two phases can be found by calculating the excess free energy per unit length of the contact length along the interface.[141] We estimate the line tension λ of the domain boundary through the following equation[142]

$$\lambda \equiv \left[\frac{1}{2}\left(U_{AA} + U_{BB}\right) - U_{AB}\right] / l_{mo} \tag{2.22}$$

where U_{AA}, $U_{BB,}$ and U_{AB} are the pair interaction energies between components A and B, and l_{mo} is the lateral size of the lipid molecules. The lateral size of the lipid molecules is given by $1.1r_c$ from the area per lipid calculation provided in Section *2.2.3*. The results for the line tension measurements as a function of the soft repulsive interaction parameter a_{t1-t2} are found to be consistent with our observations of the coarsening dynamics (see Figure 2.8), and have been averaged over all particles in the system. Our results for the line tension are in agreement with theoretical[127,143] and experimental[127] studies which demonstrate the interfacial line tension to increase with an order parameter which characterizes the degree of phase segregation. According to the theory proposed by Schick et al.,[143] there are two key factors which control the phase segregation in multi-component lipid membranes. One of the factors is the repulsive interactions between dissimilar lipid molecules (such as a mixture of saturated and unsaturated lipid molecules) which depends on the magnitude of the order parameter. The order parameter is used in the theory to provide a measure of the degree of order for the saturated lipid chains. As the order parameter increases, the repulsive interactions between the saturated and unsaturated lipid molecules will increase, which results in phase segregation. This effect is analogous to increasing the soft repulsive interaction parameter a_{ij} between the hydrocarbon tail groups of the dissimilar lipid species in our simulations.
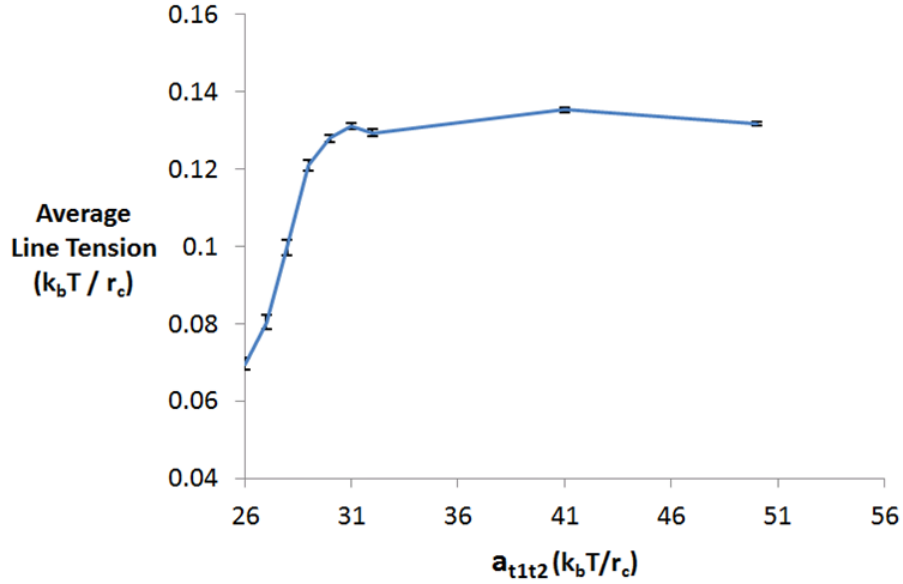
Figure 2.8: A plot of the average line tension as a function of the tail-tail soft repulsive interaction parameters $a_{t1\text{-}t2}$ (= 26, 27, 28, 29, 30, 31, 32, 41, and 50.) The measurements were performed on particle trajectories starting at 10,000τ, for a total duration of 5,000τ. Each data point has been averaged over time.

The other factor is the addition of cholesterol-like sterols which results in ordering in the saturated lipid chains, thereby inducing phase segregation. The second factor is not relevant for our investigation as we do not include sterols in our system.

The second thermodynamic property we investigate is the surface tension of the binary lipid vesicle by computing the difference between the internal and external pressures of the bilayer.[144-146] The relation between the surface tension and pressure difference across the vesicle bilayer has been shown to be given by Laplace's law which requires the following equation to hold: [146]

$$P_N(r_i) - P_N(r_j) = \frac{2\gamma_{ij}}{r_i} \qquad (2.23)$$

where r_i and r_j are the distances of the centers of mass of the particles in the inner and outer monolayers of the vesicle from the center of the vesicle, $P_N(r_i)$ and $P_N(r_j)$ are the

normal components of the pressure in the two monolayers, and γ_{ij} is macroscopic surface tension. We compute the normal pressure components by measuring the stress tensor for each bead in the bilayer of the vesicle[87,147] The stress tensor is given by

$$\Sigma^{\alpha\beta} = \begin{pmatrix} \Sigma_T & 0 & 0 \\ 0 & \Sigma_T & 0 \\ 0 & 0 & \Sigma_N \end{pmatrix} \qquad (2.24)$$

from where the diagonal component Σ_N is extracted for each bead and is correlated with its distance from center of the vesicle. The normal component of the pressure can be calculated by summing over the normal component of the stress tensor for each bead, and normalizing by the system volume. In order to calculate $P_N(r_i)$ and $P_N(r_j)$, we measure the normal pressure on the lipid head beads in the inner and outer monolayers. By using Laplace's law, we compute the surface tension as a function of the soft repulsive interaction parameter a_{t1t2} as shown in Figure 2.9.
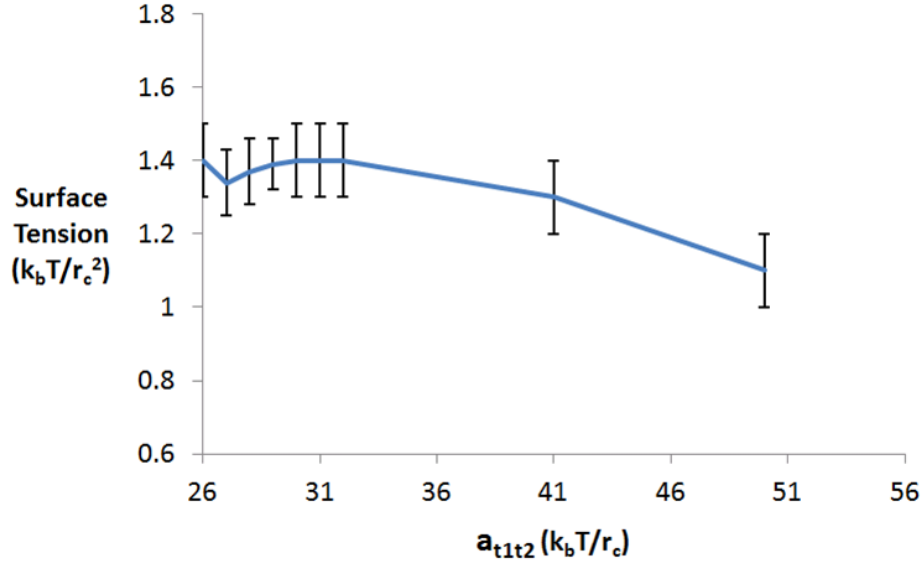
Figure 2.9: A plot of the surface tension as a function of the tail-tail soft repulsive interaction parameters a_{t1-t2} (= 26, 27, 28, 29, 30, 31, 32, 41, and 50.) The measurements were performed on particle trajectories starting at 10,000τ, for a total interval of 25,000τ. We adopt a box averaging approach to compute the errors.

For all the values of the soft repulsive interaction parameters examined, we find the average inner pressure to be greater than the average outer pressure which results in a positive surface tension. We observe the surface tension to decrease as the soft repulsive interaction parameter between the tail groups of the different lipid species increases. This finding is consistent with the trends in the area per lipid as a function of the soft repulsive interaction parameter, as shown in Table 2.3. We observe the surface tension to decrease at higher values of a_{t1t2} (41 k_bT/r_c and 50 k_bT/r_c) with corresponding increases in the area per lipid, as shown in Figure 2.9. A possible explanation for this observation could be an increase in the interstitial space between the two phases as a consequence of the strong repulsive interactions between the tail groups of the two lipid species. The repulsive interaction would increase the fluid flux from the inside to the outside of the vesicle, thereby decreasing the pressure difference, and the surface tension. We would also like to note that theoretical[148] and experimental[149] studies have also demonstrated tension to increase the degree of phase segregation in lipid membranes.

2.3.5 The relation between chain stiffness, phase separation and packing properties of the bilayer in multicomponent vesicles

The role of hydrophobic tail stiffness is explored on the phase segregation of a two-component lipid vesicle. We began with a completely mixed binary vesicle (as shown in Figure 2.1 (b)) and ran the simulations for an interval 5000 τ using a desired value of the hydrophobic tail angle coefficient $K_{angle,1}$ of one of the lipid species. The interfacial tension arising from the differences in the tail stiffness of the molecular species was sufficiently small so as to prevent macroscopic phase segregation (see Figure 2.10 (a) – (d).) However, the shape of the vesicle is observed to evolve from an

ellipsoidal to a spherical morphology with increasing chain stiffness of one of the lipid

species. The vesicle stabilizes to a spherical shape for values of chain stiffness parameter

$K_{angle,1}$ set at 10ε or higher, as shown in Figure 2.10 (d).
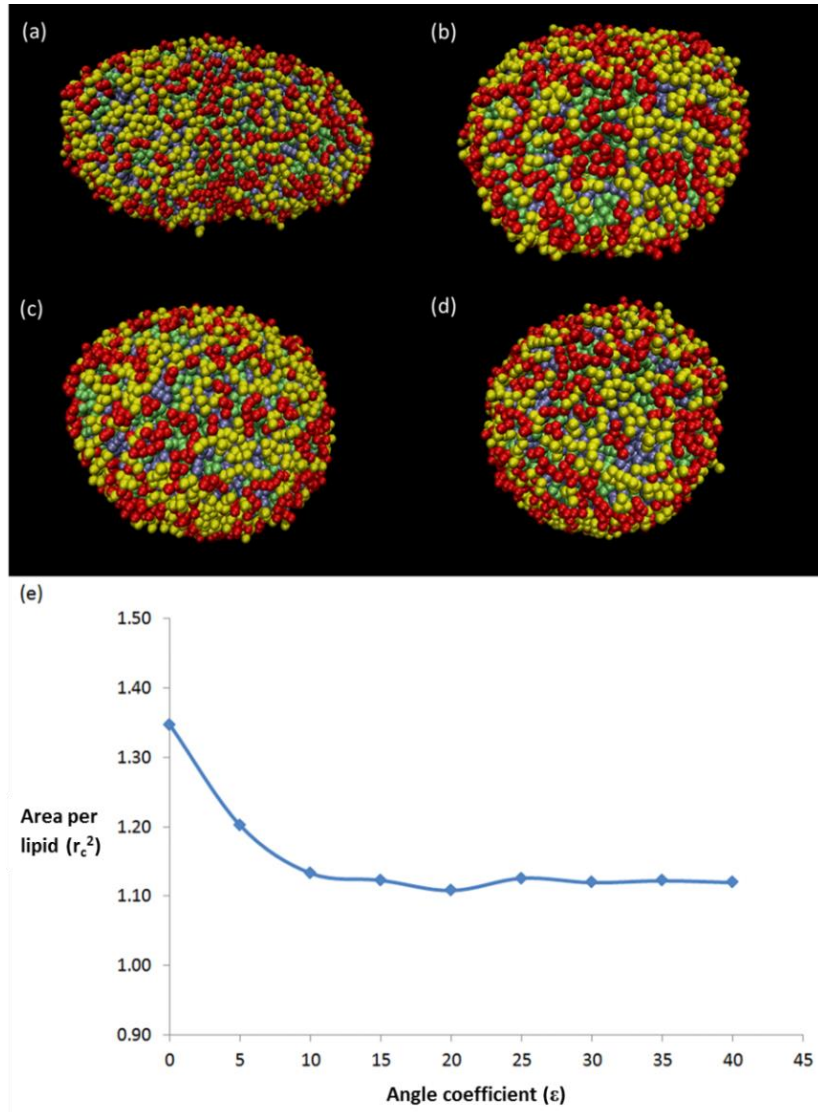
Figure 2.10: Snapshots from the final configurations of the binary component lipid vesicle at t = 5,000τ while keeping the angle coefficient of one type lipid at a constant value of $K_{angle,2}$ = 20 and varying the angle coefficient of other type of lipid for the values of (a) $K_{angle,1}$ = 0, (b) $K_{angle,1}$ = 5, (c) $K_{angle,1}$ = 10, (d) $K_{angle,1}$ = 15. All the simulations start from the completely mixed state. (e) The area per lipid of the binary component vesicle as the angle coefficient of specific type of lipid species ($K_{angle,1}$) is varied from 0 to 40 and the angle coefficient of other type of lipid species is kept at a constant value of $K_{angle,2}$ = 20. The simulations have been run for a total time of 5,000 τ.

The effect of chain stiffness on molecular packing of the lipids in the bilayer can be characterized through the measurement of the area per lipid. Using a similar approach to that detailed in Section *2.2.3*, we measure the average area per lipid for different values of the chain stiffness. The lipid molecules become more tightly packed as the chain stiffness of one of the species increases due to fewer molecular conformations sampled and smaller excluded volumes, for values of $K_{angle,1}$ set at 10ε or higher, as shown in Figure 2.10 (e).

The effect of shape change on the surface tension is also investigated by measuring the surface tension of the vesicle with ellipsoidal morphology as shown on Figure 2.10 (a). It is found that the surface tension of the ellipsoidal-shaped vesicles reduces to approximately half of the surface tension for spherical-shaped vesicles. This result is consistent with the observation that increases in the surface tension makes the vesicles more spherical in shape.[144] In addition, experimental investigations have shown mitotic cells to transform into a spherical shape by increasing their surface tension to accelerate the epithelial invagination process.[150]

2.4   Implicit solvent coarse-grained molecular dynamics (CG MD)

2.4.1 Technical background

The particle dynamics can be resolved by using classical molecular dynamics (MD) simulations.[130,135,151] The equation of motion for each bead i is given by

$$\mathbf{F}_i = m_i \mathbf{a}_i \qquad (2.25)$$

where $\mathbf{F}_i$ is the force acting on bead i, m_i is the mass and $\mathbf{a}_i$ is the acceleration of the bead i. The force can be expressed as the gradient of the potential energy U by the relations

$$\mathbf{F}_i = -\nabla_i U \tag{2.26}$$

with

$$U = U_{pair} + U_{bond} + U_{angle} \tag{2.27}$$

where U_{pair}, U_{bond} and U_{angle} are the potential energies from all its pair, bond and angle interactions, respectively. The dynamics of each bead i can be determined by the following equations

$$-\nabla_i U = m_i \mathbf{a}_i = m_i \frac{\partial^2 \mathbf{r}_i}{\partial t^2} = m_i \frac{\partial \mathbf{v}_i}{\partial t} \tag{2.28}$$

and

$$\mathbf{v}_i = \dot{\mathbf{r}}_i \tag{2.29}$$

where $\mathbf{r}_i$ and $\mathbf{v}_i$ are the position and velocity vectors of bead i. The equations of motion will be integrated using the Velocity Verlet method[130] which has greater stability, time reversibility and preserves the symplectic form in the phase space compared to the Euler method.[130]

2.4.2 Modeling and parameterization of system components

This work adopts a model introduced by Cooke and Deserno[77] and used it for developing an implicit solvent coarse-grained representation of dipalmitoylphosphatidylcholine (DPPC) phospholipid molecule. Cooke and Deserno[77] use the model to study bilayers formed from a single tail lipid molecule. The physics of the model is controlled by the external temperature (i.e. k_BT) which determines the entropy and the interaction energy (ε) which sets the enthalpy. The ratio k_BT/ε determines the phase behavior of the bilayer[77] and is the same for all the beads, for a given value of the interaction energy. This enables us to adopt the model for a two-tail representation of

a phospholipid molecule. A lipid molecule is represented by a bead-spring model with one head group encompassing three hydrophilic beads and two hydrocarbon tail groups composed of three hydrophobic beads each, as shown in the Figure 2.11 (a). The repulsive interactions due to the excluded volume effects between the beads can be modeled by the purely repulsive Weeks-Chandler-Andersen (WCA) soft-sphere potential[152]

$$U_{rep}(r,b) = 4\varepsilon[(b/r)^{12} - (b/r)^6] + \varepsilon \quad \text{(for } r \leq r_c) \tag{2.30}$$

where ε is the depth of the potential well, b is the bead diameter, r is the distance between two beads and r_c is the cutoff distance beyond which the interactions are not computed. The cut-off distance is chosen as $r_c = 2^{(1/6)}$ b. The interaction between the head-head and the head-tail beads is purely repulsive and is represented by the WCA potential. The hydrophobic effect arising from the van der Waals attraction between the beads can be suitably represented by a Lennard-Jones-style potential with its range extended via a tunable length w_f:

$$U_{\text{flat LJ}}(r) = -\varepsilon \quad \text{(for } r < r_c + w_f) \tag{2.31}$$

$$U_{\text{flat LJ}}(r) = 4\varepsilon[(b/(r - w_f))^{12} - (b/(r - w_f))^6] \quad \text{(for } r_c \leq r \leq w_f + w_{cut}) \tag{2.32}$$

$$U_{\text{flat LJ}}(r) = 0 \quad \text{(for } r > w_f + w_{cut}) \tag{2.33}$$

where the potential is cutoff beyond $w_f + w_{cut}$.[77] The underlying principle of this model is the use of a broad attractive potential $U_{\text{flat LJ}}(r)$ between the tail beads to compensate for the absence of the solvent molecules. Here, w_f is the length of the flat region at the minimum of potential and w_{cut} is the cut-off distance. In our simulations, we choose $w_f = 0.2\sigma$ and $w_c = 2.5\sigma$. The value of r_c depends on the type of beads interacting with each other and it is controlled by setting the value of b.
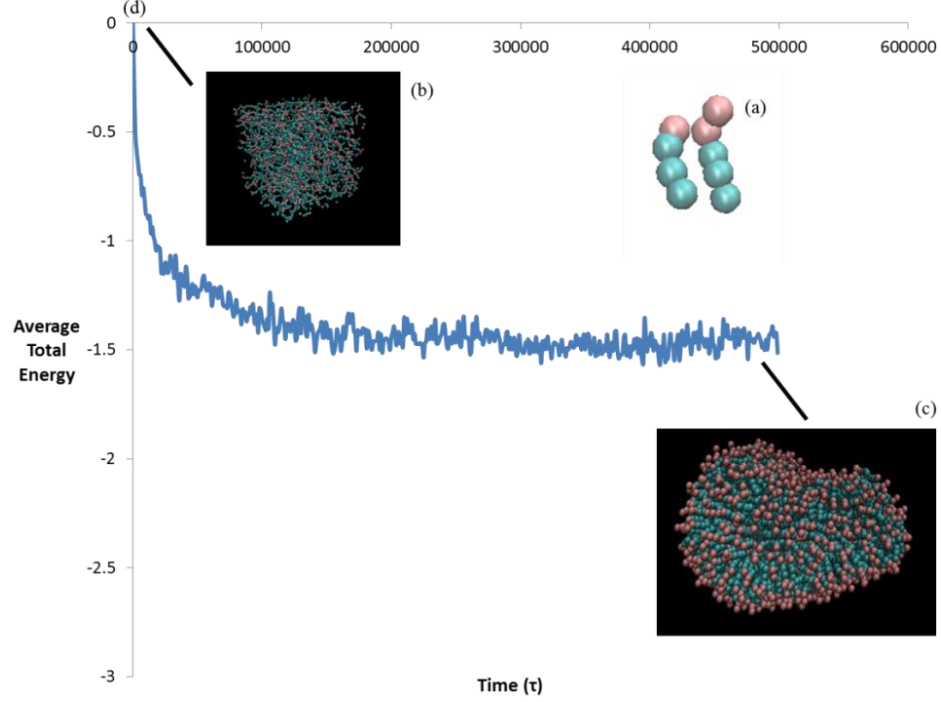
Figure 2.11: Images of (a) an amphiphilic lipid molecule, (b) randomly dispersed lipid molecules in a simulation box of 25x25x25σ at the simulation time t = 0, (c) a self-assembled single component lipid vesicle at t = 500,000τ, and (d) a plot of the average total energy of single component lipid vesicle as a function of time.

For the head-head and head-tail interactions, b is set to be 0.95σ and for tail-tail interactions, b is set to be σ. ε is the unit of energy and σ is the unit of length. The interaction between the tail beads is obtained by combining the repulsive and attractive pair potentials to yield a combined pair potential U_{comb} of the following form:

$$U_{comb}(r) = 4\varepsilon[(b/r)^{12} - (b/r)^6] \text{ (for r} \le \text{r}_c)$$
$$(2.34)$$

$$U_{comb}(r) = -\varepsilon \text{ (for r}_c < \text{r} < \text{r}_c + \text{w}_f)$$
$$(2.35)$$

$$U_{comb}(r) = 4\varepsilon[(b/(r-w_f))^{12} - (b/(r-w_f))^6] \text{ (for r}_c + \text{w}_f \le \text{r} \le \text{w}_f + \text{w}_{cut})$$
$$(2.36)$$

$$U_{comb}(r) = 0 \text{ (for r} > \text{w}_f + \text{w}_{cut})$$
$$(2.37)$$

The dissimilarity in the amphiphilic lipid species is modeled effectively through the pair potential interaction parameter ε. For a system composed of a single species of lipid

molecules, the value of ε is set to 1. We model mixtures of lipid species with distinct tail groups via the pair potential interaction energy ε, to capture the interactions between the tail beads of the like and unlike lipid species. The depth of the attractive potential represented by ε is used to effectively capture the dissimilarities in the chemistry or the length of the hydrocarbon tails, or the molecular geometry of the two lipid species. The values of the pair interaction energy ε less than 1 imply greater dissimilarity between the two interacting beads.

In the bead-spring representation of chain-like moieties, two consecutive beads along a chain are connected by an attractive finitely extensible nonlinear elastic spring (FENE)[152] given by

$$U_{FENE}(r) = -0.5 K r_{\infty}^2 \ln[1 - (r/r_{\infty})^2] \text{ (for r < r}_\infty) \tag{2.38}$$

$$U_{FENE}(r) = \infty \text{ (r} \geq r_\infty) \tag{2.39}$$

where r is the separation of the centers of mass of two bonded beads, r_∞ is the maximum extension of the spring, or the divergence length and K is the spring constant. The stiffness is K = 30ε / σ^2 and the divergence length is r_∞ = 1.5σ. The bond potential parameters were selected to model a relatively stiff spring to avoid high frequency modes and chain crossing.[77,153] The hydrophobic lipid tails are attributed stiffness through a harmonic angle potential

$$U_{angle} = K_\theta (\theta - \theta_0)^2 \tag{2.40}$$

where K_θ is the angle potential constant and is given by 8.1 ε/ rad^2. θ_0 is the equilibrium angle between three consecutively bonded beads and is set to 3.14 rad (or, 180 degrees).

The simulations were run in the canonical ensemble using the Langevin thermostat with three dimensional periodic boundary conditions. The simulation box dimensions were set to 25σ x 25σ x 25σ. The total number of beads in the system was 4500 which corresponds to a lipid density of 0.032 lipids per σ^3. This value corresponds to the lipid density used by Cooke and Deserno.[77] The simulation time step was set to δt = 0.01τ. We will be using our own distribution of LAMMPS for the investigations presented in this chapter.

2.4.3 Length, time and energy scales of the system

Using a similar procedure in Section *2.2.3*, we calculate the length, time and energy scales for our model to be σ = 0.52 nm, τ = 4.9 ns and ε = $4.5\text{x}10^{-21}$ J, respectively.

2.5   Results and discussion (Implicit solvent CG MD)

2.5.1 Formation of single component lipid vesicle via self-assembly

For the initial setup, a single species of lipid molecules are randomly placed in the simulation box, as shown in Figure 2.11 (b). To equilibrate the system, the simulation is run for a time interval of $30,000\tau$ with a repulsive pair potential acting between the different types of beads with the temperature set at 1.0. The reduced temperature corresponds to a physical temperature of 50 ^{o}C at which the DPPC bilayer is in the fluid state. Following the equilibration phase, the interaction potentials and the corresponding parameters detailed in Section *2.4.2* are used to promote the self-assembly of the amphiphilic lipid molecules to generate a stable single component lipid vesicle, as shown in Figure 2.11 (c). Figure 2.11 (d) shows the time evolution of the average total energy during the self-assembly process. The bond and angle energies fluctuate about average

values for a significant fraction of the aggregation process. The time evolution of the average pair, bond and angle energies during the self-assembly process have been provided in the Figure 2.12.

2.5.2 The effect of the temperature on the structural characteristics of a single component vesicle

A stable self-assembled vesicle is used as the initial condition and simulations are run for a range of temperatures spanning 0.7 to 0.95. Each simulation is run for an interval of 20,000τ. Figure 2.13 summarizes the final configurations of the vesicle at the different temperatures, and shows the vesicle to remain morphological robust for the values of temperatures explored.
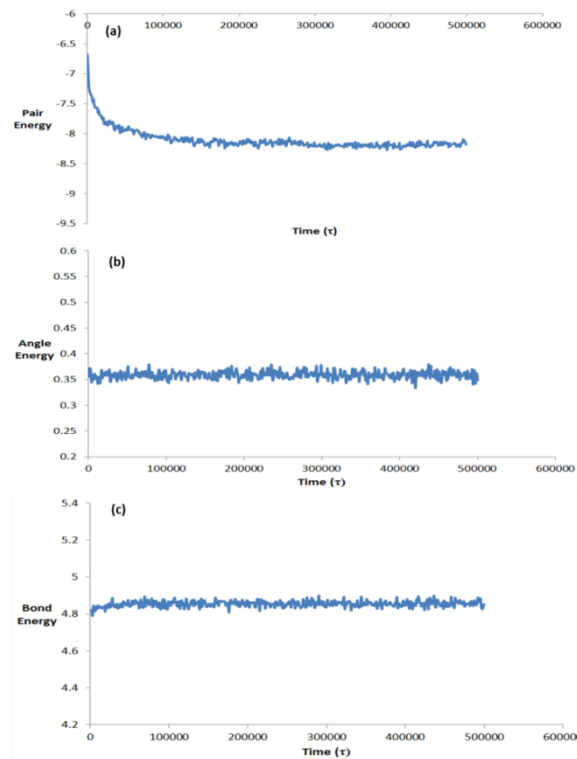
Figure 2.12: Time evolution of the average (a) pair, (b) angle and (c) bond energies during the self-assembly process of the single component lipid vesicle. The simulation has been run for a total time of 500,000τ.

We study the role of temperature on the structure of the vesicles through measurements of the bilayer thickness and the area per lipid. The bilayer thickness of the vesicle is calculated by following the same procedure detailed in Section *2.3.3*.
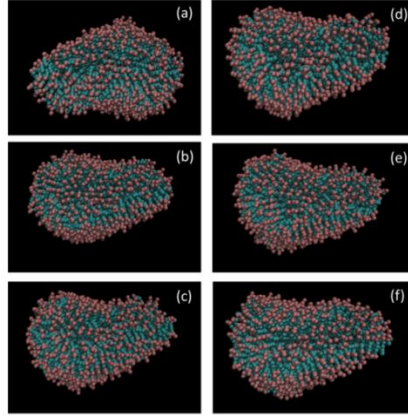
Figure 2.13: Final configuration of a single component self-assembled vesicle (at t = 20,000τ) at a temperature (a) T = 0.7, (b) T = 0.75, (c) T = 0.8, (d) T = 0.85, (e) T = 0.9, (f) T = 0.95.

For a single component vesicle, the average bilayer distance is found to be 6.5±0.1 σ which corresponds to 3.39±0.06 nm in physical units. This measurement is found to be in fairly good agreement with the theoretical and experimental results for a DPPC bilayer at 50 ^{o}C, as shown in Table 2.4.

Mechanical Properties of DPPC bilayer at 50 ^{o}C	Simulation results	Simulation results in physical units	The experimental results from the literature
Bilayer thickness	6.5±0.1σ	3.39±0.06 nm	3.3 nm (theoretical) [10] 3.6 nm (AFM) [10]
Area per lipid	2.39±0.09 σ^2	Used to obtain length scale	Used to obtain length scale

Table 2.4: Tabulation of the bilayer thickness and the area per lipid of the DPPC bilayer, at temperature of T = 50 ^{o}C. Measurements from the simulations are shown in reduced units (first column) and physical units (second column.) Published experimental and theoretical measurements are provided in the third column. The simulation results in physical units and the experimental results for the area per lipid are not provided since it is used to obtain the length scale of the system, and is discussed in the Methodology section.

Details of the average area per lipid measurements can be found in Section *2.2.3*. For a single component vesicle, we find the average area per lipid to be 2.39±0.09 σ^2, as shown in Table 2.4. Our measurements of the bilayer thickness were not influenced by changes in the temperature, as shown in Table 2.5. This behavior could manifest from the stiff angle potential functional form that provides greater resistance to variations in the hydrocarbon tail angles, in response to temperature increase. Our computations of the area per lipid, as shown in Table 2, demonstrates a slight increase with the temperature (from 2.33±0.09 σ^2 (or, 63 ± 2 A^2) at T = 0.7 to 2.39±0.09 σ^2 (or, 65 ± 2 A^2) at T = 0.95.) This observation is consistent with the theoretical and experimental studies of lipid membranes using X-ray and neutron ULV data.[154] An earlier study[154] has shown increases in the temperature to result in a higher probability of trans-gauche isomerization of the lipid molecules in a bilayer, and therefore larger values of the average area per lipid. We do not expect the stiff angle potential functional form to capture the trans-gauche isomerization of the lipid molecules in response to temperature. However, higher temperatures will increase the translational kinetic energy of the molecules in the bilayer plane, resulting in greater spacing between the lipid molecules as demonstrated by our calculations of the area per lipid. We would like to note that Cook and Deserno measured the area per lipid of their single tail lipid to lie in the range of 1.1-1.5 σ^2.[77]

2.5.3 Coarsening-dynamics in multi-component vesicles using implicit solvent conditions

We generate a stable self-assembled vesicle composed of equal concentrations of two species of lipid molecules by using the same protocol to generate a single component vesicle. The two lipid species with chemically distinct tail groups are modeled via the

interaction parameter ($\varepsilon_{t1\text{-}t2}$) between the tail beads of the two lipid types, t1 and t2, which

is varied from 0.9

T	Bilayer Thickness (σ)	Area per lipid (σ^2)
0.95	6.5±0.1	2.39±0.09
0.90	6.5±0.1	2.39±0.09
0.85	6.5±0.1	2.4±0.1
0.80	6.5±0.1	2.34±0.09
0.75	6.5±0.1	2.35±0.09
0.70	6.5±0.1	2.33±0.09

Table 2.5: The bilayer thickness and the area per lipid of the single component self-assembled vesicle as a function of temperature ranging from 0.7 to 0.95. The simulations have been run for a total time of 20,000 τ and each data point has been averaged over four simulation using different random seeds.

to 0.99. The interaction parameter ε between all the other types of beads is set at 1.0.

Beginning from a configuration where both types of lipid molecules are dispersed

randomly in the simulation box, the spatial and conformational configurations of the lipid

molecules are equilibrated by using repulsive interactions between all types of beads.

After the equilibration phase, we use parameters that capture the distinct nature of the

two lipid species. We observe the lipids to aggregate to form small clusters while the two

species phase segregate into small domains, to minimize the energetically less favorable

interactions between the dissimilar lipid molecules. After the formation of a single binary

vesicle, the clusters composed of like species diffuse in the bilayer, collide and coalesce

to grow in size, thereby reducing the interfacial tension between the different phases in

the hydrophobic region of the bilayer. Figure 2.14 (a) – (e) summarizes the final

configuration of the binary component self-assembled vesicle for different interactions

between the tail groups of the two lipid species. Our characterization of the coarsening

dynamics demonstrates the degree of phase separation to increase with the dissimilarity between the tail groups.

We study the time evolution of the coarsening dynamics by computing the total number of clusters of a given type of lipid molecule following the formation of a stable vesicle, for values of the tail-tail interaction parameter ε_{t1_t2} ranging from 0.9 to 0.99. The interfacial tension arising due to the unfavorable energetic interactions between the two lipid species will drive the phase segregation of the lipid species to form multiple domains. We anticipate the interfacial tension to increase with the dissimilarity between
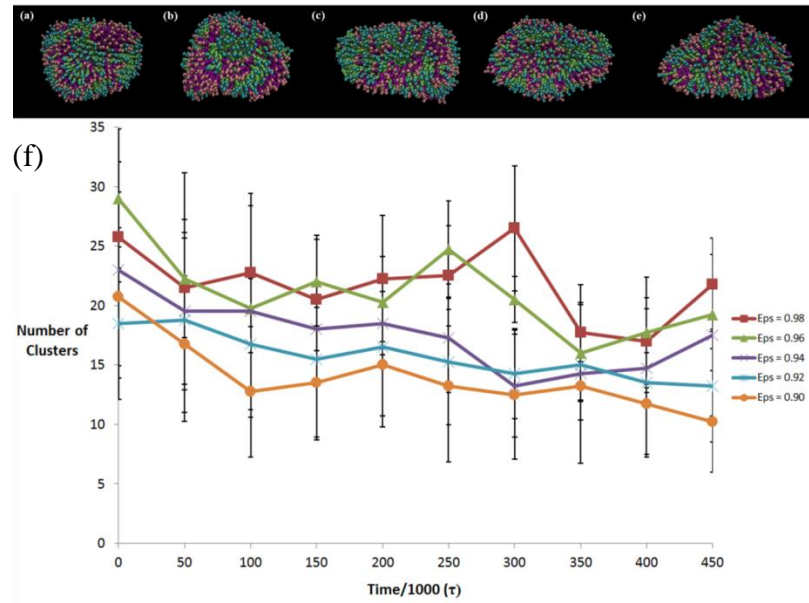
Figure 2.14: Images of the final configurations of the self-assembled binary vesicle (at time t = 500,000τ) for the inter-species inter-tail bead interaction parameters (a) $\varepsilon_{t1\text{-}t2}$ = 0.90, (b) $\varepsilon_{t1\text{-}t2}$ = 0.92, (c) $\varepsilon_{t1\text{-}t2}$ = 0.94, (d) $\varepsilon_{t1\text{-}t2}$ = 0.96, and (e) $\varepsilon_{t1\text{-}t2}$ = 0.98. (f) A plot of the time evolution of the total number of clusters of one type of lipid species after the formation of a single stable vesicle, for $\varepsilon_{t1\text{-}t2}$ = 0.90, 0.92, 0.94, 0.96, and 0.98. The simulations have been run for a total time of 500,000τ and each data point has been averaged over four simulation runs using different random seeds. The x-axis has been scaled by 1/1000 for ease of visualization.

the tail groups of the lipid species, thereby inducing the phase segregation process to minimize the interfacial tension by forming fewer clusters of a given lipid type. For

sufficiently low interfacial tension, the thermal fluctuations of the mixed bilayer can overcome the energetically favorable interactions between the like lipid species to fragment the clusters. This process is countered by the minimization of the interfacial energy via the coalescence of clusters composed of a given type of lipids. We observe the cluster growth measurements to support our expectations, as shown in Figure 2.14 (f). These computations have used results from four simulations that begin from the same initial conditions but have different random seeds.

To capture the phase segregation process in the vesicle bilayer beginning from a completely mixed state, we generate a stable self-assembled mixed binary vesicle composed of a 1:1 mixture of two species of lipid molecules by effectively treating both the lipid species as the same species. The binary system can be assumed to behave as a single component system if the interaction energy parameters between the tail beads of the like and unlike lipid species are set to the same value ($\varepsilon_{t1\_t2} = 1.0$). We follow the same protocol as detailed earlier to generate a self-assembled binary vesicle (shown in Figure 2.15 (f)), and use the pair potential parameters that capture the distinct nature of each lipid type ($\varepsilon_{t1\_t2} = 0.75, 0.80, 0.85, 0.90, 0.95$). Beginning from a mixed configuration, the lipid molecules diffuse in the bilayer, collide and coalesce to form small domains, to minimize the energetically unfavorable interactions between the dissimilar lipid molecules. The small domains diffuse, collide and coalesce to grow in size and reduce the interfacial tension between the different phases in the hydrophobic region of the bilayer. We study the phase segregation process by computing the time evolution of the number of clusters composed of a single lipid species and the average cluster size which is defined by the number of molecules in a cluster. These

measurements are performed from the time we use the pair potential parameters that are

characteristic of the two distinct lipid types. The increasing dissimilarity between the
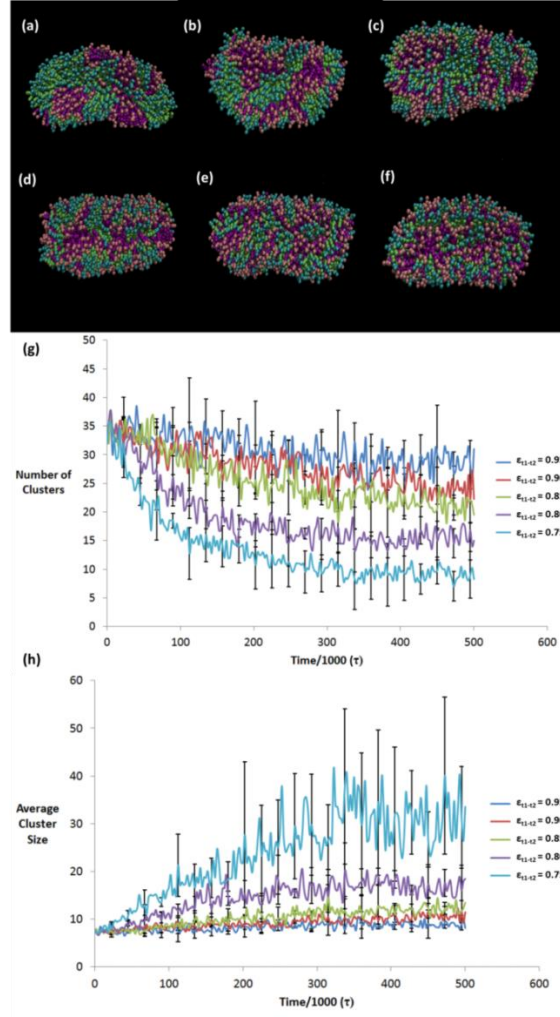
Figure 2.15: Images of the final configurations of the binary vesicle at t = 500,000τ for the inter-species inter-tail bead interaction parameters (a) ε_{t1-t2} = 0.75, (b) ε_{t1-t2} = 0.80, (c) ε_{t1-t2} = 0.85, (d) ε_{t1-t2} = 0.90, (e) ε_{t1-t2} = 0.95, and (f) ε_{t1-t2} = 1.00. All the simulations were run beginning from a completely mixed state. A plot of the time evolution of (g) the total number of clusters and (h) the average cluster size, for ε_{t1-t2} = 0.75, 0.80, 0.85, 0.90 and 0.95. The simulations have been run for a total time of 500,000τ beginning from a mixed state, and each data point has been averaged over four simulation runs using different random seeds.

lipid species drives the system to form fewer clusters of larger size. For example, we

observe 5 to 12 clusters in the final configurations of mixtures encompassing highly

dissimilar lipids (ε_{t1_t2} = 0.75.) Similarly for a lower degree of dissimilarity between the

lipid species, as captured by $\varepsilon_{t1\_t2} = 0.95$, we observe 26 to 36 clusters in the final configuration. We would like to emphasize that these cluster numbers correspond to the sum of the number of clusters in the inner and outer monolayer of the binary vesicle. We find large error bars are obtained for higher degree of dissimilarity between the tail beads of the two lipid species (see Figure 2.15 (h)) due to the presence of very few clusters with variation in the cluster sizes.

The time evolution of the coarsening dynamics can be used to compute the scaling exponents of the clustering process for the number of clusters (α) and the average size of a cluster (*β)* by using the relations 2.15 and 2.16 in demonstrated Section *2.3.2*. Our measurements of the scaling exponents ($\alpha = 0.50 \pm 0.07$ and $\beta = 0.54 \pm 0.05$) for a system which demonstrates macroscopic phase segregation ($\varepsilon_{t1\text{-}t2} = 0.75$, see Figure 2.15 (a)) are in good agreement with theoretical and simulation investigations on phase segregation in the absence of hydrodynamics.[23,155-157] We have provided the time evolution of the number of clusters and the average cluster size used to compute the exponents in Figure 2.16. The scaling exponents were computed using four simulations with different random seeds which were run for a duration of $1,000,000\tau$. We would like to note that for the range of parameters capturing the dissimilarities in the hydrocarbon tail groups, we have not observed any budding and vesiculation events.[14]

2.5.4 The effect of phase segregation on the structural characteristics of multi-component vesicle

The composition of the lipid bilayer is expected to influence its thickness and the average area per lipid. We used the same procedure as detailed earlier to measure the bilayer thickness
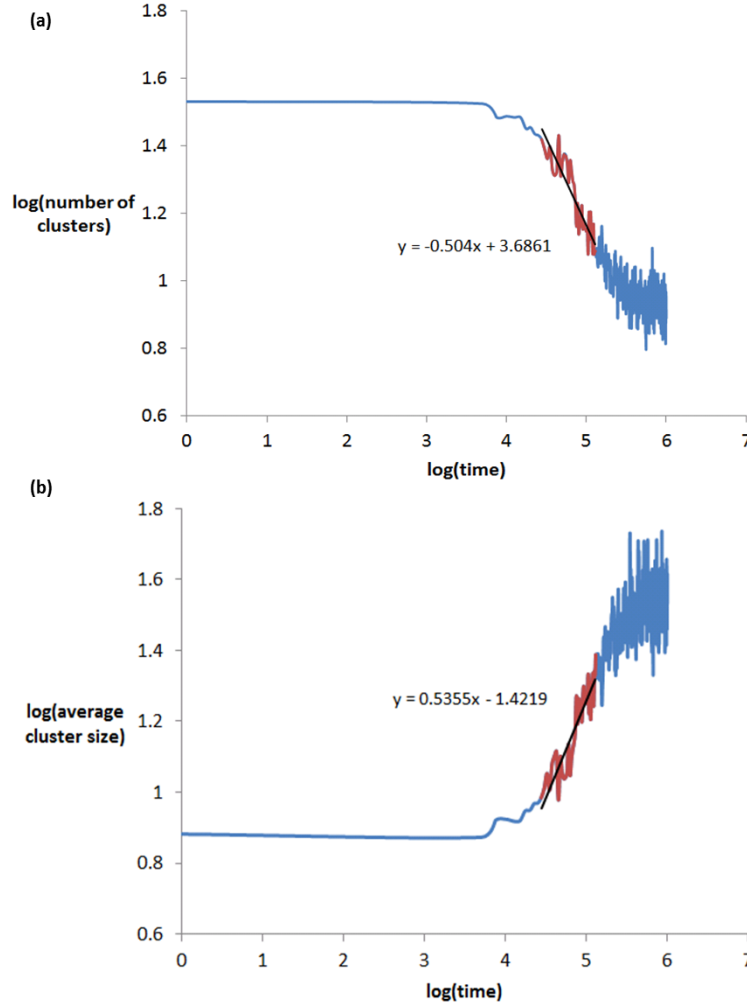
Figure 2.16: A log-log plot of the time evolution of (a) the total number of clusters and (b) the average cluster size of one type of lipid following the formation of a single stable vesicle ($\varepsilon_{t1\text{-}t2}$ = 0.75.) The simulations have been run for a time interval of 1,000,000τ from the mixed state and each data point has been averaged over four simulations which have the same initial conditions but different random seed. The scaling exponents are obtained by taking the slope of region shown in red. The trend lines and corresponding equations are shown on the figures.

for the binary vesicle, with the interaction parameter ε_{t1_t2} between the tail beads of the two lipid species ranging from 0.75 to 0.95. We do not observe any significant differences in the bilayer thickness values for intermediate to low degrees of dissimilarity in the tail groups of the lipid species. Our measurements show a slight decrease in the bilayer thickness (from 6.5 ± 0.2 σ to 6.4 ± 0.2 σ) for lower values of the tail interaction

parameter ε_{t1_t2}. We surmise that the slight increase in the bilayer thickness for lower degrees of dissimilarity between the tail groups could be an outcome of the tighter packing of the lipid molecules in the clusters formed in the bilayer. Tighter packing of the lipid molecules could result in less splaying and interdigitation of the lipid tails.

For the binary vesicle, we explore the role of the dissimilarity in the lipid hydrocarbon tail groups on the average area per lipid of the bilayer. We observe the area per lipid to be independent of the different interfacial energies between the distinct lipid species, and to be given by $2.4\pm0.1\ \sigma^2$. We surmise that with increasing dissimilarity between the lipid species, the tighter packing of the lipid molecules in the clusters is compensated by low packing density regions adjacent to the periphery of the clusters.

2.6   Chapter Conclusions

In summary, this chapter demonstrates the formation of single and binary lipid vesicles composed of two-tail amphiphilic lipid molecules and coarsening dynamics in a binary vesicle composed of phospholipid molecules with distinct chemical properties using two different simulation techniques: DPD and implicit solvent CG MD. In the early stages of the phase segregation process, the lipid molecules of the same species formed small clusters or domains via diffusion and collision to minimize their interfacial tension. For the latter stages, as the domains grow in size the clustering dynamics is determined by the diffusion and collision of clusters, and the evaporation of individual lipids from the boundaries of small clusters and their coalescence into bigger clusters. We observe the first stage for lipid mixtures with low interfacial energies or smaller degree of dissimilarity between the lipid species. For higher interfacial tension between the distinct lipid species, we demonstrate both stages through the characterization of the clustering

dynamics. Our measurements of the growth exponents using DPD and CG MD approaches for systems demonstrating macroscopic phase segregation agree with earlier numerical, theoretical and experimental studies.[4,14-17,22,23,155-157] We did not observe significant changes in the bilayer thickness and the area per lipid for different mixtures of lipid species in both techniques.

Via the use of DPD approach, the measurements of the line tension are found to be consistent with theoretical and experimental studies.[127,143] In addition, we observe the surface tension calculations to support our trends in the average area per lipid as function of the dissimilarity between the lipid species. Finally, the molecular chain stiffness of the hydrophobic tail groups was found to determine the shape of the binary vesicle, but had no noticeable effect on the phase segregation process.

Via the use of CG MD approach, the measurements of the bilayer thickness are found to be consistent with the experimental results. Our investigations on the effects of temperature on the physical properties of single component lipid vesicles were found to agree with experimental results. Contrary to expectations, our results demonstrated the bilayer thickness to be independent of temperature. A plausible explanation for this observation could be the use of stiff angle potentials that generates greater resistance to variations in the hydrocarbon tail conformations.

Chapter 3

The Design of Shape-Tunable Hairy Vesicles

The publications relevant to details of the discussions provided in this section:

- Aydin, F., Uppaladadium, G., Dutt, M., 2015, The design of shape-tunable hairy vesicles. Colloids and Surfaces B: Biointerfaces 128, 268-275.

- Aydin, F., Uppaladadium, G., Dutt, M., 2015, Harnessing nanoscale confinement to design sterically stable vesicles of specific shapes via self-assembly. J. Phys. Chem. B 119 (32), 10207-10215.

Contributions to this work:

1. Writing the computer programs to generate initial configurations for the simulations

2. Running the simulations

3. Writing the computer programs which are used to characterize the system

4. Performing the analysis and visualization of the system

5. Writing the manuscript

3.1   General overview

The stability and shape of biocompatible carriers such as lipid vesicles influence the effective delivery of therapeutic agents to target cell populations.[52] Sterically stable vesicles can be formed via the grafting of poly ethylene glycol (PEG) chains to the lipid head groups, and shape of the vesicles can be controlled by various intrinsic or extrinsic factors as previously explained in the *Introduction and Motivation* section. Experimental and computational studies have investigated the morphology of binary mixtures of PEGylated and non-PEGylated lipids;[51,52,54,56] and their dynamics and stability,[47,52,54] for species composed of the same hydrocarbon tail groups.[49,51,55] The aim of this chapter to design interfacially stable delivery vehicles or "hairy vesicles" composed of species with

different head group area and hydrocarbon tail groups with shapes conducive for unhindered passage through the circulation system and efficient internalization by desired cell populations. The specific system consists of a binary mixture of phospholipids and end-functionalized or hairy phospholipids. In this chapter, we identify the shape of the vesicles to be controlled by intrinsic factors such as the molecular geometry and the relative concentration of the molecular species or extrinsic factors such as the volume of the confinement. We have adopted a Molecular Dynamics (MD) -based mesoscopic simulation technique entitled Dissipative Particle Dynamics (DPD) (details given in Section 2.2.1) for the investigations presented in this chapter.

3.2   Modeling and parameterization of system components

3.2.1   Modeling in bulk conditions

The individual phospholipid molecules are represented by bead-spring models as shown in Figure 3.1 (a), and are modeled by a head group comprised of three hydrophilic beads and two hydrocarbon tails represented by three hydrophobic beads each. The hairy lipids, as shown in Figure 3.1 (b) – (c), encompass an identical architecture for the phospholipid, with hydrophilic tethers grafted to one of the hydrophilic head beads. The hairs or tethers are modeled by three and six hydrophilic beads. Bond and angle potential functional forms and parameters used for the lipids and tethers in this chapter are similar to those used in *Section 2.2.2*. Experimental examples of the tethers are polyethylene glycol chains with degrees of polymerization n given by 6 and 12. We select these values of the degree of polymerization to design sterically stabilize hairy vesicles with relatively short polyethylene glycol chains. In addition, earlier theoretical[158] and experimental

studies[159,160] show polymers with 6 to 17 EO units to be sufficiently effective for reducing the amount of protein adsorption on a surface at a certain surface coverage.
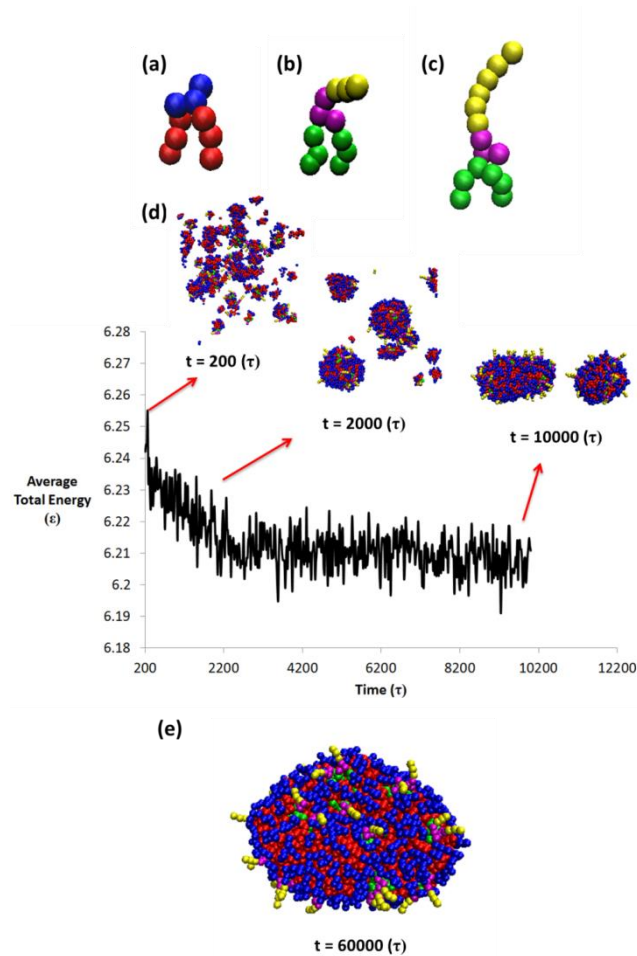
Figure 3.1: Images of the (a) amphiphilic phospholipid molecule, (b) hairy lipid molecule with a tether composed of three beads, and (c) hairy lipid molecule with a tether composed of six beads. (d) Time evolution of the average total energy of binary component hairy vesicle composed of phospholipids (90%) and hairy lipid molecules with tether composed of three beads (10%), and the corresponding images of the aggregation process. (e) An image of a stable self-assembled binary hairy vesicle composed of phospholipids (90%) and hairy lipid molecules with tethers composed of three beads (10%) at time t = 60,000τ

The soft repulsive pair potential parameters for the lipid molecule head and tail beads were selected to capture its amphiphilic nature. In addition, the hair beads are considered to be hydrophilic in nature. The soft repulsive interaction parameters between the tethers

(T), head (h), and tail (t) beads of lipid types 1 and 2, and the solvent (s) beads are assigned the following values (in units of $k_B T / r_c$): $a_{ss} = 25$, $a_{TT} = 25$, $a_{Ts} = 25$, $a_{h1h1} = 25$, $a_{t1t1} = 25$, $a_{h2h2} = 25$, $a_{t2t2} = 25$, $a_{h1t1} = 100$, $a_{h1s} = 25$, $a_{t1s} = 100$, $a_{h2t2} = 100$, $a_{h2s} = 25$, $a_{t2s} = 100$, $a_{h1T} = 25$, $a_{t1T} = 100$, $a_{h2T} = 25$, $a_{t2T} = 100$, $a_{h1t2} = 100$, $a_{h2t1} = 100$ and $a_{h1h2} = 25$. The values of the inter-specie tail-tail soft repulsive interaction parameter a_{t1t2} will span values ranging from 31 to 50, to mimic mixtures of amphiphilic species with different tail group properties. All the other parameters pertaining to DPD simulation technique, time, length and energy scales are obtained from *Section 2.2.2*.

3.2.2 Modeling under confinement

For the study of self-assembled hairy vesicle under confinement, the tethers of hairy lipids are modeled by three, five and six hydrophilic beads, which are experimentally corresponding to polyethylene glycol chains with degrees of polymerization n given by 6, 10 and 12.

Two planar walls parallel to xy-plane are used to confine the phospholipid and hairy lipid molecules, as shown in Figure 3.2 (a). The solvent molecules are both present in the region between and above the walls. Each wall consists of two layers of frozen DPD particles, with a thickness given by $0.85r_c$ and a total area of $1779r_c^2$. The beads comprising the walls are organized in a triangular lattice.
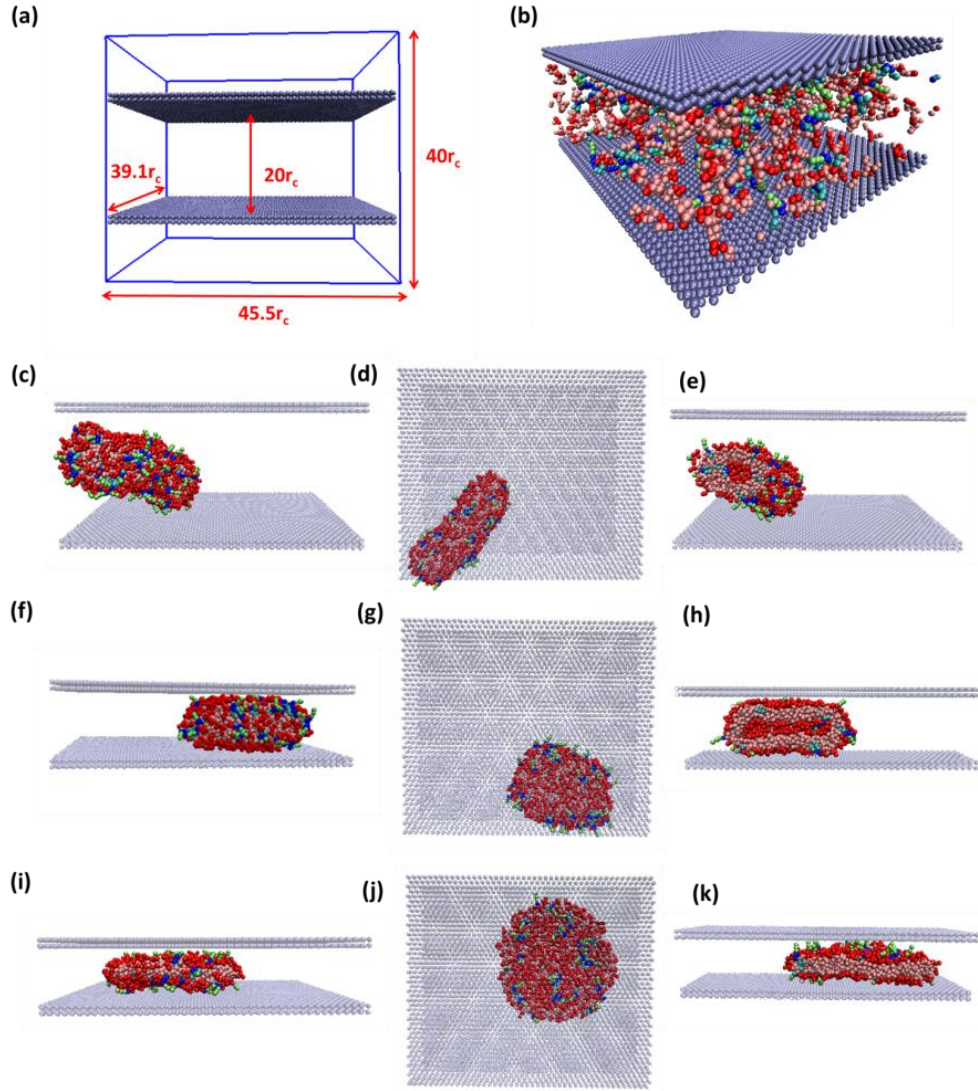
Figure 3.2: (a) The dimensions of the three-dimensional simulation box and channel used to confine the amphiphilic molecules. (b) The initial system configuration for a mixture of phospholipid and hairy lipid molecules in the confinement with a channel height of $15r_c$. (c) A side, (d) top and (e) cross-sectional view of a self-assembled prolate vesicle in the confinement with a channel height of $20r_c$ at time $t = 120,000\tau$. (f) A side, (g) top and (h) cross-sectional view of a self-assembled oblate vesicle in the confinement with a channel height of $10r_c$ at time $t = 120,000\tau$. (i) A side, (j) top and (k) cross-sectional view of a self-assembled bicelle in the confinement with a channel height of $8r_c$ at time $t = 120,000\tau$. The systems in (b) – (k) are composed of phospholipids (90%) and hairy lipid molecules with tethers composed of three beads (10%). The wall beads are reduced in size to enhance the top view of the different vesicle morphologies.

To prevent the adhesion of the vesicle onto the surface of the wall, the wall beads are modeled to have favorable interactions with the solvent molecules and unfavorable interactions with the phospholipids and hairy lipids. An experimental analogy of the wall

could be a hydrophilic surface with a charge distribution which results in unfavorable enthalpic interactions with the amphiphilic molecules.[161] Microfluidic channels can be made of materials such as glass, silicon, silicon oxide, and oxidized polystyrene. These materials can be sealed irreversibly with oxidized poly(dimethylsiloxane) (PDMS). The channel walls sealed with PDMS are found to be negatively charged in neutral and basic aqueous solutions.[162] It has been previously shown that vesicles composed of neutral and negatively charged lipid molecules, such as DOPC/DOPS, are not adsorbing onto the negatively charged silica surface.[163]

The soft repulsive interaction parameters between the tethers (T), head (h), and tail (t) beads of lipid types 1 and 2, the solvent (s) beads and the wall (w) beads are assigned the following values (in units of $k_B T / r_c$): $a_{ss} = 25$, $a_{TT} = 25$, $a_{Ts} = 25$, $a_{h1h1} = 25$, $a_{t1t1} = 25$, $a_{h2h2} = 25$, $a_{t2t2} = 25$, $a_{h1t1} = 100$, $a_{h1s} = 25$, $a_{t1s} = 100$, $a_{h2t2} = 100$, $a_{h2s} = 25$, $a_{t2s} = 100$, $a_{h1T} = 25$, $a_{t1T} = 100$, $a_{h2T} = 25$, $a_{t2T} = 100$, $a_{h1t2} = 100$, $a_{h2t1} = 100$, $a_{h1h2} = 25$, $a_{sw} = 25$, $a_{Tw} = 100$, $a_{h1w} = 100$, $a_{h2w} = 100$, $a_{t1w} = 100$ and $a_{t2w} = 100$.

3.3   Results and discussion

3.3.1 Self-assembly of hairy vesicle and characterization of the aggregation process

We design the hairy vesicles via self-assembly of the hairy and non-hairy amphiphilic species in a hydrophilic solvent. For the initial setup, a 9:1 mixture of phospholipids and short tether hairy lipids are randomly positioned in a simulation box of dimensions 30x30x30 r_c^3, along with the solvent beads. The simulation box has periodic boundaries along the three axes, and a 5.6% bead concentration of amphiphilic species. The unfavorable enthalpic interactions between the hydrophobic and hydrophilic species

drives the self-assembly of the two species to form a stable hairy vesicle, as shown in Figure 3.1. The simulations are run for a time interval of $60,000\tau$. In the early times of the aggregation process, the amphiphilic molecules diffuse in the solvent, collide and coalesce to form small size clusters. At later times, the self-assembly process proceeds via the diffusion, collision and coalescence of the small clusters to form medium to large clusters. We examine the role of the tether length and the relative concentrations of the two species on the aggregation dynamics. The relative concentration of the hairy lipids is set to 10 %, 20 %, 30 %, 40 % and 50% for the short tethers, and 10 % and 20 % for the long tethers. The characterization for each system uses particle trajectories from sixteen simulations which have identical initial conditions but different random seeds.

We characterize the dynamics of the aggregation process by computing the time evolution of the number of clusters and the average cluster size. A cluster is defined to be a group of non-solvent beads whose center-to-center distance is within their interaction cut-off range which is given by $r_c = 1$. Similarly, the average cluster size can be defined as the sum of the number of phospholipid and hairy lipid molecules divided by the total number of clusters. The aggregation process is determined by an interplay between the minimization of the unfavorable enthalpic interactions and maximization of the molecular configurational[164] and conformational entropy. One of the factors which control the equilibrium morphology of the aggregates is steric effects arising from the tethers. Increases in the steric effect results from the higher relative concentration of the hairy lipids or longer tethers which could prevent further aggregation of the smaller clusters. The steric hindrance promoted by the grafted tethers can be used to determine the size distribution of the liposomes which is important for the drug delivery applications.[49-51]

We would expect a decrease in the average cluster size with an increase in the relative concentration of the hairy lipid molecules and the tether length, as demonstrated in earlier experimental[50] and theoretical[52] studies. In addition, we surmise that the aggregate growth dynamics slows down with increase in the relative concentration of the hairy lipids and the tether chain length. Our expectations are supported by the characterization of the aggregation dynamics which is summarized in Table 3.1.

Tether length = 3		
Concentrations (%)	Scaling Exponent (α)	Scaling Exponent (β)
10	-0.84±0.07	0.85±0.07
20	-0.81±0.07	0.81±0.07
30	-0.78±0.04	0.78±0.04
40	-0.77±0.09	0.78±0.09
50	-0.75±0.05	0.76±0.06
Tether length = 6		
10	-0.80±0.07	0.81±0.07
20	-0.77±0.08	0.78±0.08

Table 3.1: Table of the scaling exponents α and β for the self-assembly of binary mixtures composed of different relative concentrations of hairy lipid and phospholipid molecules, and length of the tethers.

The time evolution of the coarsening dynamics during the self-assembly process can be used to estimate the scaling exponents of the number of clusters and the average cluster size. The scaling exponents based on number of clusters and the average size of

the clusters are respectively given by Equations 2.15 and 2.16 in *Section 2.3.2*. Our measurements demonstrate the growth dynamics to slow down with concentration of the hairy lipids and the tether length. One possible explanation for the slower growth dynamics is the higher drag forces experienced by the lipid molecules due to the additional chain-like functional groups which have favorable enthalpic interactions with the solvent.[165,166] We find our results to be in good agreement with investigations on the aggregation dynamics of phospholipid molecules and hairy nanotubes.[60] The time evolution of the aggregation dynamics is provided in Figure 3.3.
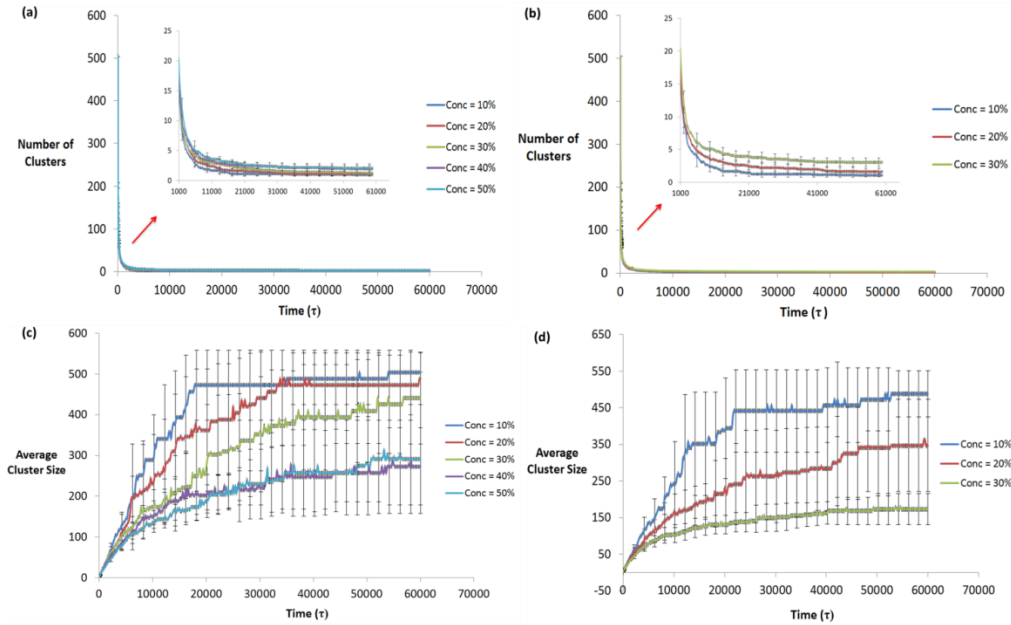
Figure 3.3: The time evolution (beginning from time t = 1,000τ) of the total number of clusters encompassing mixtures of phospholipids and hairy lipids with tethers composed of (a) three beads, for relative concentration of the hairy lipids given by 10%, 20%, 30%, 40% and 50%, and (b) six beads, for relative concentration of the hairy lipids given by 10% and 20%. The inset in (a) and (b) show the time evolution of the total number of clusters between the time interval t = 0 and t = 1,000τ. (c) The time evolution for the average cluster size for mixtures of phospholipids and hairy lipid molecules with the tethers composed of (c) three beads, for relative concentration of the hairy lipids given by 10%, 20%, 30%, 40% and 50%, and (d) six beads, for relative concentration of the hairy lipid given by 10% and 20%.

The average cluster size effectively provides the volume occupied by the non-solvent beads in a cluster as the density in the system is constant. The average linear size of the cluster becomes R(t) ~ $(< S(t) >)^{1/3}$ ~ $(t^{\beta})^{1/3}$ ~ $t^{1/3}$. A growth exponent of 1/3 is usually attributed to the evaporation-condensation effect.[4]

3.3.2 Effect of confinement on the aggregation dynamics

We examine the self-assembly of hairy and non-hairy amphiphilic species in a confined volume bound by two rectangular planar walls, located in a simulation box of dimensions 45.5x39.1x40 r_c^3 with periodic boundaries along the three axes. The walls span the x and y dimensions of the simulation box, and are located at an equidistance from the origin of the simulation box as shown in Figure 3.2 (a). The distance between their planar surfaces is varied from $8r_c$ to $20r_c$. The distance is chosen to effectively model different degrees of confinement. We use a 8:2, 8.5:1.5 and 9:1 binary mixture of phospholipid and hairy lipid molecules, with the hairs comprised of three, five and six beads. Each system consists of 504 molecules. This corresponds to 50 hairy lipid molecules and 454 phospholipids for a 9:1 mixture, 76 hairy lipid molecules and 428 phospholipids for a 8.5:1.5 mixture and 101 hairy lipid molecules and 403 phospholipids for a 8:2 mixture. We randomly place the molecules from each species in the confined volume between the two walls, as shown in Figure 3.2 (b). The solvent beads are both present between and above the two walls. We observe the formation of a single stable hairy vesicle via the self-assembly of the two species, as shown in Figure 3.2 (c). The simulations are run for a time interval of 120,000τ. We observe the amphiphilic molecules to aggregate to form small clusters at the initial stages of the self-assembly process, which is followed by the formation of medium to large-sized clusters via the

diffusion, collision and coalescence of the small clusters, similar to our observations in *Section 3.3.1*. We examine the role of the confining volume on the aggregation dynamics, for different hair lengths and relative concentrations of the two species. The relative concentration of the hairy lipids is set to 10 %, 15 % and 20 % for three different lengths of the hairs. The characterization presented in this section uses particle trajectories from four simulations which have identical initial conditions but different random seeds.

We characterize the aggregation dynamics during the self-assembly process by measuring the scaling exponents of the time evolution of the number of clusters by following similar procedure in *Section 3.3.1*. We observe the aggregation dynamics at the channel heights of $15r_c$ to be quite similar to the aggregation dynamics at the channel heights of $20r_c$, as shown in Figure 3.4.
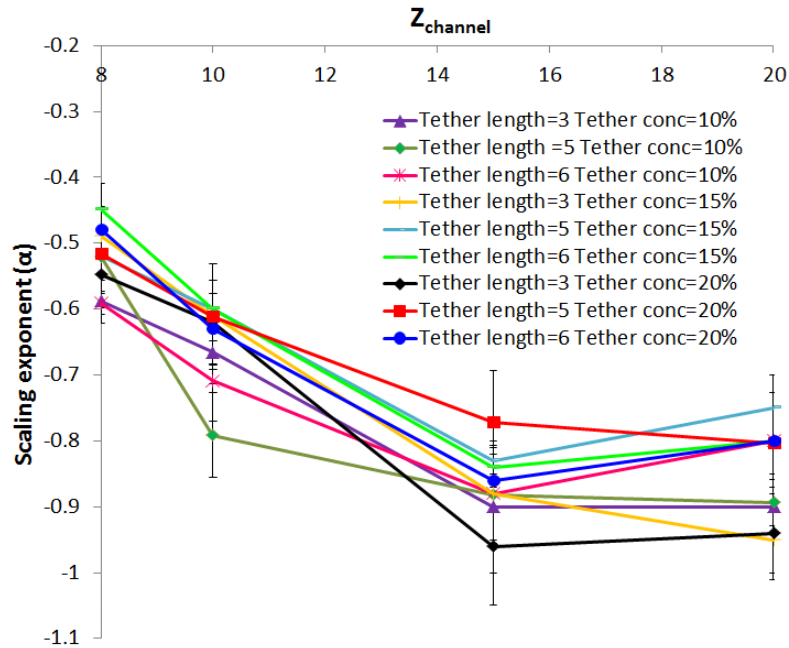
Figure 3.4: A plot of the scaling exponent α as a function of the distance between two planar surfaces for the self-assembly of binary mixtures composed of different relative concentrations of hairy lipid and phospholipid molecules, and length of the tethers.

We also calculate the scaling exponents for the self-assembly in bulk condition and find the results to be within 2 – 5 % of the scaling exponents at the channel height of $20r_c$. This implies that confinement at the channel heights of $20r_c$ and $15r_c$ have negligible effects on the aggregation dynamics. The effect of the confinement on the aggregation dynamics has been observed when the channel height is reduced to $10r_c$ and $8r_c$. As the degree of confinement increases, the aggregation dynamics slows down, as evidenced from Figure 3.4. We surmise that increasing the degree of confinement results in greater steric hindrance between the small clusters encompassing phospholipids and hairy lipids. In addition, we expect the aggregation dynamics to slow down with an increase in the length of the tethers due to the higher steric hindrance and hydrodynamic drag, as we observed in *Section 3.3.1*. We demonstrate that the growth dynamics slows down with an increase in the length of tethers when the distance between two planar surfaces is $15r_c$ and $20r_c$ in line with our expectations. However, we do not observe the length of tethers to influence the growth dynamics as the degree of confinement increases. Our measurements demonstrate the growth dynamics to change negligibly with the relative concentration of the hairy lipids. We also measure the constant C in the relation $N(t) \sim C\ t^{\alpha}$ in order to understand the effect of confinement on the aggregation dynamics at the initial stage of self-assembly process. The duration of initial stage of aggregation dynamics (prior to the measurement of scaling exponents) and the rate of aggregation dynamics at later stages (where the scaling exponent is measured) will affect the value of C. We expect a higher C value with a longer initial stage of aggregation dynamics where the individual molecules collide and coalescence to form small clusters. The value of C is also expected to increase with faster aggregation dynamics at later stages. As shown in

Figure 3.5, our measurements of the constant C as a function of the channel height and relative concentration of the hairy lipids for three different lengths of tethers are in agreement with our expectations. We demonstrate the value of C to increase with channel height and find its value in bulk conditions to be higher than that in the channel height of $20r_c$ (C ~ 21000 – 23000 for short tethers and C ~ 14000 - 16000 for long tethers).
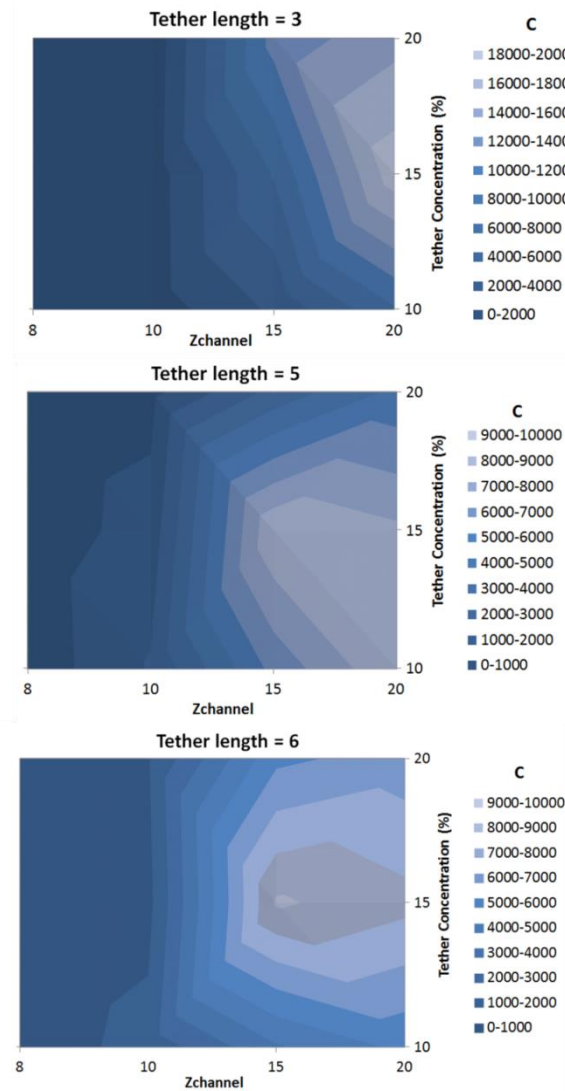
Figure 3.5: The constant C in the scaling exponent relation $N(t) \sim C\,t^\alpha$ as a function of the channel height and relative concentration of the hairy lipids for three different lengths of tethers.

We surmise that the reason for higher values of C with decreasing confinement is the longer duration of the aggregation dynamics at the initial stage as longer time intervals are required for collision and coalescence encounters between the individual molecules. In addition, the scaling exponents at the channel height of $15r_c$ and $20r_c$ as well as in bulk conditions are indistinguishable, and do not show any increasing trends. Our results also show that the value of C decreases with longer tethers due to the slowdown in the aggregation dynamics.

3.3.3 Distribution of tethers in the monolayers

To illustrate the organization of the two species in the hairy vesicle, we have examined the distribution of the hairy lipids in the monolayers. The molecules are more tightly packed in the inner monolayer as it occupies a spherical shell of smaller volume than the outer monolayer. The number of hairy molecules which could pack into each monolayer would depend upon the excluded volume of the tethers. For negligible differences in the excluded volume of the tethers in the two monolayers, we would expect fewer hairy lipid molecules in the inner monolayer. The excluded volume of a tether can be measured through the radius of gyration given by

$$R_g^2 = \frac{\left[\sum_{i=1,N+1}(\mathbf{r}_i - \mathbf{r}_{cm})^2\right]}{(N+1)} \tag{3.1}$$

where $\mathbf{r}_i$ is the position vector for the each tether bead, $\mathbf{r}_{cm}$ is the center-of-mass position of a tether and N is the number of beads per tether. We calculate the radius of gyration of each hair in a given monolayer after the formation of a single stable hairy vesicle, and average over all the hairs. Table 3.2 shows the distribution of the hairy lipids and the R_g of the tethers, in the two monolayers. For the short tethers, we report an asymmetric distribution of the hairy lipid molecules in the two monolayers, with negligible

differences in the radius of gyration. The asymmetry in the inter-monolayer distribution is found to become increasingly prominent with the length of the hairs. We also note that the radius of gyration for the longer tethers is higher in the outer than the inner monolayer. A possible explanation is that the excluded volume of the tethers decreases to pack into the inner cavity of the vesicle. Our findings are consistent with experimental[49] and theoretical[51,52] studies which have shown the asymmetric distribution of the

	Conc. (%)	Number of Hairy Lipids in the Inner Monolayer	Number of Hairy Lipids In the Outer Monolayer	Radius of Gyration in the Inner Monolayer (r_c)	Radius of Gyration In the Outer Monolayer (r_c)	Minimum Radius (r_c)	Maximum Radius (r_c)
Tether length = 3	10	10	40	0.37±0.02	0.37±0.02	4.3±0.2	10.7±0.5
	20	11	90	0.36±0.02	0.36±0.02	3.8±0.3	11.8±0.4
	30	15	137	0.36±0.01	0.36±0.01	4.0±0.2	11.3±0.3
	40	39	163	0.37±0.01	0.37±0.01	4.2±0.01	11.1±0.3
	50	50	202	0.37±0.01	0.37±0.01	4.7±0.2	10.3±0.3
Tether length =6	10	6	44	0.56±0.04	0.56±0.04	4.1±0.2	11.3±0.4
	20	4	97	0.54±0.03	0.54±0.03	4.1±0.2	11.3±0.3

Table 3.2: The number of hairy lipid molecules and the radius of gyration of the tethers present in the inner and outer monolayers of the self-assembled vesicles, and maximum and minimum distances from the center of mass of the vesicle to the lipid head groups in the outer monolayer for different relative concentrations of the hairy lipids and tether lengths.

molecular species in pegylated-lipid/phospholipid mixtures between the two monolayers due to the volumetrically constrained inner region of the lipid vesicular aggregates, and demonstrate the distribution to be optimal for spontaneously forming liposomes. We do not observe the radius of gyration of the tether and their distribution in the self-assembled hairy vesicles to be influenced by the confinement, as shown in Table 3.3 and Table 3.4.

	Conc. (%)	Radius of gyration in the inner monolayer (r_c)	Radius of gyration in the outer monolayer (r_c)
Tether length = 3 $Z_{channel} = 10r_c$	10	0.43±0.01	0.43±0.02
	15	0.41±0.02	0.42±0.01
	20	0.42±0.01	0.44±0.02
Tether length = 5 $Z_{channel} = 10r_c$	10	0.59±0.06	0.72±0.02
	15	0.59±0.06	0.73±0.02
	20	0.58±0.04	0.74±0.02
Tether length = 6 $Z_{channel} = 10r_c$	10	0.73±0.07	0.89±0.03
	15	0.72±0.07	0.87±0.03
Tether length = 3 $Z_{channel} = 15r_c$	10	0.40±0.03	0.41±0.02
	15	0.40±0.03	0.43±0.01
	20	0.42±0.02	0.42±0.01
Tether length = 5 $Z_{channel} = 15r_c$	10	0.63±0.04	0.71±0.03
	15	0.61±0.04	0.70±0.03
	20	0.64±0.04	0.71±0.02
Tether length = 6 $Z_{channel} = 15r_c$	10	0.74±0.06	0.84±0.04
	15	0.71±0.05	0.87±0.02
	20	0.74±0.04	0.84±0.04
Tether length = 3 $Z_{channel} = 20r_c$	10	0.40±0.01	0.43±0.01
	15	0.41±0.02	0.43±0.01
	20	0.40±0.01	0.42±0.01
Tether length = 5 $Z_{channel} = 20r_c$	10	0.64±0.05	0.71±0.03
	15	0.61±0.03	0.70±0.01
	20	0.64±0.04	0.70±0.02
Tether length = 6 $Z_{channel} = 20r_c$	10	0.78±0.04	0.83±0.02
	15	0.72±0.05	0.85±0.04
	20	0.72±0.05	0.84±0.02

Table 3.3: The radius of gyration of the tethers presents in the inner and outer monolayers of the self-assembled vesicles for different relative concentrations of the hairy lipids and tether lengths in the confinement with a channel height of $10r_c$, $15r_c$ and $20r_c$.

3.3.4 Intrinsic factors controlling shape of hairy vesicle

We investigate the dimensions of the vesicles through the minimum and maximum distances from its center of mass to the lipid head groups in the outer

monolayer, as shown in Table 3.2. The large difference in the minimum and maximum distances indicates that the self-assembled hairy vesicles favor an ellipsoidal morphology.

The local curvature of the hairy vesicle can be influenced by the molecular stiffness of the species, or their spatial distribution in the bilayer, specifically as one the species has a

	Conc. (%)	Number of tethers in the inner monolayer	Number of tethers in the outer monolayer
Tether length = 3 $Z_{channel}$ = 10r_c	10	7±1	43±1
	15	12±4	64±4
	20	17±1	84±1
Tether length = 5 $Z_{channel}$ = 10r_c	10	6	44
	15	6±1	70±1
	20	7	94
Tether length = 6 $Z_{channel}$ = 10r_c	10	5	45
	15	4	72
Tether length = 3 $Z_{channel}$ = 15r_c	10	5±1	45±1
	15	11±2	65±2
	20	14±2	87±2
Tether length = 5 $Z_{channel}$ = 15r_c	10	4±1	46±1
	15	7±3	69±3
	20	9+1	92+1
Tether length = 6 $Z_{channel}$ = 15r_c	10	2±1	48±1
	15	5±2	71±2
	20	4±1	97±1
Tether length = 3 $Z_{channel}$ = 20r_c	10	9±1	41±1
	15	10±2	66±2
	20	17±1	84±1
Tether length = 5 $Z_{channel}$ = 20r_c	10	5±1	45±1
	15	5±2	71±2
	20	9±2	92±2
Tether length = 6 $Z_{channel}$ = 20r_c	10	3±1	47±1
	15	8	68
	20	7±1	94±1

Table 3.4: The number of hairy lipid molecules present in the inner and outer monolayers of the self-assembled vesicles for different relative concentrations of the hairy lipids and tether lengths at different degrees of confinement.

curvature-inducing functional group.[57-59] We examine the role of these factors on the shape of the hairy vesicle for different relative concentrations of the hairy lipids and tether lengths. The angle potential constant of the hairy lipid is set to a value of 0, while that for the phospholipid tails is varied from 5 to 20. An experimental example of a

saturated lipid molecular species with stiffer tails is 1,2-distearoyl-sn-glycero-3-phosphocholine (18 carbons atoms[154]), where as DPPC molecule is a saturated phospholipid with 16 carbon atoms in each hydrocarbon tail. We begin with a hairy vesicle, and run the simulations for a time interval of 5000 τ using different values of K_{angle} for the phospholipid species. We anticipate the chain stiffness of the phospholipid molecules to control the packing of the molecules in the bilayers i.e., a higher molecular chain stiffness would result in tighter packing of the molecules. However with increasing concentrations of the hairy lipids, the excluded volume of the tethers disrupts the tighter packing of the hydrocarbon tails. Our results show the shape of the vesicle to transform from an ellipsoidal to a spherical shape with increasing chain stiffness of the non-hairy lipid species for low concentrations of the hairy lipids, as shown in Figure 3.6. The shape of the vesicle remains unchanged for higher concentrations of the hairy lipids. To develop a systematic parameterization of the shape transformation of the hairy vesicle, we have examined the role of factors such as the concentration of the hairy lipids (x_{tether}) and the molecular stiffness of the phospholipid tails (K_{angle}) on the interfacial line tension, the ratio of minimum to maximum distance of the head groups in the outer monolayer from the center of mass of the hairy vesicle (r_{min}/r_{max}), and the reduced volume (υ). We summarize our results in phase diagrams, as shown in Figure 3.7.

Figure 3.7 (a) and (b) show the reduced volume of the hairy vesicle as a function of the concentration of the hairy lipids and the chain stiffness of the phospholipid hydrocarbon tails, for tethers composed of three and six beads. The reduced volume is defined as[167]

$$\upsilon \equiv V / ((4\pi / 3)\, R^3) \qquad (3.2)$$

where V is the volume of the vesicle and R is the radius of the sphere with the same area

as the vesicle surface area given by

$$R \equiv (A / 4\pi)^{1/2} \qquad (3.3)$$
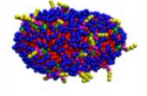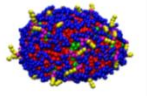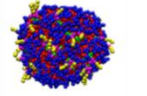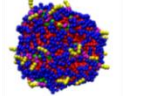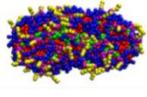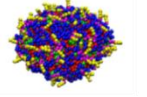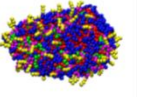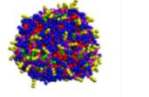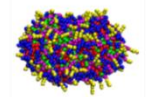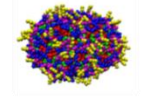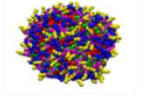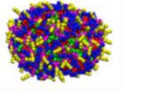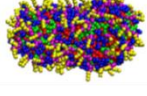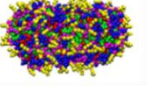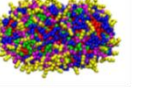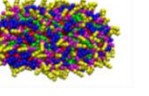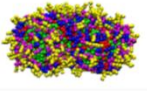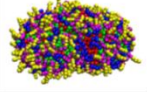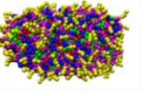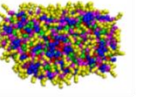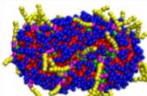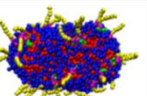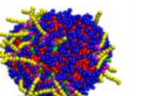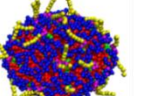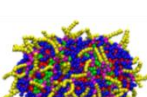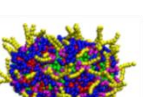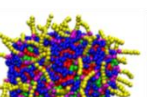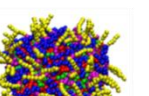
Tether Length	Relative Concentration of Tethers (%)	K_{angle}			
		5	10	15	20
Tether length of 3	10				
	20				
	30				
	40				
	50				
Tether length of 6	10				
	20				

Figure 3.6: Equilibrium configurations of the binary hairy vesicle composed of a range of concentrations of the hairy lipids (10% to 50% for the short tethers and 10% to 20% for the long tethers) at t = 5,000τ, for different hydrocarbon chain stiffness of the phospholipid specie given by K_{angle} = 5, 10, 15, and 20. The angle coefficient of the hairy lipid hydrocarbon chain was set at K_{angle} = 0.

The results are consistent with our observations presented in Figure 3.6; as we increase the chain stiffness at lower concentrations of the hairy lipids, the reduced volume approaches to 1.0 which corresponds to a more spherical morphology. We also observe similar trends in the phase diagram for r_{min}/r_{max} as a function of x_{tether} and K_{angle}, as shown in Figure 3.7 (c) and (d). These results indicate that the equilibrium morphology of the binary hairy vesicle is determined by an interplay between the packing of the molecular species and the excluded volume of the curvature-inducing groups. Our results indicate that the shape changes with the molecular stiffness of the phospholipid hydrocarbon tails to be independent of the tether length. We find our observations to be in good agreement with experimental results by Dobereiner et al.[39] where they use a vesicle composed of two lipid species which have different hydrocarbon tail lengths. As they increase the temperature, vesicles change their morphology to adopt a more elongated shape accompanied by a simultaneous decrease in the reduced volume from $\upsilon = 0.954$ to $\upsilon = 0.912$. The lipid molecules with shorter hydrocarbon tails will be more susceptible to changes in temperature, and thus have lower chain stiffness. This property is analogous to increasing the difference between the chain stiffness of the two lipid species in our model.

The phase diagrams that relate the composition of the tethers and the chain stiffness of the phospholipid tails to the interfacial line tension are shown in Figure 3.7 (e) and (f). The line tension can be measured through Equation 2.22. Our observations demonstrate the line tension to decrease with higher relative concentrations of the hairy lipids. A plausible explanation for this observation is the reduced interactions between neighboring hairy lipids due to the excluded volume of the tethers. We would like to note

that an earlier computational study[168] reported similar observations for a bicellar structure

composed of a mixture of zwitterionic and PEGylated lipid molecules.
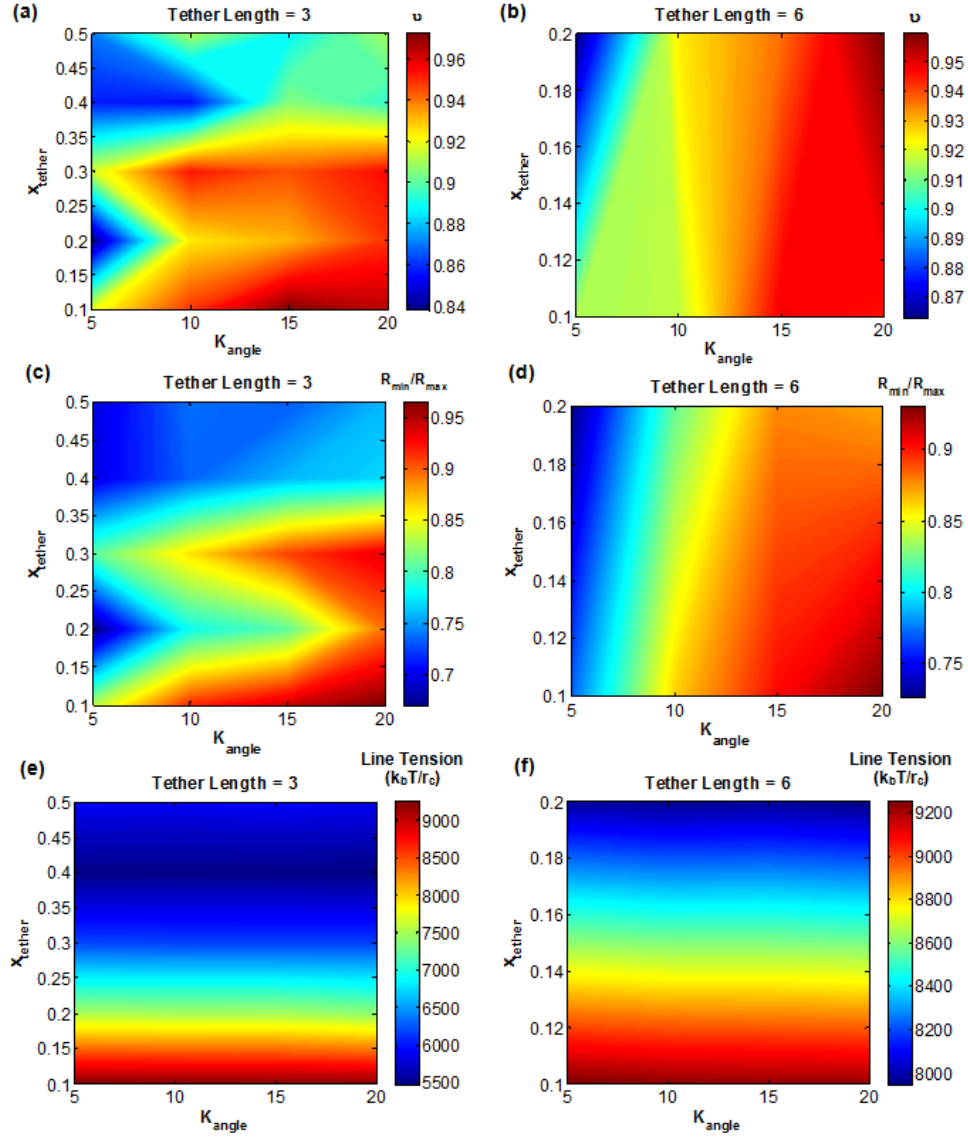
Figure 3.7: The phase diagram for the reduced volume of the self-assembled hairy vesicles with tethers composed of (a) three beads, (b) six beads as a function of x_{tether} and K_{angle}. The phase diagram for the r_{min}/r_{max} of the self-assembled hairy vesicles with tethers composed of (c) three beads, (d) six beads as a function of x_{tether} and K_{angle}. The phase diagram for the interfacial line tension of the self-assembled hairy vesicles with tethers composed of (e) three beads, (f) six beads as a function of x_{tether} and K_{angle}. x_{tether} is varied from 0.1 to 0.5 for lipid species with short tethers and from 0.1 to 0.2 for lipid species with long tethers. K_{angle} for the phospholipids is varied from 5 to 20.

The effect of the spatial distribution of the species on the shape can be queried by using suitable conditions, such as temperature, which promote macroscopic phase segregation[59] in the bilayer. We investigate the phase segregation within the bilayer of a hairy vesicle composed of equal concentrations of hairy lipids and phospholipids with different hydrocarbon tails. We begin with a stable pre-assembled mixed hairy vesicle in a 40 r_c x 40 r_c x 40 r_c periodic simulation box composed of 1178 molecules. The differences in the hydrocarbon tail groups such as the length is reflected in the transition temperature for the lipid molecules, and can be effectively captured by the tail-tail interaction parameter a_{t1t2}. The range of the tail-tail interaction parameter a_{t1t2} used in this investigation (31 to 50) has been demonstrated to promote macroscopic phase segregation in a binary phospholipid vesicle, and can model differences in the length of the hydrocarbon tails of the molecules. The simulations have been run for a time interval of 10,000τ. The characterization has been performed using particle trajectories from four simulations that begin from the same initial conditions but have different random seeds.

To demonstrate that the latter dynamics of the phase separation process is determined by the evaporation-condensation effect,[4,140] we measure the scaling exponents of the time evolution of the number of clusters and the average cluster, as shown in Figure 3.8. A cluster is composed of hairy lipid molecules whose head group beads are within interaction range from each other. Table 3.5 shows the cluster growth dynamics to become faster with increasing dissimilarity between the hydrocarbon tail groups and for shorter tethers. We surmise that longer tethers experience greater drag which results in a slow down in the domain growth dynamics. The average radius of a domain can be shown to be given by the following relation $R(t) \propto t^{\beta/2}$.

The higher excluded volume of the longer tethers, as indicated in Table 3.2, could sufficiently increase the separation between neighboring hairy lipids so that the corresponding head groups are outside the interaction range from each other.
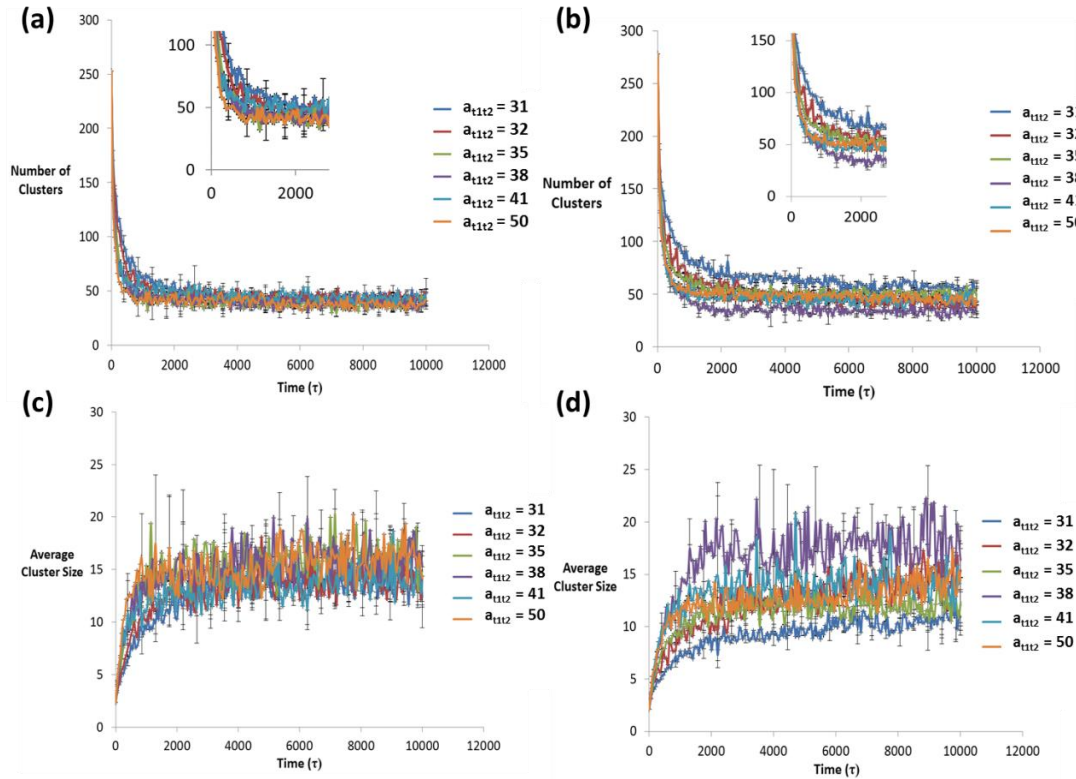
Figure 3.8: A plot of the time evolution of the total number of clusters of the hairy lipid molecules with (a) short and (b) long tethers. A plot of the time evolution for the average size of the clusters composed of hairy lipids with (c) short and (d) long tethers. The simulations have been run for a time interval of 10,000τ, and each data point has been averaged over four simulations using identical initial conditions but different random seeds. All the simulations start from a completely mixed state. The inter-specie tail-tail soft repulsive interaction parameter was set at the following values: a_{t1t2} = 31, 32, 35, 38, 41, and 50.

We find the area per hairy lipid increases, respectively, by 30% and 50% for the short and long tethers (as shown in Table 3.6), in comparison to the area per phospholipid which is calculated to be 1.12 r_c^2. The increase in the area per molecule with the inclusion of the PEGylated moeities has also been reported by earlier experimental[54] and computational

studies.[168] We would like to note that measurements of the radius of gyration of the short

and long hairs for the

a_{ij} (k_bT/r_c)	Scaling Exponent (α)	Scaling Exponent (β)
Tether length = 3		
31	-0.45	0.46
32	-0.50	0.50
35	-0.50	0.52
38	-0.51	0.52
41	-0.51	0.48
50	-0.51	0.54
Tether length = 6		
31	-0.33	0.34
32	-0.33	0.34
35	-0.36	0.37
38	-0.46	0.46
41	-0.47	0.48
50	-0.47	0.48

Table 3.5: Table of the scaling exponents α and β for the coarsening dynamics in the bilayer of a binary hairy vesicle induced by the dissimilarity of the hydrocarbon tail groups of the phospholipid and hairy lipids, for different tether lengths.

outer monolayers are respectively given by $0.450\pm0.002r_c$, and $0.925\pm0.003r_c$, and is not sensitive to the distinction in the hydrocarbon tail groups. This observation would also hold for the area occupied by the hairy lipids.

	a_{t1t2} (k_bT/r_c)	Area Per Hairy Lipid Molecule in the Inner Monolayer (r_c^2)	Area Per Hairy Lipid Molecule In the Outer Monolayer (r_c^2)
Tether length = 3	31	1.2 ± 0.1	1.7 ± 0.1
	32	1.2 ± 0.1	1.8 ± 0.1
	35	1.3 ± 0.1	1.8 ± 0.2
	38	1.2 ± 0.1	1.8 ± 0.2
	41	1.3 ± 0.2	1.8 ± 0.2
	50	1.3 ± 0.2	1.8 ± 0.2
Tether length = 6	31	1.5 ± 0.1	2.0 ± 0.1
	32	1.4 ± 0.2	1.9 ± 0.1
	35	1.5 ± 0.1	2.0 ± 0.1
	38	1.4 ± 0.1	1.9 ± 0.1
	41	1.5 ± 0.2	2.0 ± 0.2
	50	1.5 ± 0.2	2.0 ± 0.2

Table 3.6: The area per hairy lipid for tethers composed of three and six beads in the inner and outer monolayers of the binary hairy vesicle as a function of the inter-specie tail-tail soft repulsive interaction parameters a_{t1t2}. The simulations have been run for a total time of 10,000 τ and each data point has been averaged over four simulation runs using identical initial conditions but different random seeds.

To capture the shape change for a phase segregated hairy vesicle, we measure the maximum and minimum distance of the lipid head groups from the center of mass of the vesicle, as shown in Figure 3.9 (e). Our results demonstrate the shape of the vesicle to transform from a spherical to an ellipsoidal shape with increasing dissimilarity between the hydrocarbon tail groups, as shown in Figure 3.9. The shape change for a range binary mixtures composed of different phospholipid and hairy lipid species can be related to thermodynamic properties such as the interfacial line tension. The measurements in Figure 3.9 (f) were performed on particle trajectories beginning from $10,000\tau$, for a total duration of $5,000\tau$. Each data point has been averaged over time and the total number of beads in the system. The line tension is observed to increase with the degree of distinction between the hydrocarbon tails and the length of the tethers, and influences the shape of the phase segregated hairy vesicle.

3.3.5 Effect of confinement on the shape of hairy vesicle

Our measurements of the reduced volume for hairy vesicles under confinement, as shown in Figure 3.10, demonstrate the shapes of the vesicles to deviate significantly from a spherical morphology ($\upsilon = 1$) and adopt either prolate and oblate shapes or bicelles depending on the degree of confinement during the self-assembly of the hairy vesicles. The results for the tether concentration of 15% are not shown in the figure as they are very similar to the results for the tether concentrations of 10% and 20%. Our findings show that the self-assembly of the phospholipid and hairy lipid molecules favors the formation of cigar-shaped (prolate) vesicles for various relative concentrations of the hairy lipids and the length of the hairs when the distance between the planar surfaces is set to $15r_c$ or $20r_c$. The corresponding reduced volumes of prolate vesicles are found to be

within the range of 0.7-0.8. The side, top and cross-sectional views of the prolate vesicles are shown in Figure 3.2 (c) – (e), respectively.

To understand the role of volumetric confinement on the reduced volume, we examine the self-assembly of phospholipid and hairy lipid molecules in the absence of the confining walls (by using the same relative concentrations of the hairy lipids and the length of the hairs).
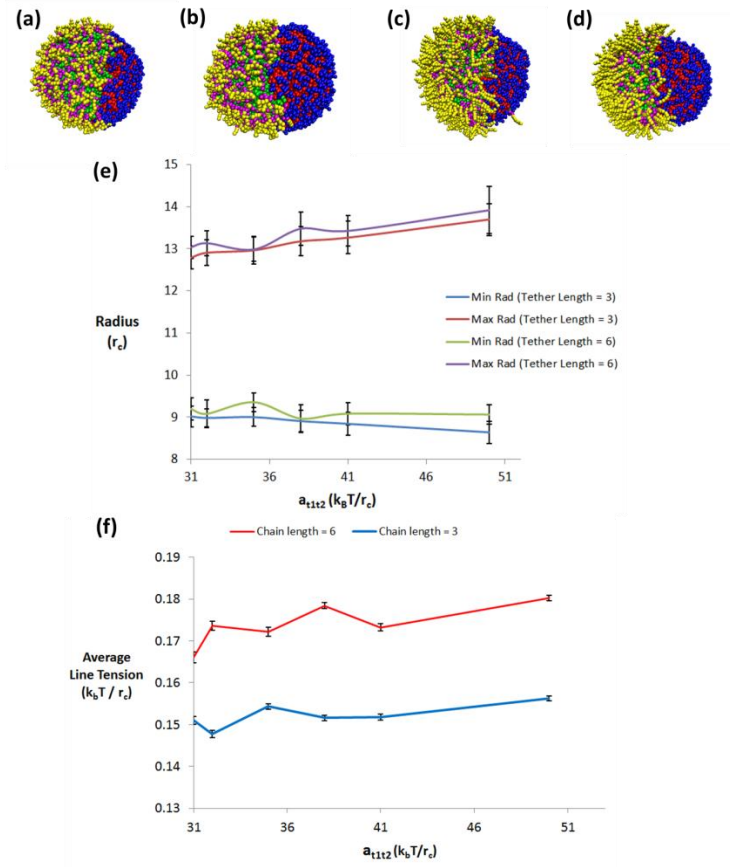
Figure 3.9: Final configurations of the binary hairy vesicle at time t = 10,000τ for different soft repulsive interaction parameters between the tail groups of the phospholipids and hairy lipids given by (a) a_{t1t2} = 31, (b) a_{t1t2} = 50, and (c) a_{t1t2} = 31, (d) a_{t1t2} = 50, respectively for short and long tethers. Plots of the (e) minimum and maximum distance of the lipid head beads from the COM of vesicle, and (f) average line tension as function of a_{t1t2}.
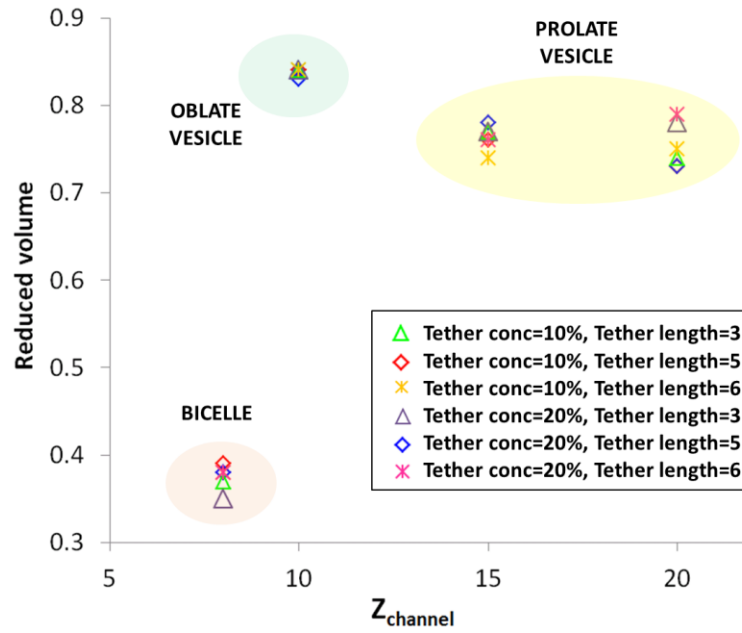
Figure 3.10: A plot of the reduced volume of the self-assembled hairy vesicles as a function of the distance between two planar surfaces for different relative concentrations of the hairy lipids and tether lengths.

Our results for the reduced volume, as shown in Table 3.7, indicate the formation of hairy vesicles which have a very similar morphology to the vesicles in a confined region with heights of $15r_c$ and $20r_c$. We conclude the self-assembled morphology to be similar to that obtained in the bulk phase at these degrees of confinement. In order to increase the effect

	Conc. (%)	Reduced volume (υ)	x-axis (r_c)	y-axis (r_c)	z-axis (r_c)
Tether length = 3 No wall	10	0.76±0.05	16±2	5.5±0.5	4.5±0.3
	15	0.74±0.03	16±1	5.5±0.5	4.4±0.2
	20	0.81±0.07	14±3	6±1	4.6±0.3
Tether length = 5 No wall	10	0.75±0.06	17±2	5.5±0.6	4.3±0.3
Tether length = 6 No wall	10	0.75±0.06	16±2	5.6±0.6	4.4±0.4

Table 3.7: The reduced volume and the x, y, z - principal axes of the self-assembled hairy vesicles for different relative concentrations of the hairy lipids and tether lengths in bulk conditions (without walls).

of the confinement, we set the distance between the planar surfaces to $10r_c$, and repeat the simulations examining the self-assembly of the phospholipid and hairy lipid molecules. An increase in the degree of confinement is found to favor the formation of disc-shaped (oblate) hairy vesicles, as captured by the side, top and cross-sectional views respectively in Figure 3.2 (f) – (h). The corresponding reduced volumes of oblate vesicles are found to be within the range of 0.8-0.9. This result indicates a shape transformation of the hairy vesicles from prolate to oblate shape with an increase in the degree of confinement. We surmise that for sufficiently large distances between the planar walls, the prolate shape of the vesicle allows the self-assembled aggregate to maximize its rotational entropy about principal axes which are parallel or perpendicular to the planar walls. With a reduction in the separation distance between the walls, the vesicle maximizes its rotational entropy by adopting an oblate shape which enables rotation about a principal axes perpendicular to the plane of walls. The shape transformation from a prolate to an oblate shape has been theoretically shown in a previous study[169] via the use of area difference elasticity model (ADE). Helal et al.[169] investigated the stability of prolate and oblate shaped vesicles in a two-dimensional slit or one-dimensional cylinder by varying the degree of confinement. Although the reduced volumes for the prolate shaped vesicles are in good agreement with the model ($\upsilon_{prolate} > 0.65$); the reduced volumes for the oblate vesicles was measured to be higher than those for prolate vesicles, contrary to their findings ($\upsilon_{oblate} < 0.65$). This might be due to the fact that the self-assembly of vesicles, under the confinement, did not preserve the total volume or area of the membrane on account of the inter-monolayer asymmetric distribution of the hairy lipids, as shown in Table 3.8.

	Conc. (%)	Surface area (r_c^2)	Enclosed volume (r_c^3)
Tether length = 3 $Z_{channel}$ = 10r_c	10	690±7	1430±10
	20	694±9	1440±20
Tether length = 3 $Z_{channel}$ = 15r_c	10	730±20	1500±40
	20	760±30	1530±50
Tether length = 3 $Z_{channel}$ = 20r_c	10	800±40	1590±60
	20	760±30	1530±50
Tether length = 3 Without walls	10	790±30	1570±60
	20	780±30	1580±50
Tether length = 6 $Z_{channel}$ = 10r_c	10	700±10	1440±20
Tether length = 6 $Z_{channel}$ = 15r_c	10	810±30	1560±60
	20	780±30	1550±50
Tether length = 6 $Z_{channel}$ = 20r_c	10	790±40	1570±50
	20	750±30	1530±50
Tether length = 6 Without walls	10	830±30	1640±60

Table 3.8: The total outer surface area and enclosed volume of the self-assembled hairy vesicles for different relative concentrations of the hairy lipids and tether lengths at different degrees of confinement.

We would like to note that Helal et al. use preconfigured vesicle shapes, and fixed enclosed volume and total area of the membrane. In addition they do not include the thermal fluctuations of the bilayer in their model. Further reduction in the separation distance between the planar walls (to 8r_c) results in a stable bicellar morphology, as captured by the side, top and cross-sectional views respectively in Figure 3.2 (i) − (k). The corresponding reduced volumes of bicelles are found to be within the range of 0.3-0.4. These results demonstrate that the morphology of the self-assembled vesicles can be finely tuned by harnessing suitable confinement conditions. These findings enable the design of stable hairy vesicles with a well-defined shape and low polydispersity for applications such as liposomal drug delivery and gene therapy.[170,171]

The shape of the vesicle can also be characterized through the measurement of the principal axes[5] of the resulting aggregates and the projections along the axes (through the mapping of the coordinates of the head beads in the outer monolayer onto an ellipsoid, as shown in Figure 3.11). In order to find the principal axes, the algebraic expression of
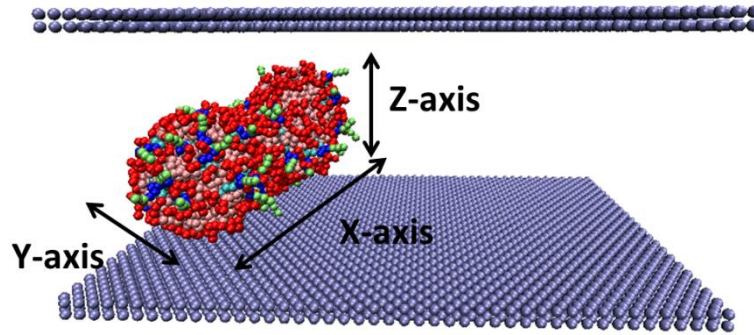
Figure 3.11: An image that shows the principal axes (x, y and z) of the self-assembled binary hairy vesicle with a prolate morphology.

the ellipsoid is formed in the matrix of the quadratic form. The ellipsoid is centered in the Cartesian coordinate system by first finding its center and then forming its corresponding translation matrix. The translation matrix can be used to determine the principal axes by solving the eigenvalue problem. We compute the projections along the principal axes of the self-assembled hairy vesicles both with and without volumetric confinement, for different relative concentrations of the hairy lipids, the length of the hairs and the distance between the surfaces of the walls. These results are shown in Table 3.7 (for bulk conditions) and in Table 3.9 (for channel heights of $8r_c$, $10r_c$, $15r_c$ and $20r_c$). Our measurements of the principal axes are consistent with our previous observations; the self-assembled hairy vesicles in the bulk and in channels of heights $15r_c$ and $20r_c$ have prolate shapes, whereas the self-assembled hairy vesicles in a channel of height of $10r_c$

have oblate shapes. In addition, the self-assembled bicelles in a channel height of $8r_c$ have disc-shaped morphology but they have longer x and y dimensions and shorter z dimension, compared to the dimensions of oblate vesicles present in a channel of height of $10r_c$. As shown in Table 3.7 and Table 3.9, the least variation in the vesicle dimensions is observed along the z-axis which coincides with the direction of confinement. We find that shape fluctuations due to the hydrodynamics and thermal fluctuations can be reduced by increasing the degree of confinement as is evidenced from the standard deviations of the projections along the principal axes.

	Conc. (%)	x-axis (r_c)	y-axis (r_c)	z-axis (r_c)
Tether length = 3	10	16±1	13±1	2.0±0.1
$Z_{channel}$ = $8r_c$	15	16±1	14±1	2.0±0.1
	20	16±1	14±1	2.0±0.1
Tether length = 5	10	15±1	13±1	2.1±0.2
$Z_{channel}$ = $8r_c$	15	15±1	13±1	2.1±0.2
	20	15±1	13±1	2.1±0.1
Tether length = 6	10	15±1	13±1	2.1±0.1
$Z_{channel}$ = $8r_c$	15	15±1	13±1	2.1±0.2
	20	15±1	13±1	2.1±0.2
Tether length = 3	10	10±1	8.1±0.4	4.2±0.1
$Z_{channel}$ = $10r_c$	15	11±2	7±1	4.2±0.1
	20	10±1	8.2±0.4	4.2±0.1
Tether length = 5	10	10±1	8.0±0.4	4.2±0.1
$Z_{channel}$ = $10r_c$	15	10±1	8.0±0.5	4.2±0.1
	20	11±1	7.8±0.6	4.2±0.1
Tether length = 6	10	10±1	7.9±0.5	4.2±0.1
$Z_{channel}$ = $10r_c$	15	10±1	8.1±0.4	4.2±0.1
Tether length = 3	10	15±1	5.4±0.3	4.5±0.2
$Z_{channel}$ = $15r_c$	15	15±1	5.4±0.3	4.5±0.2
	20	15±1	5.4±0.3	4.6±0.2
Tether length = 5	10	15±1	5.4±0.3	4.5±0.2
$Z_{channel}$ = $15r_c$	15	16±1	5.3±0.3	4.4±0.2
	20	15±1	5.4±0.3	4.6±0.2
Tether length = 6	10	16±1	5.3±0.4	4.3±0.1
$Z_{channel}$ = $15r_c$	15	16±1	5.3±0.3	4.4±0.2
	20	15±1	5.4±0.3	4.5±0.1
Tether length = 3	10	16±1	5.4±0.4	4.4±0.2
$Z_{channel}$ = $20r_c$	15	16±1	5.4±0.4	4.4±0.2
	20	15±1	5.4±0.3	4.6±0.2
Tether length = 5	10	16±2	5.3±0.4	4.4±0.2
$Z_{channel}$ = $20r_c$	15	16±2	5.4±0.4	4.4±0.2
	20	16±1	5.4±0.4	4.4±0.2
Tether length = 6	10	16±1	5.4±0.4	4.4±0.2
$Z_{channel}$ = $20r_c$	15	14±1	5.6±0.2	4.7±0.1
	20	14±1	5.5±0.3	4.7±0.2

Table 3.9: The x, y, z - principal axes of the self-assembled hairy vesicles for different relative concentrations of the hairy lipids and tether lengths in the confinement with a channel height of $8r_c$, $10r_c$, $15r_c$ and $20r_c$.

The interfacial line tension measurements (shown in Figure 3.12) on self-assembled hairy vesicle under confinement demonstrate a decrease in line tension with higher relative concentrations of the hairy lipids, similar to our observations in Section 3.3.4 for the bulk conditions. In addition, we do not observe the line tension of the self-assembled hairy vesicles to be influenced by the height of the confinement.
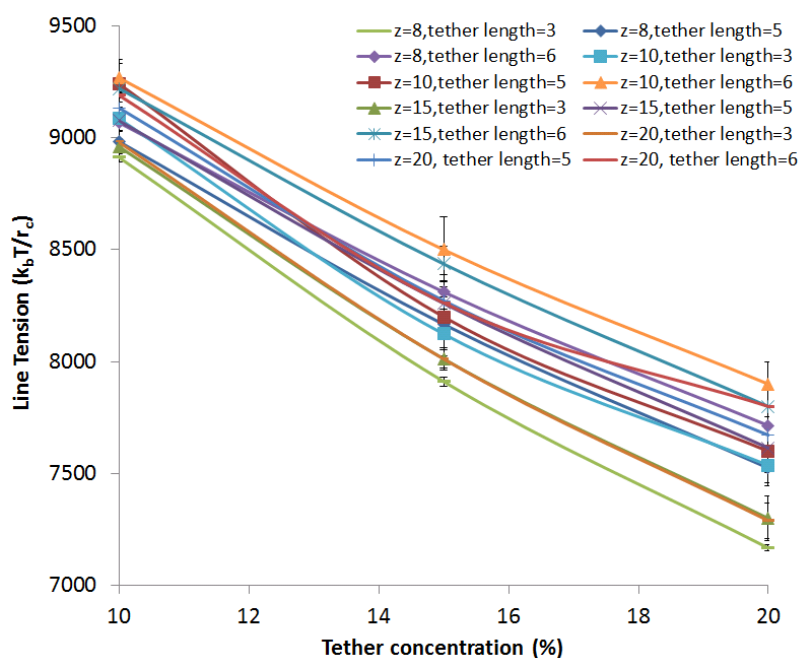
Figure 3.12: A plot of interfacial line tension of the self-assembled hairy vesicles as a function of tether concentration for different distances between two planar surfaces and different tether lengths.

3.4   Chapter conclusions

In this chapter, we have demonstrated the design of a stable hairy vesicle composed of phospholipid and pegylated lipid molecules via self-assembly, and identified the factors which control the shape of the vesicle. Our results demonstrate the relative concentration of the end-functionalized lipids, tether length, molecular stiffness, the degree of dissimilarity in the hydrocarbon tail groups and the volume of confinement

to determine the shape of the hairy vesicle. The asymmetric distribution of the hairy lipid molecules in the monolayers of the self-assembled hairy vesicles is caused by the excluded volume of the tethers, and is in good agreement with theoretical and experimental results.[49,51] The shape of the hairy vesicle evolves from an ellipsoidal to a spherical morphology with increasing hydrocarbon tail stiffness of the phospholipid species, and the equilibrium morphology is found to depend upon the interplay between the packing of the molecular species and the excluded volume of the tethers. We have demonstrated a good correspondence between our results for the shape transformation of the hairy vesicles and experimental studies.[39-41] In addition, as the degree of confinement increases, the prolate shaped vesicles transform into an oblate shape for different relative concentrations of the hairy lipids and the length of the hairs. We find our observations to be in good agreement with earlier theoretical investigations that demonstrate oblate vesicles to be increasingly favored over prolate vesicles as the degree of confinement increases.[169] For a higher degree of confinement, we report the formation of stable bicellar structures.

Chapter 4

Modeling Interactions between Patchy Nanoparticles and Multi-component Nanostructured Soft Biomaterials

The publications relevant to details of the discussions provided in this section:

- Aydin, F., Uppaladadium, G., Dutt, M., Controlling Interactions between Patchy Nanoparticles and Vesicles via Steric Stabilization. Submitted.

- Aydin, F., Dutt, M., Modeling interactions between charged nanoparticles and multi-component vesicles. In preparation.

Contributions to this work:

- Running the simulations

- Writing the computer programs which are used to characterize the system

- Performing the analysis and visualization of the system

- Writing the manuscript

- Implementing long range electrostatic interactions into the implicit solvent CG MD model using Large-scale Atomic/Molecular Massively Parallel Simulator (LAMMPS).

4.1 General overview

The study of interactions between macromolecules and surfaces has attracted increasing attention in recent years due to their role in various biological applications such as design of efficient antifouling surfaces[172], biomedical implants[173] and drug delivery vehicles such as stable liposomes.[174] Biocompatible materials are designed so as to completely eliminate or significantly reduce the adsorption of proteins onto a surface in order to avoid surface-induced thrombosis.[158,175] One of the methods to prevent protein adsorption is through the grafting of polymer chains on to a surface by mimicking the protective polysaccharide layer on cell membranes.[174] This approach has been used in liposomal therapeutic formulations to increase circulation time and steric stability.[47-51] Experimental studies include investigations of the interactions of PEGylated vesicles with plasma proteins like fibrinogen, hemoglobin[176,177] or cytochrome c.[178]

The study of interactions between various biomolecules can give us new insight into the design of biomaterials and biosensors as well as understanding the underlying

mechanisms of cellular activities.[179] For example, electrostatic interactions between charged nanoparticles and cell mimetic membranes can be used to induce reorganization of the molecules in the bilayer. This will enable us to obtain biomaterials with different functional properties, varying from one spot to another.

The interactions between NPs and biomembranes have been studied by using various computational techniques including the Molecular Dynamics (MD) simulation method[180-185]. We have adopted Dissipative Particle Dynamics (DPD) approach to understand the mechanisms and factors underlying the interaction between patchy nanoparticles (NPs) and hairy vesicles. In addition, we have used implicit solvent coarse-grained molecular dynamics approach to investigate the effects of nanoparticle adsorption on the surface reconstruction of multicomponent vesicle.

4.2 Modeling interactions between patchy nanoparticles and hairy vesicles via dissipative particle dynamics simulation technique

4.2.1 Modeling and parameterization of system components

Our system consists of a stable hairy vesicle composed of phospholipid and hairy lipid molecules, and patchy NPs in a hydrophilic solvent. We use the same models for phospholipids and hairy lipid molecules described in *Chapter 3*.
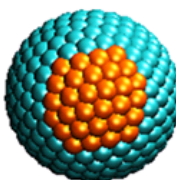
Figure 4.1: Spherical patchy NP with a radius of $2.25r_c$

The NPs, shown in Figure 4.1, are hollow spheres composed of 312 hydrophilic beads with a patch covering 20% of the surface. The patch is set to have highly favorable enthalpic interactions with the hydrophilic head group of the phospholipid molecules, or the tethers. The distance between the centers of neighboring beads of the NP is set to $0.5rc$. Three different sizes of NPs are used with the following radii: $0.75r_c$ (small), $1.50r_c$ (medium) and $2.25r_c$ (large) that correspond respectively to 50%, 100% and 150% of the length of the long tethers. Experimental counterparts of the NPs can be proteins or drug molecules with moieties grafted on to its surface.[176] We model the complex topography and asymmetric charge distribution of NPs via patchy spherical counterparts.[186]

The soft repulsive interaction parameters between the patch (p), non-patch (n) beads of the NPs, tether (T), head (h), and tail (t) beads of lipid types 1 and 2, and the solvent (s) beads are assigned the values (in units of $k_B T / r_c$): $a_{ss} = 25$, $a_{ps} = 25$, $a_{ns} = 25$, $a_{pp} = 50$, $a_{nn} = 50$, $a_{nT} = 25$, $a_{TT} = 25$, $a_{Ts} = 25$, $a_{h1h1} = 25$, $a_{t1t1} = 25$, $a_{h2h2} = 25$, $a_{t2t2} = 25$, $a_{h1t1} = 100$, $a_{h1s} = 25$, $a_{t1s} = 100$, $a_{h2t2} = 100$, $a_{h2s} = 25$, $a_{t2s} = 100$, $a_{ph1} = 25$, $a_{nh1} = 25$, $a_{nh2} = 25$, $a_{pt1} = 100$, $a_{pt2} = 100$, $a_{nt1} = 100$, $a_{nt2} = 100$, $a_{h1T} = 25$, $a_{t1T} = 100$, $a_{h2T} = 25$, $a_{t2T} = 100$, $a_{h1t2} = 100$, $a_{h2t1} = 100$ and $a_{h1h2} = 25$. The repulsion between the NPs can represent the electrostatic repulsion between identically charged NPs. The attraction between the NP patch and the phospholipid head groups, or tethers, can represent attraction between oppositely charged moieties. For favorable enthalpic interactions between the patch and the phospholipid head groups, the soft repulsive interaction parameter is given by $a_{ph2} = 5$, with patch-tether interaction given by $a_{pT} = 25$. For favorable interactions between the patch and tether, the corresponding interaction parameters are $a_{ph2} = 25$ and $a_{pT} = 5$.

All the other parameters pertaining to DPD simulation technique, time, length and energy scales are obtained from *Section 2.2.2*.

4.2.2   Results and Discussion

The hairy vesicles are composed of 1:1 mixture of phospholipids and hairy lipids; we examine hairy lipids with short and long tethers. We begin with a preassembled hairy vesicle, which is placed in a simulation box of dimensions 40 r_c x 40 r_c x 40 r_c containing hydrophilic solvent beads. The total number of beads in the simulation box is 192,000. The simulation box has periodic boundaries along the three coordinate axes and a total of 1178 phospholipid and hairy lipid molecules. A mixed stable hairy vesicle is obtained in a simulation spanning a time interval of 10,000τ. We introduce NPs into the simulation box such that they are outside the interaction range from the vesicle surface. The total number of beads is conserved by removing the corresponding number of solvent beads for each NP. We run the simulations until all the NPs interfacially adsorb onto the vesicle surface. The characterization for each system uses particle trajectories from four simulations which have identical initial conditions but different random seeds.

We investigate two different scenarios for the interactions between the NPs and hairy vesicle: favorable enthalpic interactions between the NP patch with (A) the phospholipid head groups, and (B) the tethers. In part A, we perform the investigations for both the tether lengths. Where as part B, we focus on hairy vesicles composed of long tethers as they are more commonly used in the experimental studies.[46,49,50]

A. NP adsorption promoted by favorable interaction between patch and phospholipid head groups

We begin with a hairy vesicle in the hydrophilic solution and place 4 large NPs at randomly selected locations in the simulation box. The initial configuration of the hairy vesicle with four patchy NPs, for both the short and long tethers is respectively shown in Figure 4.2 (a) and (b). The adsorption of the NP on to the phospholipid head groups will be determined by: (1) the degree of deterrence offered to the approach of the NP to the bilayer-solvent interface by the tethers, (2) the suitable orientation of the NP such that the patch faces the phospholipid head groups, and (3) whether the NP patch and the phospholipid head groups are within interaction range. Our results show that NPs diffuse in the solvent until a NP patch is able to bypass the tethers and approach the phospholipid head groups on the vesicle surface, such that they are within interaction range. The highly favorable enthalpic interactions between the NP patch and the phospholipid head group results in the adsorption of NPs. This observation holds for hairy vesicles with different tether lengths, as shown in Figure 4.2 (c) and (d).
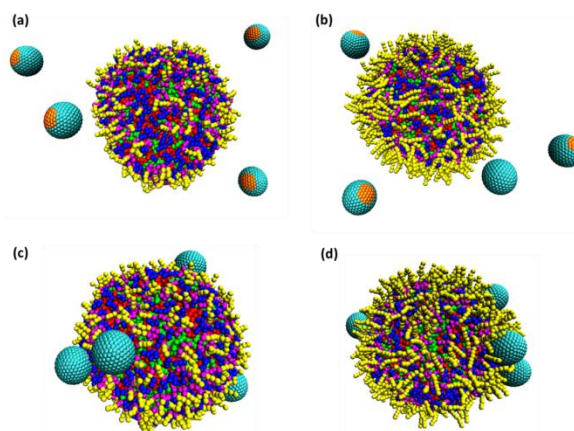
Figure 4.2: Initial configuration of (a) binary component hairy vesicle composed of phospholipids (50%) and hairy lipid molecules with short tethers (50%), and 4 NPs placed outside the interaction range of the hairy vesicle, (b) binary component hairy vesicle composed of phospholipids (50%) and hairy lipid molecules with long tethers (50%), and 4 NPs placed outside the interaction range of the hairy vesicle, (c) short tether hairy vesicle with 4 NPs adsorbed onto the phospholipid head groups at t = 160,000τ, (d) long tether hairy vesicle with 4 NPs adsorbed onto the phospholipid head groups at t = 160,000τ.

Our observations show that NPs are constantly hitting the hairy vesicle surface as they are diffusing in the solvent and are quite often are pushed away by the tethers. This is captured by the number of interactions between the NPs and long tethers as a function of time, as given in Figure 4.3.
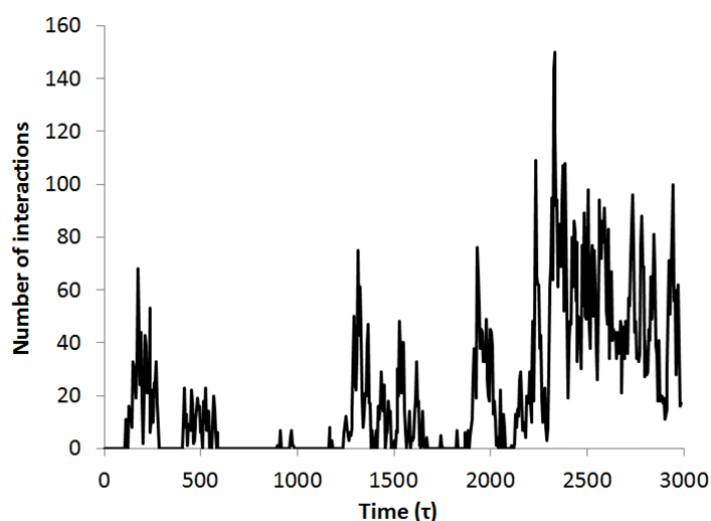
Figure 4.3: A plot of number of interactions between nanoparticle and tethers as a function of time for 4 nanoparticles interacting with hairy vesicle composed of long tethers.

A pair of beads is considered to be interacting if their center-to-center distance is less than the interaction cut-off distance ($r_c = 1$). The number of interactions between the NPs and tethers constantly varies from zero to positive values until the first interaction occurs between a NP patch and the phospholipid head groups. From this point, the interaction count between the NP and the tethers varies about a positive value due to the neighboring tethers. The NPs and the phospholipid head groups can only reach close proximity to each other for regions with low tether density. We would like to note that high tether density promotes steric stabilization and decreases the interfacial adsorption of particles.[4] Our results show that the capture of the NP by the bilayer is not necessarily occurring via

direct approach of the NP patch towards the phospholipid head groups. We observe that some NPs are bypassing the tethers while their patches are oriented in a different direction to the vesicle surface, as shown in Figure 4.4 (a) and (b). After bypassing the tethers and having a close proximity to the vesicle surface, the NPs keep changing their orientation until their patches are within the interaction range from the nearby phospholipid head groups, as shown in Figure 4.4 (c). Upon orienting its patch towards vesicle surface, the first interaction occurs between the NP and a single phospholipid molecule, as demonstrated by Figure 4.4 (d). Following the initial interaction, there is a steep increase in the number of interactions between the NP patch and the phospholipid head groups. There onwards, the number of interactions quickly reaches a steady state value, as shown in Figure 4.4 (g). This demonstrates that the initial contact between the NP patch and the phospholipid head group activates the subsequent adsorption of the NP to a group of phospholipid molecules, as shown in Figure 4.4 (e) and (f). The number of phospholipid molecules interacting with each NP patch is found to be around 6-8, and this value does not change after the number of interactions reaches a steady value. In addition, we observe the NPs to be moving on the vesicle surface with a constant change in the phospholipid molecules that are within interaction range of the NP patch.

We examine the time evolution in the interaction count between the NP patch and the phospholipid head group using four NPs for different tether lengths and simulation runs, as shown in Figure 4.5. We anticipate longer time intervals between subsequent NP absorption events for hairy vesicles with longer tethers. This premise is based upon the larger excluded volume and hence, higher steric hindrance exerted by the tethers on the approaching NPs. Where as there is some variability in the outcomes for the different

simulation runs, we observe the adsorption of the NPs to occur in a relatively shorter interval of time for hairy vesicles with short tethers. Figure 4.5 (b) shows some of the NPs to take longer than 160,000τ tethers. Figure 4.5 (b) shows some of the NPs to take
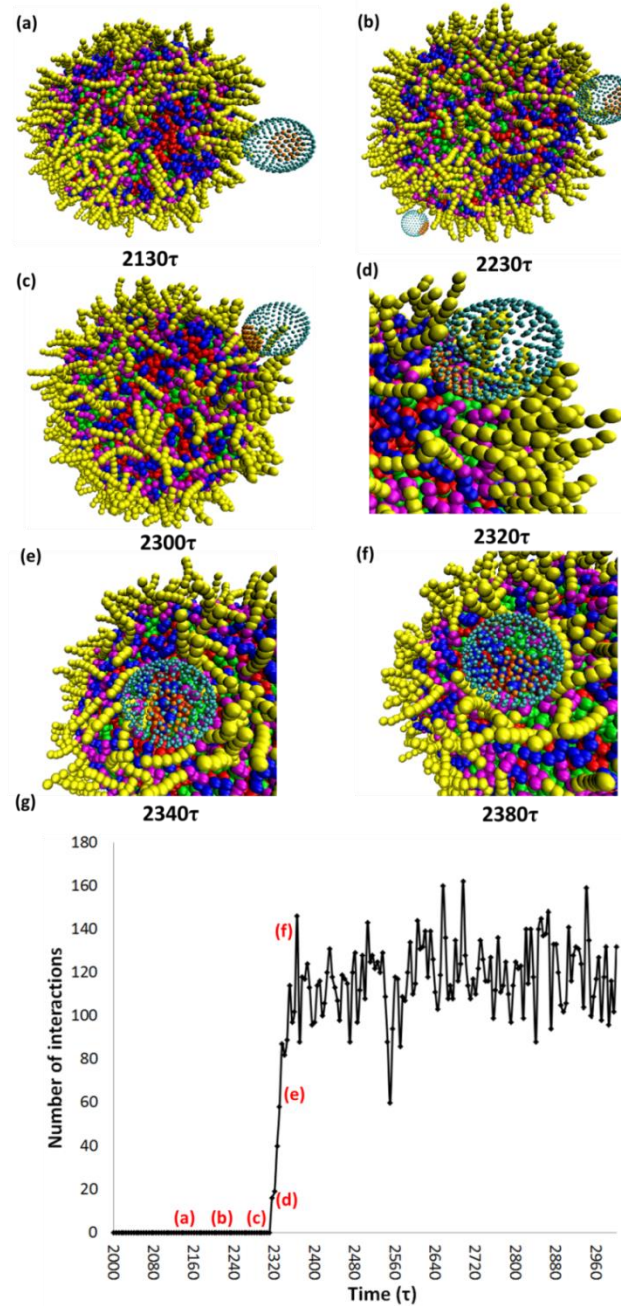
Figure 4.4: Images of the capture of a single NP by phospholipid head groups of a hairy vesicle composed of long tethers at (a) t = 2130τ, (b) t = 2230τ, (c) t = 2300τ, (d) t = 2320τ, (e) t = 2340τ, (f) t = 2380τ and (g) a plot of the number of interactions between NP patch and tethers as a function of time during the capturing process.
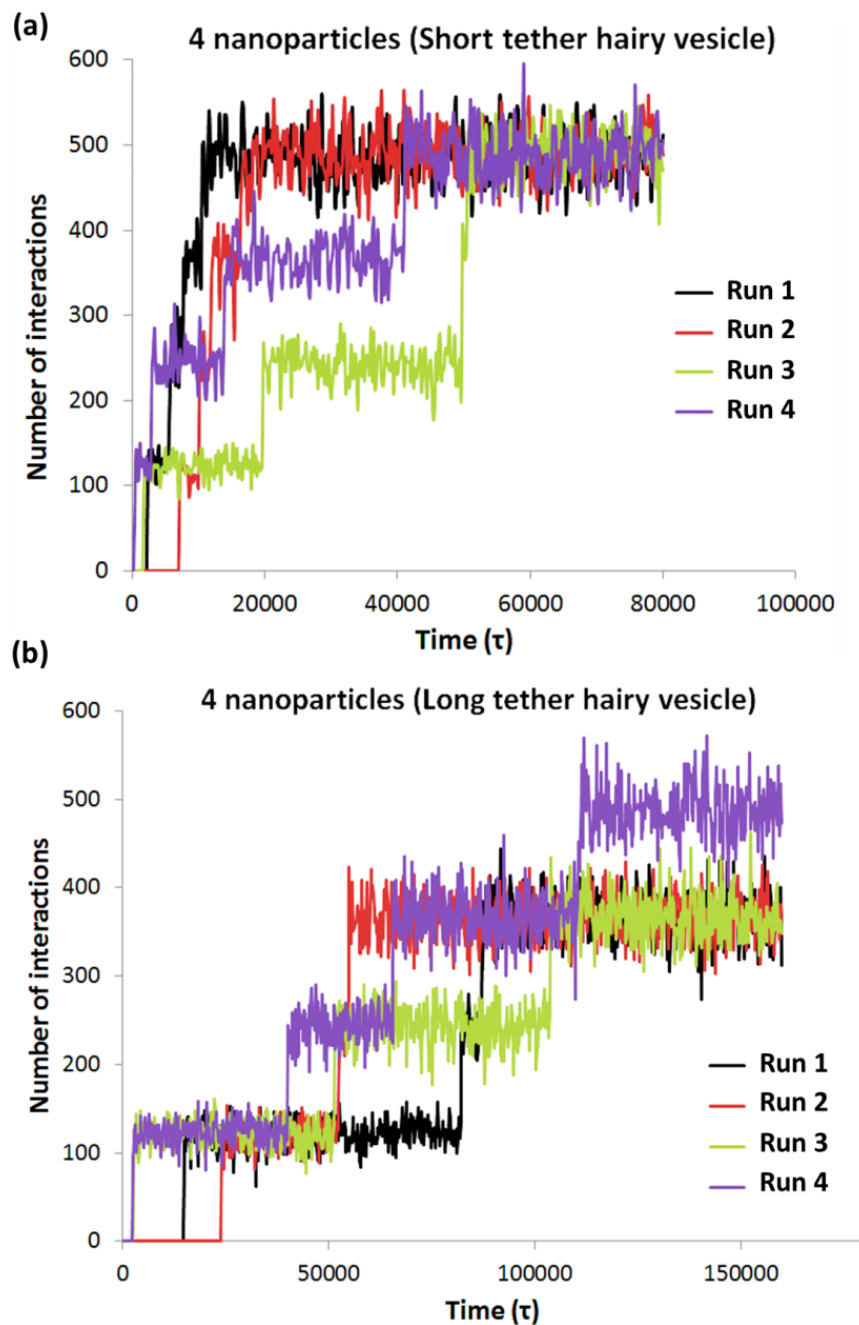
Figure 4.5: Plots of the number of interactions between the NP patch and phospholipid head groups as a function of time for 4 NPs interacting with hairy vesicle composed of (a) short and (b) long tethers. The simulations of hairy vesicles composed of short and long tethers have been run for a total time of 80,000τ and 160,000τ, respectively. The measurements from four simulation runs using different random seeds are shown separately in the plot.

longer than 160,000τ to adsorb onto the surface of a vesicle with long tethers. We find that prior adsorbed NPs do not affect the number of phospholipid head groups interacting with the subsequently adsorbing NPs, so there is no limiting effect of the availability of phospholipids on the adsorption dynamics of multiple NPs. We repeat the studies using eight and twelve NPs. As the number of NPs increases, the absorption time per NP is found to decrease, as shown in Figure 4.6.
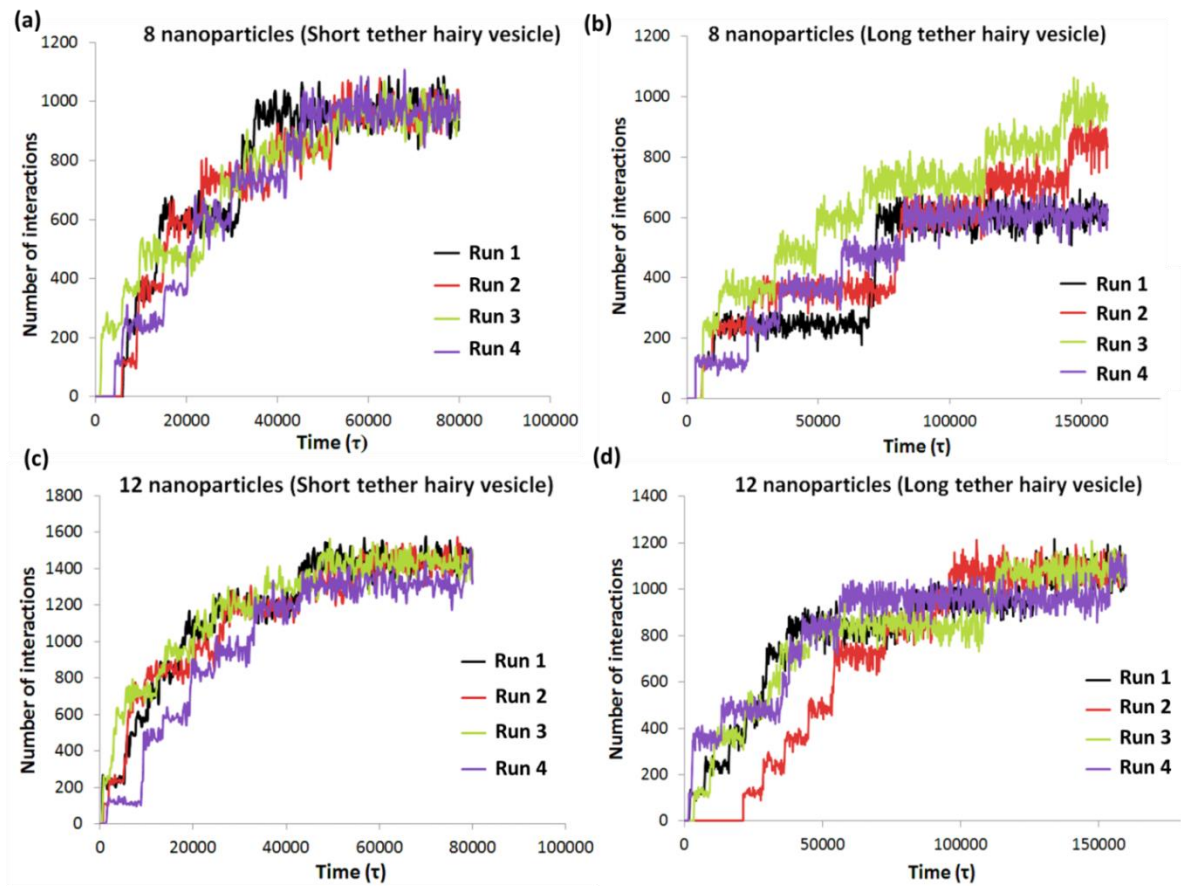
Figure 4.6: Plots of number of interactions between nanoparticle patch and phospholipid head groups as a function of time for (a) 8, (b) 12 nanoparticles interacting with hairy vesicle composed of short tethers and (c) 8, (d) 12 nanoparticles interacting with hairy vesicle composed of long tethers. The simulations of hairy vesicles composed of short and long tethers have been run for a total time of 80,000τ and 160,000τ, respectively. The measurements of four simulation runs using different random seeds are shown separately in the plot.

The adsorption time is defined to be the time interval spanning the beginning of the simulation to the time the NP gets adsorbed onto the vesicle surface. A possible explanation for this observation might be the unfavorable enthalpic interactions between the NPs that constrain their diffusion in the solvent, effectively *pushing* the NPs towards the vesicle surface. This would accelerate the adsorption of the NPs onto the vesicle surface. We would like to note that interaction count measurements demonstrate each NP to interact with approximately the same number of phospholipid head groups, as is evidenced from the number of interactions between the NP patch and the phospholipid head groups for different number of NPs shown in Table 4.1.

Interaction type	Interaction count (4 nanoparticles)	Interaction count (8 nanoparticles)	Interaction count (12 nanoparticles)
Lipid head-NP	490±30	970±50	1440±60
Tether-NP	490±40	970±50	1450±60

Table 4.1: A comparison of the number of interactions between NP patch – phospholipid head groups and NP patch – tethers after all the NPs adsorb on to the vesicle.

In order to understand the role of tether concentration on the adsorption time of the NPs, we measure the number of NPs adsorbed within a time interval of $30,000\tau$ for a range of relative concentration of the hairy lipids spanning 10% to 50%. We use lipids with short and long tethers and twelve NPs, for the adsorption time measurements. We also examine the influence of NP size on the adsorption time. We do not observe the small NPs to get adsorbed on to the vesicle surface with the long tethers, regardless of tether concentration. For the medium and large sized NPs, we find the number of

adsorbed NPs to decrease linearly with increasing relative concentrations of the hairy

lipids with longer tethers, as shown in Figure 4.7. We observe a similar linear decrease

for the small and medium sized NPs (whose dimensions correspond respectively to 100%

and 150% of the length of the short tethers) on to the vesicle surface with the short

tethers.
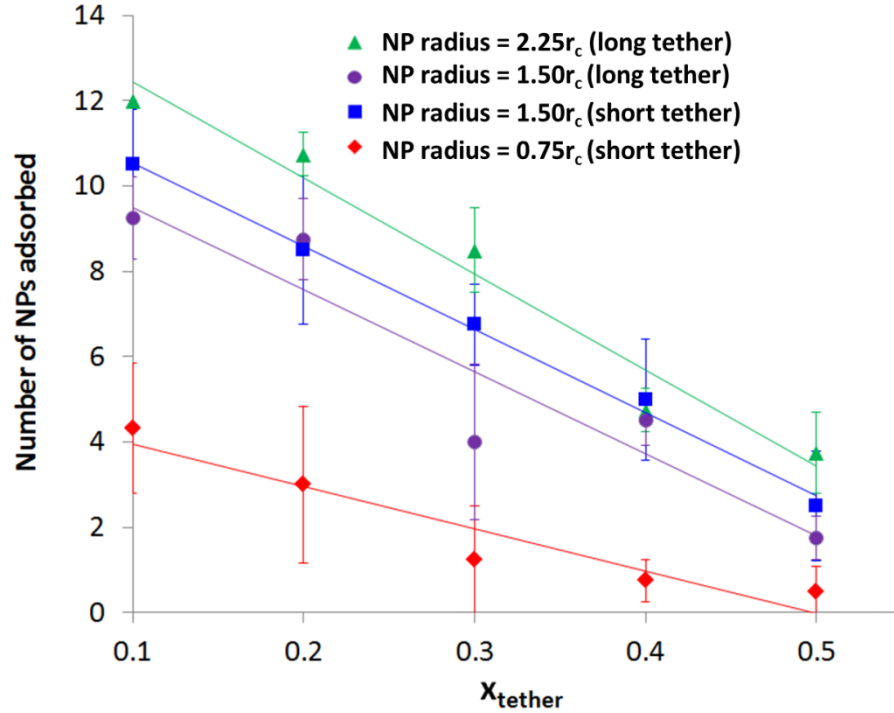
Figure 4.7: A plot of the number of NPs adsorbed on to the phospholipid head groups of hairy vesicle composed of short and long tethers as a function of tether composition (0.1 to 0.5) respectively for the NP radius of $0.75r_c$ and $1.50r_c$, and the NP radius of $1.50r_c$ and $2.25r_c$. The simulations have been run for a total time of $30,000\tau$ and each data point has been averaged over four simulation runs using different random seeds.

These results are in a good agreement with previous theoretical[158] and experimental

findings[159,160] that report a linear decrease in the adsorption of proteins (such as lysozyme

and fibrinogen) on a gold surface covered with short oligomeric polyethylene oxide

chains. In addition, we demonstrate that the adsorption of the NPs to decrease with its

dimensions. This observation is found to be independent of the relative concentration of

the hairy lipids. The difference in the number of adsorbed NPs is small when the size of the NPs is comparable to the length of the tethers (for the medium and large sized NPs). When the size of the NPs is smaller than the length of tethers, there are no adsorption events. These results agree with previous findings that show the amount of protein adsorbed on the surface becomes independent of the polymer chain length when the thickness of the polymer layer is greater than the protein size.[187]

We measure the residence time to understand the dynamics of the phospholipids interacting with the NPs following their adsorption. We define the residence time as the number of times a phospholipid molecule is found to be interacting with a NP during a time interval spanning $10,000\tau$. For this measurement, we track the interactions between the phospholipid head groups and the NP patch at time intervals of 50τ. A phospholipid molecule can have a maximum residence time of 200 ($10,000\tau$ / 50τ) if it is in contact with a NP patch during the entire interval of the measurement. The residence time distribution is obtained by binning the number of phospholipid molecules based upon their residence time. For these measurements we use four, eight and twelve large NPs, and hairy lipids with short and long tethers, as respectively shown in Figure 4.8. Our results demonstrate the population of the lipid molecules interacting with the NP patch to be in flux. The phospholipid molecules diffuse in the bilayer until they are within interaction range of the NP patch. These molecules will interact with the patch for a short time interval before diffusing away. This behavior is captured by a large population of phospholipid molecules with short residence times. We observe an increase in the residence time of the phospholipids with the number of NPs, as shown by the residence

time distribution shifting towards the right. We surmise that a higher number of adsorbed

NPs results in a smaller number of phospholipids that are free to diffuse in the bilayer,
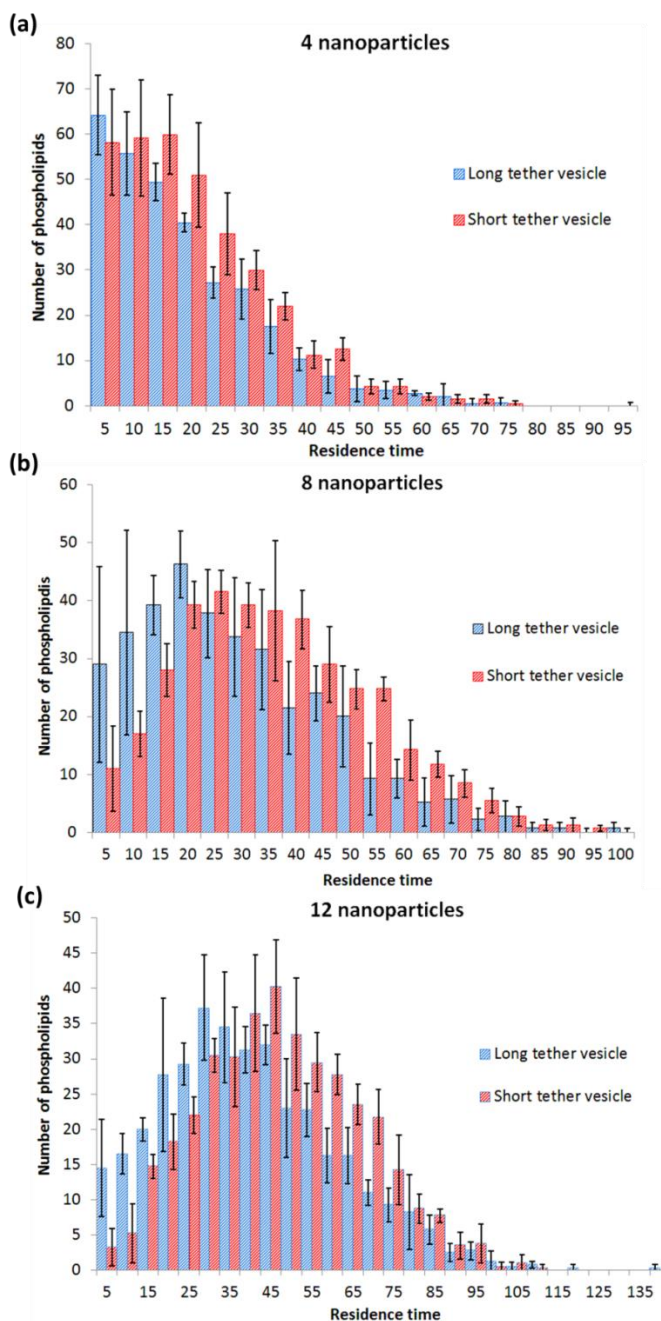
Figure 4.8: Residence time measurements of NPs after their adsorption on to the phospholipid head groups of hairy vesicle composed of short and long tethers for (a) 4, (b) 8 and (c) 12 NPs.

and can contribute to the population of phospholipids interacting with the patch but are in flux. This effect also explains the difference between the residence time distributions for vesicles with the short and long tethers since all the NPs were unable to adsorb on to the hairy vesicle with the long tethers in the prescribed time interval, as discussed earlier. The simulations have been run for a total time of 10,000τ and each data point has been averaged over four simulation runs using different random seeds.

B. NP adsorption promoted by interaction between patch and tethers

We have also examined the effect of highly favorable interactions between the NP patch and the tethers. These investigations were performed on a hairy vesicle with long tethers, with four, eight and twelve large NPs. For these studies, we use the following soft repulsive interaction parameters between the NP patch, and the phospholipid head groups and the tethers: $a_{ph2} = 25$ and $a_{pT} = 5$.

We repeat the investigations by placing a hairy vesicle and the NPs in a simulation box such that the NPs are outside the interaction range from the vesicle surface. The NPs will diffuse in the solution (as shown in Figure 4.9 (a), for a single NP) until they lie within an interaction range from the tethers. The capture of the NP by the tethers is activated by an initial contact between NP patch and a tether bead, as evidenced by Figure 4.9 (b). This is immediately followed by the interaction of two to three tethers with the patch, and the reorientation of the NP to maximize the interactions between the patch and the tethers, as respectively shown in Figure 4.9 (c) and (d). We observe the number of interactions between the patch and the tethers to reach a steady state value, as shown in Figure 4.9 (e). Similar to our observations for favorable patch − phospholipid

head group interactions, we observe the NPs to move on the vesicle surface following their adsorption onto the tethers.
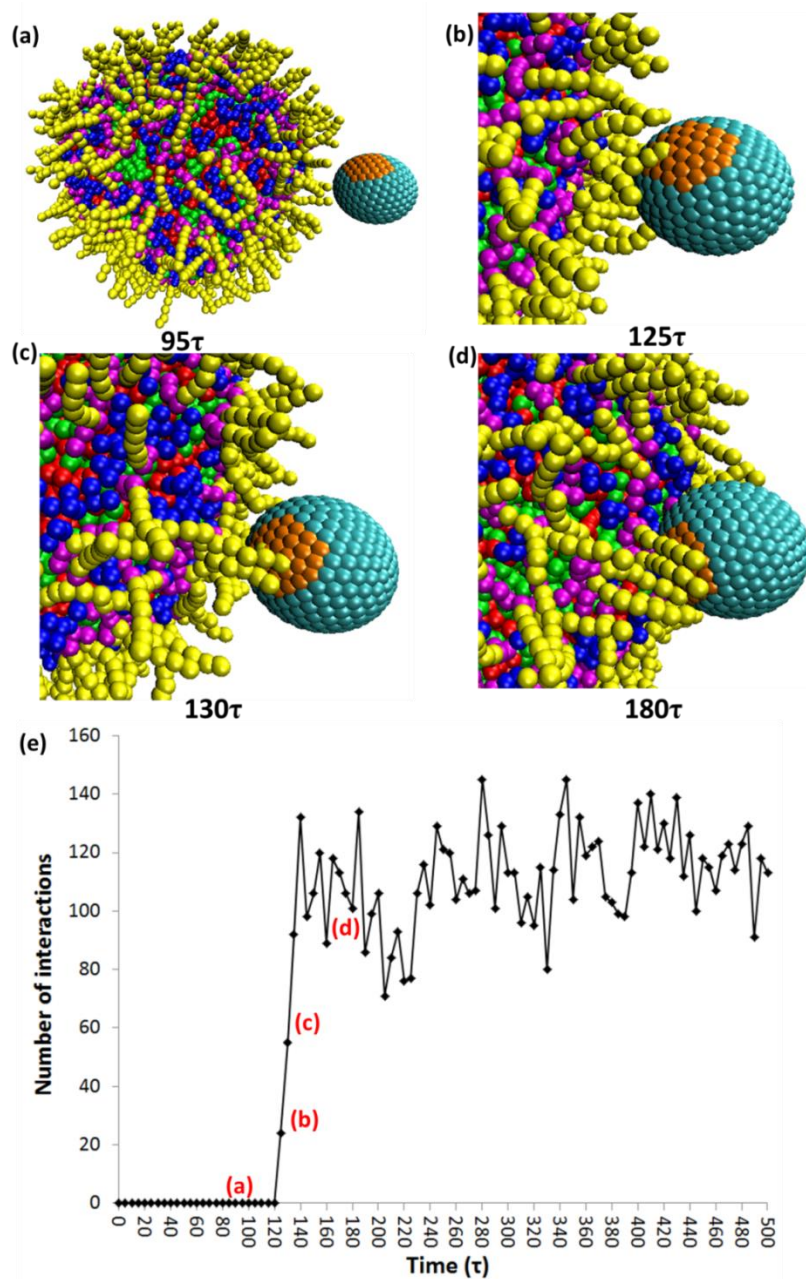
Figure 4.9: Images of the capture of single NP by tethers of hairy vesicle composed of long tethers at (a) t = 95τ, (b) t = 125τ, (c) t = 130τ, (d) t = 180τ, and (e) a plot of number of interactions between NP patch and tethers as a function of time during the capturing process.

We measure the time evolution of the interaction count between the patch and the tethers, for different number of NPs introduced simultaneously into the system, as shown in Figure 4.10. A comparison of the interaction counts between the patch and the phospholipid head group with that corresponding to the patch and the tethers indicate no significant differences for a given number of adsorbed NPs (see Table 4.1). This implies that a NP does not adsorb onto a single tether; instead it maximizes the favorable enthalpic interactions by adsorbing onto multiple tethers. The notable difference between patch – head and patch – tether interaction plots (see Figures 4.5 and 4.10) is absence of the discrete increase in the interaction count in the latter with the adsorption of the NPs. In addition, the time required for all the NPs to adsorb onto the tethers is significantly shorter than the adsorption time of the NPs onto the phospholipid head groups. The latter can be attributed to the lack of steric hindrance by the tethers, which facilitates the adsorption of the NPs onto the tethers.

We measure the residence time for the systems exhibiting favorable interactions between the patch and the tethers, for four, eight and twelve large NPs introduced simultaneously into the solution. We define the residence time as the number of times that a tether is found to be in contact with a patch during the time interval of $10,000\tau$. For this measurement, we track the interactions between the tethers and a patch at intervals of 50τ.

To understand the distinctive behavior of adsorbed NPs on phospholipid head groups and tethers, we compare the respective residence time distribution while ensuring that the same number of NPs is adsorbed in the time interval of $10,000\tau$. Figure 4.11 shows the residence time measurements for systems with favorable interactions between

the patch and the phospholipid head group (for short tethers) and the patch and the tethers

(for long tethers). Our calculations demonstrate the residence time distribution for
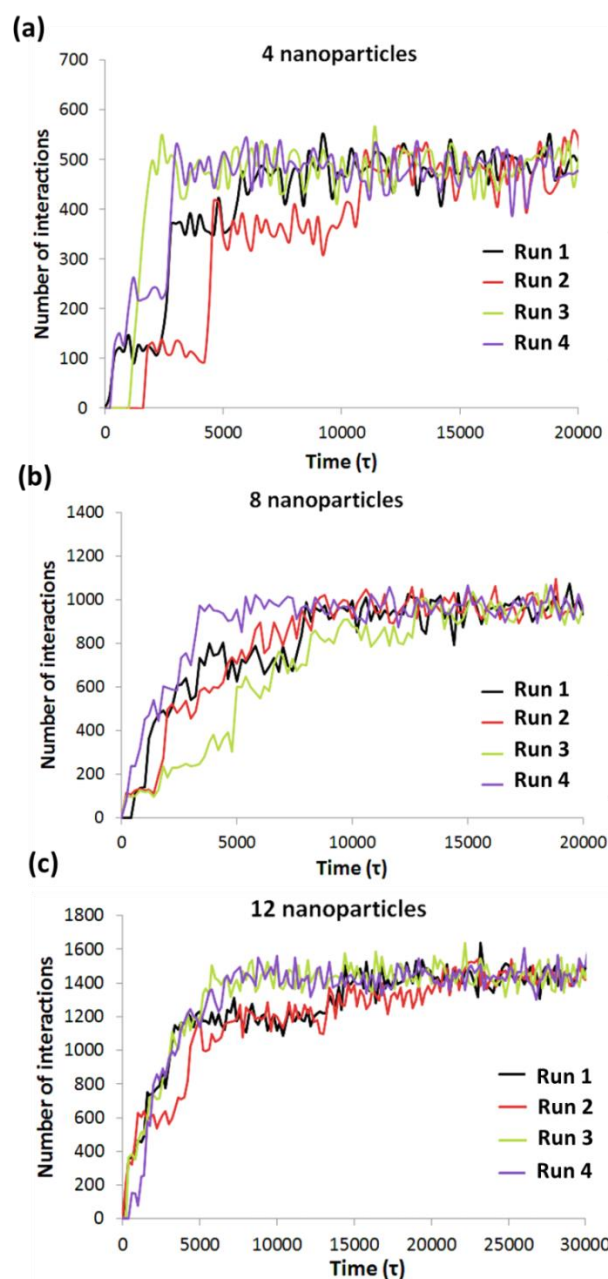
Figure 4.10: Plots of number of interactions between NP patch and tethers as a function of time for (a) 4, (b) 8, (c) 12 NPs interacting with hairy vesicle composed of long tethers. The simulations have been run for a total time of 80,000τ. The measurements from four simulation runs using different random seeds are shown separately in the plot.

systems with favorable enthalpic interactions between the patch and the tethers to support

short-lived interactions. We surmise that the conformational entropy of the tethers will
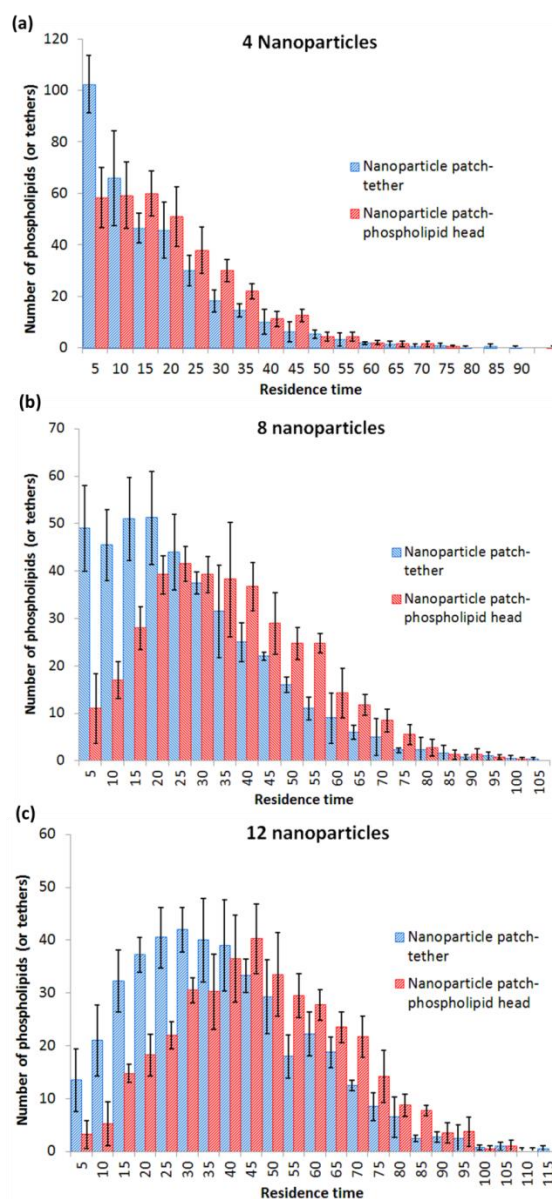
Figure 4.11: Residence time measurements of NPs following their adsorption on to the phospholipid head groups of the hairy vesicle composed of short tethers and tethers of hairy vesicles composed of long tethers for (a) 4, (b) 8 and (c) 12 NPs. The simulations have been run for a total time of 10,000τ and each data point has been averaged over four simulation runs using different random seeds.

reduce the lifetime of the interactions between the patch and the tethers. Another possible contribution is the higher degree of obstruction encountered by the NPs adsorbed on to the phospholipid head groups during their lateral diffusion due to the excluded volume of the tethers. The excluded volume of the tethers would constrain the motion of the NPs and phospholipids, thereby increasing the lifetime of their interactions. The decrease in the lateral diffusion of adsorbed proteins on a liposome surface by grafted PEG chains has been previously shown in experiments.[178] As the total number of adsorbed NPs increases, we observe the residence time distribution to favor longer lived interactions due to the decreasing population of tethers and phospholipids which are available to participate in new interactions with the NP patch.

4.3   Modeling interactions between charged nanoparticles and multi-component vesicles via implicit solvent coarse-grained molecular dynamics simulation technique

4.3.1 Modeling and parameterization of system components

We have used an implicit solvent model introduced by Cooke and Deserno[77] (as described in *Sections 2.4.1 and 2.4.2*) to develop a coarse-grained representation of two-tail lipid molecules which we extend to implement screened electrostatic interactions in the model. Our system consists of a stable multicomponent vesicle composed of zwitterionic and neutral lipid molecules, and NPs with negatively charged patches. A lipid molecule is represented by a bead-spring model with one head group encompassing three hydrophilic beads and two hydrocarbon tail groups composed of three hydrophobic beads each, as shown in the Figure 4.12 (a). We use a multicomponent vesicle composed of zwitterionic and neutral lipid molecules. Positive and negative charges are added into

two hydrophilic beads in the head group of zwitterionic lipid molecules, as shown in Figure 4.12 (b). The experimental examples of zwitterionic and neutral lipid molecules are dipalmitoylphosphatidylcholine (DPPC) and 1,2-dipalmitoyl-sn-glycerol, respectively. Same bonded and non-bonded potentials (as detailed in *Section 2.4.2*) are used to model attractive and repulsive interactions between lipid beads. In addition, screened electrostatic interaction between the charged groups is modeled via the Yukawa potential $U(r) = A\dfrac{e^{-kr}}{r}$ (for r < r_c^{elec}) where 1/k is the Debye screening length and r_c^{elec} is the cutoff distance for screened electrostatic interactions. The cut-off distance is chosen as r_c^{elec} = 6σ. A is a constant which embodies the strength of the electrostatic potential and given by $A = \dfrac{q_1 q_2}{4\pi\varepsilon_0\varepsilon}$ where q_1 and q_2 are charges belong to charged groups, ε_0 is vacuum permittivity and ε is dielectric constant of water. The strength of the screened electrostatic interactions will be determined by the concentration of the counterions. We choose 1/k = 1 nm which corresponds to Debye length for 0.1 M solution of a monovalent salt and is commonly used approximation of the cytoplasm.[188] DPPC phospholipid molecule has positively charged choline and negatively charged phosphate groups which bear charges +e and −e, respectively (e = 1.602x10^{-19} C). By using ε_0 = 8.854x10^{-12} C^2/Nm^2 and ε = 80, we get A ~ ± k_bT for the electrostatic interactions between charged groups of DPPC phospholipid molecules.

The NPs, shown in Figure 4.12 (c), are hollow spheres composed of 312 hydrophilic beads with a patch covering 20% of the surface and the radii of 2.25σ. The patch is set to be negatively charged (anionic patch) so it has highly favorable interactions with the positively charged head bead of phospholipid molecule. The

remaining part of NP is modelled as neutral. Experimental counterparts of the NPs can be proteins, drug molecules or synthetic particles with moieties grafted on to its surface.[176] We model the complex topography and asymmetric charge distribution of NPs via patchy spherical counterparts.[186] Negatively charged nanoparticles can be obtained by modifying the surface of white polystyrene (PS) latex with carboxyl groups ($\sim$0.91e^-/nm^2).[179] The surface area of the NP patch is found to be 4.4 nm^2, which corresponds to $q_{patch} \sim 4e^-$ by using the charge density of 0.91 e^-/nm^2. For the attractive interactions between the negatively charged patch and the positively charged phospholipid head bead, A parameter is found to be -4k_BT. Similarly, for the repulsive interactions between the negatively charged patch and the negatively charged phospholipid head bead, A parameter is found to be +4k_BT. In addition, A parameter for patch – patch interactions is set to +16k_BT by using the previously defined relation $A = \dfrac{q_1 q_2}{4\pi\varepsilon_0\varepsilon}$. All the remaining interactions between NP and lipid molecules are described by WCA potential with $\varepsilon = 1$, $r_c = 2^{(1/6)}$ b and b = σ.
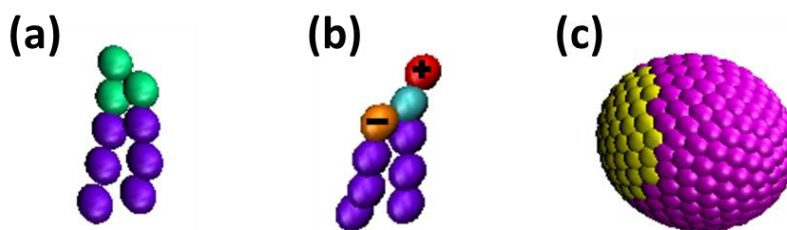
Figure 4.12: Images of the (a) neutral lipid molecule, (b) zwitterionic phospholipid molecule such as DPPC, and (c) spherical NP with a negatively charged patch. NP has a radius of 2.25r_c.

The simulations were run in the canonical ensemble using the Langevin thermostat with three dimensional periodic boundary conditions. The simulation box dimensions were set to 60σ x 60σ x 60σ. The total number of beads in the system was 36000 which corresponds to a lipid density of 0.019 lipids per σ^3. The simulation time

step was set to δt = 0.01τ. All the other parameters pertaining to implicit solvent CG MD simulation technique, time, length and energy scales are obtained from *Section 2.4.2* and *Section 2.4.3*.

4.3.2 Results and discussion

The binary component vesicles are composed of 1:2 mixture of zwitterionic phospholipids and neutral lipids. We begin with a preassembled binary component vesicle, which is placed in a simulation box of dimensions 60 σ x 60 σ x 60 σ. The total number of lipid beads in the simulation box is 36000. The simulation box has periodic boundaries along the three coordinate axes and a total of 4000 zwitterionic phospholipid and neutral lipid molecules. A mixed stable vesicle is obtained in a simulation spanning a time interval of 100,000τ. We introduce NPs into the simulation box such that their center-of-masses are 6σ away from the vesicle surface. We run the simulations until all the NPs interfacially adsorb onto the vesicle surface. The characterization for each system uses particle trajectories from four simulations which have identical initial conditions but different random seeds.

We start with a mixed vesicle composed of zwitterionic and neutral lipid molecules in implicit solvent conditions and place 24 charged patchy NPs at randomly selected positions in the simulation box, as shown in Figure 4.13. The strong electrostatic interactions between the negatively charged NP patch and the positively charged phospholipid head group result in the adsorption of NPs while vesicle keeps its integrity, as shown in Figure 4.13. This is consistent with the previous studies demonstrating that anionic and cationic NPs adsorb to the PC group of phospholipids and liposomes maintain their integrity in the presence of adsorbed NPs on their surface.[179]

We examine the time evolution in the interaction count between the negatively charged NP patch and the positively charged phospholipid head group using 24 NPs, as shown in Figure 4.14. A pair of beads is considered to be interacting if their center-to-center distance is less than the cut-off distance ($r_c = 1.07$) based on WCA potential. We observe the adsorption of the NPs to occur in a very short interval of time as the NP patch is already present within the interaction range of phospholipid head groups at the beginning of the simulation run. The system is setup in this way due to the lack of solvent
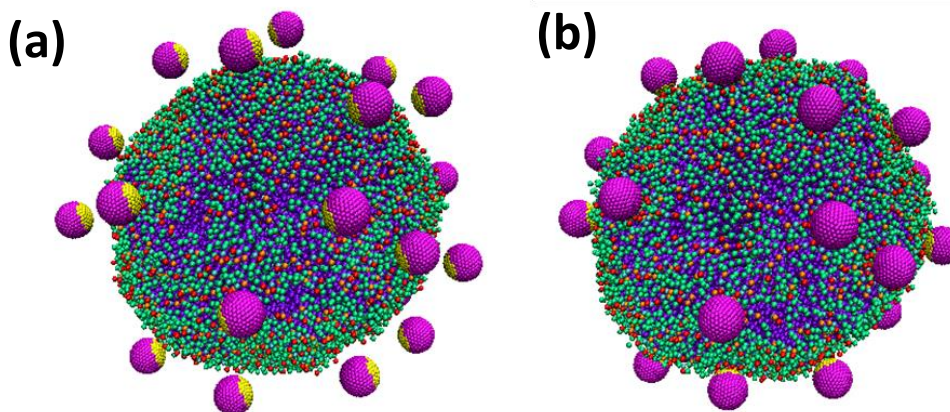
Figure 4.13: (a) Initial configuration of binary component vesicle composed of zwitterionic phospholipids (33%) and neutral lipid molecules (67%), and 24 NPs with negatively charged patches randomly placed outside the vesicle surface, (b) binary component vesicle with 24 NPs adsorbed onto the phospholipid head groups at t = 100,000τ.

molecules. Solvent could be used to bring NPs into close proximity of phospholipid head groups via hydrodynamic forces, as we observe in *Section 4.2.2* by using DPD approach. We demonstrate that there is a steep increase in the number of interactions between the NP patch and the phospholipid head groups and it quickly reaches a steady state value. The number of phospholipid molecules interacting with each NP patch is found to be around 6-12, and this value does not change after the number of interactions reaches a

steady value. We find that prior adsorbed NPs do not affect the number of phospholipid head groups interacting with the subsequently adsorbing NPs, so there is no limiting effect of the availability of phospholipids on the adsorption dynamics of multiple NPs, similar to our observations in *Section 4.2.2*.

We measure the residence time to understand the dynamics of the phospholipids interacting with the NPs via electrostatic interactions following their adsorption. We define the residence time as the number of times positively charged head group of a phospholipid molecule is found to be interacting with negatively charged patch of a NP during a time interval spanning $80,000\tau$. For this measurement, we track the interactions between the phospholipid head groups and the NP patch at time intervals of 100τ. A phospholipid molecule can have a maximum residence time of 800 ($80,000\tau$ / 100τ) if it
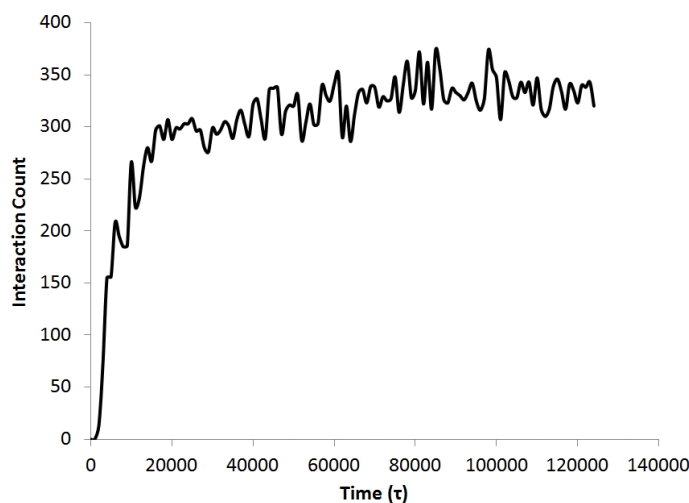
Figure 4.14: Plot of the number of interactions between the negatively charged NP patch and positively charged phospholipid head groups as a function of time for 24 NPs interacting with binary vesicle composed of zwitterionic phospholipids (33%) and neutral lipid molecules (67%). The simulations have been run for a total time of $100,000\tau$. The interaction count has been averaged over four simulation runs using different random seeds.

is in contact with a NP patch during the entire interval of the measurement. The residence time distribution for a system composed of 4000 lipid molecules and 24 NPs is obtained by binning the number of phospholipid molecules based upon their residence time, as shown in Figure 4.15. Our results demonstrate that a large population of phospholipid molecules has long lasting interactions with the NP patch, evidenced from the fact that residence time distribution is completely shifted towards right. This indicates that phospholipid molecules are not diffusing away after interacting with NP patch for a short time interval. One of the reasons for long lasting interactions between phospholipid head groups and NP patch could be the absence of solvent molecules in the implicit solvent CG MD approach, where NPs lack the momentum resulted from solvent molecules.
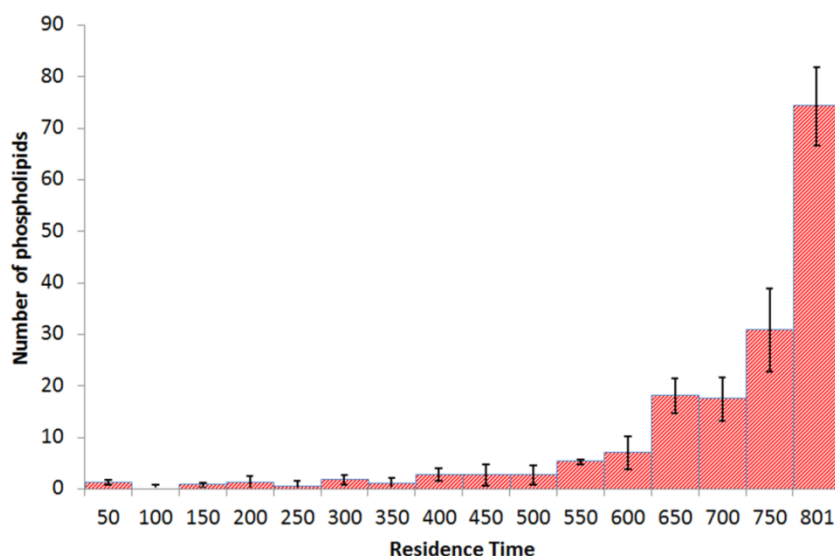
Figure 4.15: Residence time measurements of 24 NPs after their adsorption on to the phospholipid head groups of binary component vesicle composed of zwitterionic phospholipids and neutral lipid molecules.

Another reason could be the formation of distinct domains of zwitterionic lipid molecules at the site of interaction, which are surrounded by neutral lipid molecules. We observe the formation of the domains upon the adsorption of NPs on the vesicle surface, as shown in Figure 4.16. The reconstruction of the vesicle surface by the formation of small domains

is also captured quantitatively via measuring number of interactions between the head groups of zwitterionic lipid molecules, as shown in Figure 4.16 (c). We surmise that strong electrostatic interactions between phospholipid head groups and NP patches prevent phospholipid molecules from diffusing away in a short time interval.
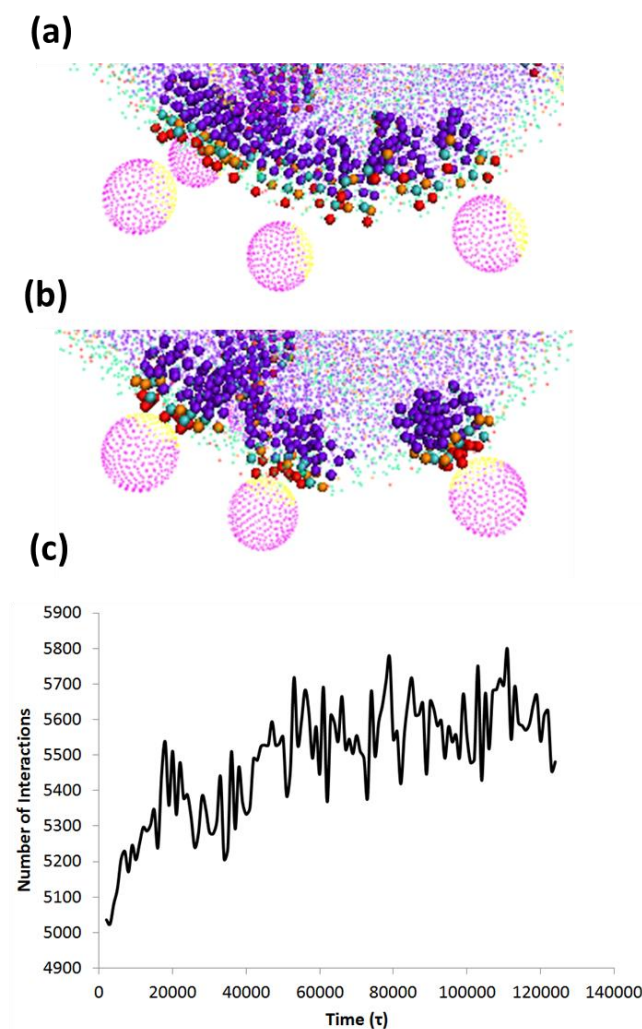
Figure 4.16: (a) Initial configuration of zwitterionic phospholipid molecules within the interaction range of NPs before their adsorption. (b) Formation of small domains composed of zwitterionic phospholipid molecules upon adsorption of NPs on to the vesicle surface. (c) Plot of the number of interactions between phospholipid head groups as a function of time during the adsorption of NPs on to the vesicle surface.

4.4   Chapter conclusions

We have demonstrated the interactions between a stable vesicle and NPs can be controlled via steric stabilization through the use of DPD approach. We implement the steric stabilization on the vesicle by using a mixture of phospholipids and hairy lipids. We identified the factors which control the adsorption of NPs on the vesicle surface as well as their behavior on the surface after the adsorption. Our results demonstrate the relative size of the NPs to the tether length, the relative concentration of the hairy lipids and the relative affinity of the NP patch for the tethers and phospholipid head groups to determine the adsorption behavior of the NPs. The decrease in the adsorption of NPs onto the vesicle surface with increasing concentration of hairy lipids is found to be good agreement with previous experimental and theoretical studies on the adsorption of proteins on a gold surface covered with short oligomeric polyethylene oxide.[158-160] The residence time measurements show the NPs to be moving over the surface of the vesicle, and the lateral diffusion of the NPs to be obstructed by the presence of hairy lipid molecules, which is in a good agreement with experimental results.[178]

In addition, we demonstrate the formation of binary component vesicle composed of zwitterionic and neutral lipid molecules via the use of implicit solvent CG MD approach. We investigated the interactions of NPs with negatively charged patches with the positively charged head group of phospholipid molecules as well as the behavior of NPs on the vesicle surface after the adsorption. We demonstrated the adsorption of charged NPs to induce reorganization of phospholipid molecules on the vesicle surface. The residence time measurements show the NPs to have long lasting interactions with phospholipid head groups, as opposed to our observations in the interactions of NPs with

the surface of hairy vesicle using DPD approach. This difference could be resulted from the absence of solvent molecules in the implicit solvent CG MD approach, where NPs lack the momentum resulted from solvent molecules. Another reason can be the formation of distinct domains on the vesicle surface due to the strong electrostatic interactions between NP patch and phospholipid head groups, as we do not observe any domain formation for the interactions of NPs with phospholipids using DPD approach.

Chapter 5

Conclusions

To summarize, we carried out our investigations on the multi-component bio-inspired phospholipid vesicles composed of phospholipid species with different interfacial areas or hydrocarbon tail groups in both hydrodynamic and non-hydrodynamic conditions in order to understand the factors affecting the organization, stiffness, shape and stability, and the underlying mechanisms of the interactions between biological particles or synthetic particles with them by using two different coarse-grained MD based simulation methods. We utilized DPD method to capture the hydrodynamic effects and the coarse-grained implicit solvent MD to capture larger length and time scales. Using these modeling tools enabled us to address physical phenomena at a desired spatio-temporal scale such as length scale from 1 nm up to 1 μm and time scale from nano-seconds to micro-seconds.

In chapter 2, we focused on the development of the vesicle models by using more realistic coarse-grained representations of lipid molecules such as double tail

phospholipid species. We investigated the formation of single and binary lipid vesicles composed of two-tail amphiphilic lipid molecules and coarsening dynamics in a two-component vesicle composed of phospholipid molecules with distinct chemical properties in hydrodynamic and non-hydrodynamic conditions using DPD and implicit solvent CG MD, respectively. We demonstrated that the degree of dissimilarity between the phospholipid species affects their ability to form distinct domains in the lipid bilayer and the occurrence of macroscopic phase separation for phospholipid mixtures composed of species with different hydrocarbon tail groups. We observed the characteristics of the macroscopic phase segregation to agree with earlier numerical, theoretical and experimental studies. We showed that the variations in the molecular chain stiffness affect the structural properties and shape transformations of the vesicle but have no effect on the phase segregation process. We did not observe significant changes in the bilayer thickness and the area per lipid for different mixtures of lipid species in both techniques. We obtained the relation between phase segregation in the multicomponent vesicles and thermodynamic variables such as interfacial line tension and surface tension via the use of DPD approach, and they were found to be consistent with theoretical and experimental studies. We found our investigations on the effects of temperature on the physical properties of single component lipid vesicles to agree with experimental results via the use of CG MD approach.

In chapter 3, we designed sterically stable biocompatible vehicles aka "hairy vesicles" encompassing two species of phospholipids with different interfacial areas and hydrocarbon tail groups via self-assembly and identified the factors which control the shape of the vesicles. The relative concentration of the end-functionalized lipids, tether

length, molecular stiffness, degree of dissimilarity in the hydrocarbon tail groups, and the volume of confinement were found to determine the shape of the hairy vesicle. The asymmetric distribution of the hairy lipid molecules in the inner and outer monolayers of the self-assembled hairy vesicles was shown to occur due to the excluded volume of the tethers, and we found these results to be in good agreement with theoretical and experimental results. The final equilibrium morphology of the hairy vesicles was shown to depend upon the packing of the molecular species, and the excluded volume of the tethers. The transition from an ellipsoidal to a spherical morphology is promoted with increasing hydrocarbon tail stiffness while the excluded volume of tethers counteracts this transition by disrupting the tight packing of the molecules. These observations for the shape transformation of the hairy vesicles were found to agree with experimental studies. In addition, the degree of confinement was found to cause the prolate shaped vesicles to transform into an oblate shape for different relative concentrations of the hairy lipids and the length of the hairs, which was found to be in good agreement with earlier theoretical investigations. The formation of stable bicellar structures was found to be favored with a higher degree of confinement.

In chapter 4, we demonstrated that the relative size of the NPs to the hair length, and the relative concentration of the hairy lipids to affect the adsorption behavior of the NPs on two different vesicle surfaces: (i) phospholipid head groups and (ii) hairs. The amount of adsorbed NPs was found to decrease significantly as their dimensions get smaller than the length of the hairs. We also found that the number of adsorbed NPs decreases linearly with increasing relative concentrations of the hairy lipids, which is in good agreement with previous experimental and theoretical studies of nanoparticle

adsorption on the surfaces decorated with short tethers. Thus, the hairs provide a means of regulating the adsorption of NPs onto the biocompatible vesicles. We demonstrated that the adsorption behavior of the NPs to depend on the relative affinity of the NP patch for the tethers and phospholipid head groups. A shift in the relative affinity of the NPs towards the tethers facilitates their adsorption due to the lack of steric hindrance, and this result in a significant reduction in the adsorption time of the NPs onto the vesicle surface. Our measurements showed that adsorbed NPs are moving over the surface of the vesicle instead of anchoring to a specific location, and their lateral diffusion is obstructed by the presence of hairy lipid molecules.

In the second part of this chapter, we demonstrated the formation of binary component vesicle composed of zwitterionic and neutral lipid molecules via the use of implicit solvent CG MD approach. In order to achieve this goal, we implemented screened electrostatic interactions in the implicit solvent CG MD model by using Yukawa potential. By using this reduced model, we investigated the interactions between NPs with negatively charged patches and the positively charged head group of phospholipid molecules. We demonstrated the adsorption of charged NPs to cause reconstruction of the vesicle surface by inducing reorganization of phospholipid molecules in the lipid bilayer. The residence time measurements show the NPs to have long lasting interactions with phospholipid head groups, as opposed to our observations in the interactions of NPs with the surface of hairy vesicle using DPD approach. This difference could be resulted from two possible reasons. One of the reasons is the absence of solvent molecules in the implicit solvent CG MD approach, where NPs lack the momentum resulted from their interactions with solvent. The other reason can be that strong electrostatic interactions

between the negatively charged NP patch and positively charged phospholipid head groups induce the formation of distinct domains on the vesicle surface and NPs are anchored to these domains. We do not observe any domain formation for the interactions of NPs with phospholipids using DPD approach as NP – phospholipid interactions are found to be quite transient.

Overall, the aim of this dissertation is to understand the underlying mechanisms that affect the organization, shape, stiffness and interfacial stability of biomaterials and their interactions with biological or synthetic particles. Each chapter demonstrated the cooperative relations among these factors which determine the final structural and functional state of the lipid based systems by using suitable modeling tools which can address physical phenomena at longer time and length scales such as length scale from 1 nm up to 1 μm, and time scale from nano-seconds to micro-seconds.

Future directions

Our investigations can be extended to model larger model bilayer systems which mimic the composition of the cell membranes by introducing other cellular components such as various phospholipid species, sterols, carbohydrates and membrane proteins. This will enable us to validate our models against experimental results, and use the models for predicting the processes and mechanisms underlying the interactions of biological or synthetic nanoparticles with cell membranes. One type of critical cellular component with a potential interest to model in the future scope of this research is actin cytoskeleton system. The cytoskeleton is a polypeptide network that surrounds the inner monolayer of the cells and play important role in the structural integrity and physiological functions of the cells by controlling their stiffness, shape and mobility. The bilayer-actin cytoskeleton system with

various membrane proteins can be modeled in order to understand the role of cytoskeletal on the interaction between nanoparticles and cell membranes as well as the impact of these interactions on the organization of membrane proteins.

One of the challenges in transporting drug delivery vehicles through blood capillaries is their disruption and rupture before delivering their cargo to the target cells. In order to design drug delivery systems with improved transportation efficiency in blood capillaries, it is important to investigate the shape characteristics of sterically stable bioinspired vesicles or "hairy vesicles" in more realistic environment such as during their flow through blood capillaries. Cylindrical microfluidic channels and Poiseuille flow in the channel can be implemented to model the transport of hairy vesicles in the blood capillaries. These models can be used to investigate various effects such flow rate and vesicle composition on the deformation dynamics and morphology of the vesicles, which would be difficult to study by using real-time in vivo conditions.

Another future direction in line with the objectives of this dissertation work is developing a computational model by coupling implicit solvent coarse-grained molecular dynamics model with a Lattice-Boltzmann fluid in order to design and characterize nanostructured soft materials. Lattice-Boltzmann fluid can be used to implement long range hydrodynamic effects in the system instead of using computationally expensive explicit solvent molecules. This hybrid model can be used to generate a stable vesicle composed of single and multiple phospholipid species in order to investigate physiological processes occurring on the mesoscopic spatio-temporal scales. The results of these investigations can be used for the design and prediction of novel hybrid soft and bio-materials at the mesoscale for various applications in medicine, sensing and energy.

Bibliography

1   Gao, L. H.; Shillcock, J.; Lipowsky, R. Improved Dissipative Particle Dynamics Simulations of Lipid Bilayers. *J. Chem. Phys.* **2007**, 126, 015101.

2   Alberts, B.; Johnson, A.; Lewis, J.; Raff, M.; Roberts, K.; Walter, P. Molecular Biology of the Cell. Garland Science: New York, 2007.

3   Shillcock, J. C.; Lipowsky, R. EquilibriumSstructure and Lateral Stress Distribution of Amphiphilic Bilayers from Dissipative Particle Dynamics Simulations. *J. Chem. Phys.* **2002**, 117, 5048–5061.

4   Laradji, M.; Kumar, P.B.S. Dynamics of Domain Growth in Self-assembled Fluid Vesicles. *Phys. Rev. Lett.* **2004**, 93, 198105.

5   Lipowsky, R.; Sackmann, E. Structure and Dynamics of Membranes, Handbook of Biological Physics. *Elsevier*, Amsterdam, 1995.

6   Israelachivili, J. Intermolecular and Surface Forces. *Academic Press*, Boston, 2011.

7   Koufos, E.; Muralidharan, B.; Dutt, M. *AIMS Press Materials Science* **2014**, 1 (2), 103 − 120.

8   Rubenstein, J.L.R.; Smith, B.A.; McConnell, H.M. Lateral Diffusion in Binary Mixtures of Cholesterol and Phosphatidylcholines. *Proc. Natl. Acad. Sci. USA* **1979**, *76*, 15-18.

9   Kahya, N.; Scherfeld, D.; Schwille, P. Differential Lipid Packing Abilities and Dynamics in Giant Unilamellar Vesicles Composed of Short-chain Saturated Glycerol-phospholipids, Sphingomyelin and Cholesterol. *Chem. Phys. Lipids* **2005**, *135*, 169–180.

10 Leonenko, Z. V.; Finot, E.; Ma, H.; Dahms, T. E. S.; Cramb, D. T. Investigation of Temperature-Induced Phase Transitions in DOPC and DPPC Phospholipid Bilayers Using Temperature-Controlled Scanning Force Microscopy. Biophys. J. **2004**, *86*, 3783–3793.

11 Veatch, S. L.; Keller, S. L. Separation of Liquid Phases in Giant Vesicles of Ternary Mixtures of Phospholipids and Cholesterol. Biophys. J. **2003**, *85*, 3074–3083.

12 Lipowsky, R. Budding of Membranes Induced by Intramembrane Domains. *J. Phys. II* **1992**, *2*, 1825.

13 Esposito, C.; Tian, A.; Melamed, S.; Johnson, C.; Tee, S-Y.; Baumgart, T. Flicker Spectroscopy of Thermal Lipid Bilayer Domain Boundary Fluctuations. Biophys. J**. 2007**, *93*, 3169-3181.

14 Laradji, M.; Kumar, P.B.S. Dynamics of Domain Growth in Self-assembled Fluid Vesicles. *Phys. Rev. Lett.* **2004**, *93*, 198105.

15 Ramachandran, S.; Laradji, M.; Kumar, P.B.S. Lateral Organization of Lipids in Multi-component Liposomes. *J. Phys. Soc. Jpn.* **2009**, *78*, 041006.

16 Stanich, C.A.; Honerkamp-Smith, A.R.; Putzel, G.G.; Warth, C.S.; Lamprecht, A.K.; Mandal, P.; Mann, E.; Hua, T.-A.D.; Keller, S.L. Coarsening Dynamics of Domains in Lipid Membranes. *Biophys. J.* **2013**, *105*, 444-454.

17 Taniguchi, T. Shape Deformation and Phase Separation Dynamics of Two-component Vesicles. *Phys. Rev. Lett.* **1996**, *76*, 4444-4447.

18 Fan, J.; Han, T.; Haataja, M. Hydrodynamic Effects on Spinodal Decomposition Kinetics in Planar Lipid Bilayer Membranes. *J. Chem. Phys.* **2010**, *133*, 235101.

19 Bagatolli, L.A.; Gratton, E. Direct Observation of Lipid Domains in Free Standing Bilayers Using Two-photon Excitation Fluorescence Microscopy. *J. of Fluorescence* **2001**, *11*, 141-160.

20 Ramachandran, S.; Komura, S.; Gommper, G. Effects of an Embedding Bulk Fluid on Phase Separation Dynamics in a Thin Liquid Film. *EPL* **2010**, *89*, 56001.

21 Ursell, T.S.; Klug, W.S.; Phillips, R. Morphology and Interaction between Lipid Domains. *Proc. Natl. Acad. Sci. USA* **2009**, *106*, 13301.

22 Bagatolli, L.; Kumar, P.B.S. Phase Behavior of Multicomponent Membranes: Experimental and Compuatational Techniques. *Soft Matter* **2009**, *5*, 3234-3248.

23 Cooke, I. R.; Kremer, K.; Deserno, M. Tunable Generic Model for Fluid Bilayer Membranes. *Phys. Rev. E.* **2005**, *72*, 011506.

24 Marrink, S. J.; de Vries, A. H.; Tieleman, D. P. Lipids on the Move: Simulations of Membrane Pores, Domains, Stalks and Curves. *Biochim. Biophys. Acta, Biomembr.* **2009**, *1788*, 149–168.

25 Boal, D. *Mechanics of the cell.* Cambridge University Press: New York, 2012.

26 Liang, X.; Mao, G.; Ng, K.Y.S. Mechanical Properties and Stability Measurement of Cholesterol-containing Liposome on Mica by Atomic Force Microscopy. *J. Colloid Interface Sci.* **2004**, *278*, 53–62.

27 Baumgart, T.; Das, S.; Webb, W.W.; Jenkins, J.T. Membrane Elasticity in Giant Vesicles with Fluid Phase Coexistence. *Biophys. J.* **2005**, *89*, 1067–1080.

28 Brannigan, G.; Brown, F.L.H. Composition Dependence of Bilayer Elasticity. *J. Chem. Phys.* **2005**, *122*, 07490.

29 Lodish, H.; Baltimore, D.; Berk, A.; Zipursky, S.L.; Matsudaira, P.; Darnell, J. *Molecular Cell Biology.* Scientific American Books: New York, 1995.

30 Lipowsky, R. Domains and Rafts in Membranes—Hidden Dimensions of Selforganization. *J. Biol. Phys.* **2002**, *28*, 195–210.

31 Simons, K.; Vaz, W. L. C. Model Systems, Lipid Rafts, and Cell Membranes. *Annu. Rev. Biophys. Biomol. Struct.* **2004**, *3*, 269.

32 Illya, G.; Lipowsky, R.; Shillcock, J. C. Effect of Chain Length and Asymmetry on Material Properties of Bilayer Membranes. *J. Chem. Phys.* **2005**, *122*, 244901.

33 Rawicz, W.; Olbrich, K. C.; McIntosh, T.; Needham, D.; Evans, E. Effect of Chain Length and Unsaturation on Elasticity of Lipid Bilayers. *Biophys. J.* **2000**, *79*, 328–339.

34 Szleifer, I.; Kramer, D.; Ben-Shaul, A.; Roux, D.; Gelbart, W. M. Curvature Elasticity of Pure and Mixed Surfactant Films. *Phys. Rev. Lett.* **1988**, *60*, 1966-1969.

35 Dutt, M.; Kuksenok, O.; Little, S.R.; Balazs, A.C. Designing Tunable Bio-nanostructured Materials via Self-assembly of Amphiphilic Lipids and Functionalized Nanotubes. *MRS Spring 2012 Conference Proceedings* **2012**, 1464.

36 Olbrich, K.; Rawicz, W.; Needham, D.; Evans, E. Water Permeability and Mechanical Strength of Polyunsaturated Lipid Bilayers. *Biophys J.* **2000**, *79*, 321-327.

37 Merkel, T. J. et al. Using Mechanobiological Mimicry of Red Blood Cells to Extend Circulation Times of Hydrogel Microparticles. *PNAS*, **2011**, 108, 586–591.

38 Geng, Y.; Dalhaimer, P.; Cai, S.; Tsai, R.; Tewari, M.; Minko, T.; Discher, D. E. Shape Effects of Filaments versus Spherical Particles in Flow and Drug Delivery. *Nature Nanotechnology* **2007**, *2*, 249 − 255.

39 Dobereiner, H.-G.; Evans, E.; Kraus, M.; Seifert, U.; Wortis, M. Mapping Vesicle Shapes into the Phase Diagram: A Comparison of Experiment and Theory. *Phys. Rev. E.* **1997**, *55*, 4458.

40 Nieh, M.-P.; Pencer, J.; Katsaras, J.; Qi, X. Spontaneously Forming Ellipsoidal Phospholipid Unilamellar Vesicles and Their Interactions with Helical Domains of Saposin C. *Langmuir* **2006,** *22,* 11028-11033.

41 Sandstrom, M. C.; Johansson, E.; Edwards, K. Structure of Mixed Micelles Formed in PEG-Lipid/lipid Dispersions. *Langmuir* **2007**, 23, 4192-4198.

42 Allen, T. M. Long-circulating (Sterically Stabilized) Liposomes for Targeted Drug Delivery. *Trends Pharmacol. Sci.* **1994**, 15, 215−220.

43 Klibanov, A. L.; Maruyama, K.; Torchilin, V. P.; Huang, L. Amphipathic Polyethyleneglycols Effectively Prolong the Circulation Time of Liposomes. *FEBS Lett.***1990**, *268,* 235−237.

44 Harris, J. M.; Chess, R. B. Effect of Pegylation on Pharmaceuticals. *Nat. Rev. Drug Discovery* **2003**, *2*, 214–221.

45 Lasic, D. D.; Woodle, M. C.; Papahadjopoulos, D. On the Molecular Mechanism of Steric Stabilization of Liposomes in Biological Systems. *J. Liposome Res.* **1992**, *2*, 335–353.

46 Blume, G.; Cevc, G. Liposomes for the Sustained Drug Release in Vivo. *Biochim. Biophys. Acta* **1990**, 1029, 91–97.

47 Rex, S.; Zuckermann, M. J.; Lafleur, M., Silvius, J. R. Experimental and Monte Carlo Simulation Studies of the Thermodynamics of Polyethyleneglycol Chains Grafted to Lipid Bilayers. *Biophys. J.* **1998**, *75*, 2900–2914.

48 Szleifer, I.; Gerasimov, O. V.; Thompson, D. H. Spontaneous Liposome Formation Induced by Grafted Poly (Ethylene Oxide) Layers: Theoretical Prediction and Experimental Verification. *Proc. Natl. Acad. Sci. U.S.A.* **1998**, *95*, 1032–1037.

49 Nicholas, A. R.; Scott, M. J.; Kennedy, N. I.; Jones, M. N. Effect of Grafted Polyethylene Glycol (PEG) on the Size, Encapsulation Efficiency and Permeability of Vesicles. *Biochimica Biophysica Acta* **2000**, *1463*, 167–178.

50 Garbuzenko, O.; Barenholz, Y.; Priev, A. Effect of Grafted PEG on Liposome Size and on Compressibility and Packing of Lipid bilayer. *Chemistry and Physics of Lipids* **2005**, *135*, 117–129.

51 Lee, H.; Pastor, R. W. Coarse-grained Model for PEGylated Lipids: Effect of PEGylation on the Size and Shape of Self-assembled Structures. *J. Phys. Chem. B* **2011**, *115*, 7830–7837.

52 Bru, M. R.; Thompson, D. H.; Szleifer, I. Size and Structure of Spontaneously Forming Liposomes in Lipid/PEG-Lipid Mixtures. *Biophys. J.* **2002**, *83*, 2419–2439.

53 Shinoda, W.; DeVane, R.; Klein, M. L. Coarse-grained Molecular Modeling of Non-ionic Surfactant Self-assembly. *Soft Matter* **2008**, *4*, 2454–2462.

54 Stepniewski, M.; Gierula, M. P.; Rog, T.; Danne, R.; Orlowski, A.; Karttunen, M.; Urtti, A.; Yliperttula, M.; Vuorimaa, E.; Bunker, A. Study of PEGylated Lipid Layers as a Model for PEGylated Liposome Surfaces: Molecular Dynamics Simulation and Langmuir Monolayer Studies. *Langmuir* **2011**, *27*, 7788–7798.

55 Kasbauer, M.; Lasic, D. D.; Winterhalter, M. Polymer Induced Fusion and Leakage of Small Unilamellar Phospholipid Vesicles: Effect of Surface Grafted Polyethylene-glycol in the Presence of Free PEG. *Chemistry and Physics of Lipids* **1997**, *86*, 153–159.

56 Lee, H.; Kim, H. R.; Park, J. C. Dynamics and Stability of Lipid Bilayers Modulated by Thermosensitive Polypeptides, Cholesterols, and PEGylated lipids. *Phys.Chem.Chem.Phys.* **2014**, *16*, 3763.

57 Simon, J.; Kfihner, M.; Ringsdorf, H.; Sackmann, E. Molecules *Chem. Phys. Lipids* **1995**, *76*, 241–258.

58 Nikolov, V.; Lipowsky, R.; Dimova, R. Behavior of Giant Vesicles with Anchored DNA. *Biophys J.,* **2007**, *92*, 4356–4368.

59 Seifert, U.; Lipowsky, R. Morphology of Vesicles. In: Lipowsky, R.; Sackmann, E. (eds) Structure and Dynamics of Membranes, vol 1. *Elsevier*, 1995, Amsterdam.

60 Dutt, M.; Kuksenok, O.; Nayhouse, M. J.; Little, S. R.; Balazs, A. C. Modeling the Self-Assembly of Lipids and Nanotubes in Solution: Forming Vesicles and Bicelles with Transmembrane Nanotube Channels. *ACS Nano* **2011**, *5*, 4769–4782.

61 Shi, A. -C.; Li, B. Self-Assembly of Diblock Copolymers Under Confinement. *Soft Matter* **2013**, *9*, 1398–1413.

62 Li, X.; Tang, Y. -H.; Liang, H.; Karniadakis, G. E. Large-Scale Dissipative Particle Dynamics Simulations of Self-Assembled Amphiphilic Systems. *Chem. Commun.* **2014**, *50*, 8306–8308.

63 Stewart-Sloan, C. R.; Thomas, E. L. Interplay of Symmetries of Block Polymers and Confining Geometries. *Eur. Polym. J.* **2011**, *47*, 630–646.

64 Sushko, M. L.; Liu, J. Surfactant Two-Dimensional Self-Assembly under Confinement. *J. Phys. Chem. B*. **2011**, *115*, 4322–4328.

65 Bianchi, E.; Likos, C. N.; Kahl, G. Self-assembly of Heterogeneously Charged Particles under Confinement. *ACS Nano* **2013**, *7*, 4657–4667.

66 Yang, G.; Tang, P.; Yang, Y.; Cabral, J. T. Self-assembly of AB Diblock Copolymers under Confinement into Topographically Patterned Surfaces. *J. Phys. Chem. B*. **2009**, *113*, 14052–14061.

67 Wang, Z.; Li, B.; Jin, Q.; Ding, D.; Shi, A. -C. Self-Assembly of Cylinder-Forming ABA Triblock Copolymers under Cylindrical Confinement. *Macromol. Theor. Sim*. **2008**, *17*, 301–312.

68 Khoo, H. S.; Li, C.; Huang, S. -H.; Tseng, F. -G. Self-Assembly in Micro- and Nanofluidic Devices: A Review of Recent Efforts. *Micromachines* **2011**, *2*, 17– 48.

69 Helal, K.; Biben, T.; Hansen, J. -P. Influence of Capillary Confinement on the Equilibrium Shape of Vesicles. *J. Phys.: Condens. Matter.* **1999**, 11, 51–58.

70 Farago, O. "Water-free" Computer Model for Fluid Bilayer Membranes. *O. J. Chem. Phys.* **2003**, *119*, 596−605.

71 Brannigan, G.; Brown, F.L.H. Solvent-free Simulations of Fluid Membrane Bilayers. *J. Chem. Phys.* **2004**, *120*, 1059.

72 Shillcock, J. C. Spontaneous Vesicle Self-Assembly: A Mesoscopic View of Membrane Dynamics. *Langmuir* **2012**, *28*, 541– 547.

73 Tieleman, D. P.; Leontiadau, H.; Mark, A. E.; Marrink, S. J. Simulation of Pore Formation in Lipid Bilayers by Mechanical Stress and Electric Fields. *J. Am. Chem. Soc.* **2003**, *125*, 6382–6383.

74 Damodaran, K.V.; Merz, K.M. A Comparison of DMPC- and DLPE-based Lipid Bilayers. *Biophys. J.* **1994**, *66*, 1076–1087.

75 Moore, P. B.; Lopez, C. F.; Klein, M. L. Dynamical Properties of a Hydrated Lipid Bilayer from a Multinanosecond Molecular Dynamics Simulation *Biophys. J.* **2001**, *81*, 2484–2494.

76 Essmann, U.; Perera, L.; Berkowitz, M. L. The Origin of the Hydration Interaction of Lipid Bilayers from MD Simulation of Dipalmitoylphosphatidylcholine Membranes in Gel and Liquid Crystalline Phases. *Langmuir* **1995**, *11*, 4519–4531.

77 Cooke, I.R.; Deserno, M. Solvent-free Model for Self-assembling Fluid Bilayer Membranes: Stabilization of the Fluid Phase based on Broad Attractive Tail Potentials. *J. Chem. Phys.* **2005**, *123*, 224710.

78 West, B.; Schmid, F. Fluctuations and Elastic Properties of Lipid Membranes in the Gel L-beta State: A Coarse-grained Monte Carlo Study. *Soft Matter* **2010**, *6*, 1275.

79 Farago, O. Mode Excitation Monte Carlo Simulations of Mesoscopically Large Membranes. *J. Chem. Phys.* **2008**, *128*, 184105.

80 Farago, O. Fluctuation-induced Attraction between Adhesion Sites of Supported Membranes. *Phys. Rev. E*. **2010**, *81*, 050902.

81 Farago, O. Membrane Fluctuations near a Plane Rigid Surface. *Phys. Rev. E*. **2008**, *78*, 051919.

82 Dutt, M.; Nayhouse, M.J.; Kuksenok, O.; Little, S.R.; Balazs, A.C. Interactions of End-Functionalized Nanotubes with Lipid Vesicles: Spontaneous Insertion and Nanotube Self-organization. *Current Nanoscience* **2011**, *7*, 699-715.

83 Dutt, M.; Kuksenok, O.; Little, S.R.; Balazs, A.C. Forming Transmembrane Channels Using End-Functionalized Nanotubes. *Nanoscale* **2011**, *3*, 240-250.

84 Ludford, P.; Aydin, F.; Dutt, M. Design and Characterization of Nanostructured Biomaterials via the Self-assembly of Lipids. *MRS Fall 2013 Conference Proceedings* **2013**, 1498.

85 Koufos, E.; Dutt, M. Design of Nanostructured Hybrid Inorganic-biological Materials via Self-assembly. *MRS Spring 2013 Conference Proceedings* **2013**, 1569.

86 Smith, K. A.; Jasnow, D.; Balazs, A. C. Designing Synthetic Vesicles that Engulf Nanoscopic Particles. *J. Chem. Phys.* **2007**, *127*, 084703.

87 Goetz, R.; Lipowsky, R. Computer Simulations of Bilayer Membranes: Self-assembly and Interfacial Tension. *J. Chem. Phys.* **1998**, *108*, 7397–7409.

88 Kranenburg, M.; Venturoli, M.; Smit, B. Phase Behavior and Induced Interdigitation in Bilayers Studied with Dissipative Particle Dynamics. *J. Phys. Chem.* **2003**, *41*, 11491.

89 Kranenburg, M.; Laforge, C.; Smit, B. Mesoscopic Simulations of Phase Transitions in Lipid Bilayers. *Phys. Chem. Chem. Phys.* **2004**, *6*, 4531–4534.

90 Yamamoto, S.; Maruyama, Y.; Hyodo, S. Dissipative Particle Dynamics Study of Spontaneous Vesicle Formation of Amphiphilic Molecules. *J. Chem. Phys.* **2002**, *116*, 5842.

91 Yamamoto, S.; Hyodo, S. Budding and Fission Dynamics of Two-Component Vesicles. *J. Chem. Phys.* **2003**, *118*, 7937–7943.

92 Stevens, M. J.; Hoh, J. H.; Woolf, T. B. Insights into the Molecular Mechanism of Membrane Fusion from Simulation: Evidence for the Association of Splayed Tails. *Phys. Rev. Lett.* **2003**, *91*, 188102.

93 Stevens, M.J. Coarse-grained Simulations of Lipid Bilayers. *Chem. Phys.* **2004**, *121*, 11942−11948.

94 Arkhipov, A.; Yin, Y.; Schulten, K. Membrane-bending Mechanism of Amphiphysin N-BAR Domains. *Biophys. J.* **2009**, *97*, 2727–2735.

95 Shih, A.Y.; Arkhipov, A.; Freddolino, P. L.; Schulten, K. A Coarse-grained Protein-lipid Model with Application to Lipoprotein Particles. *J. Phys. Chem.* **2006**, *110*, 3674-3684.

96 Marrink, S. J.; Risselada, H. J.; Yefimov, S.; Tieleman, D. P.; de Vries, A. H. The MARTINI Forcefield: Coarse-grained Model for Biomolecular Simulations. *J. Phys. Chem. B*. **2007**, *111*, 7812–7824.

97 Wang, Z.; Frenkel, D. J. Modeling Flexible Amphiphilic Bilayers: A Solvent-free Off-lattice Monte Carlo Study. *Chem. Phys.* **2005**, *122*, 234711.

98 Brannigan, G.; Philips, P.F.; Brown, F.L.H. Flexible Lipid Bilayers in Implicit Solvent. *Phys. Rev. E*. **2005**, *72*, 011915.

99 Noguchi, H.; Takasu, M. Self-assembly of Amphiphiles into Vesicles: A Brownian Dynamics Simulation. *Phys. Rev. E*. **2001**, *64*, 041913.

100 Noguchi, H. Fusion and Toroidal Formation of Vesicles by Mechanical Forces: A Brownian Dynamics Simulation. *J. Chem. Phys*. **2002**, *117*, 8130-8137.

101 Katsov, K.; Mueller, M.; Schick, M. Field Theoretic Study of Bilayer Membrane Fusion I Hemifusion Mechanism. *Biophys. J.* **2004**, *87*, 3277.

102 Schick, M. *Membranes: A Field-theoretic Description. Encyclopedia of Biophysics*. Roberts, G.C.K., Ed., Springer-Verlag: Berlin Heidelberg, 2012.

103 May, S.; Kozlovsky, Y.; Ben-Shaul, A.; Kozlov, M.M. Tilt Modulus of a Lipid Monolayer. *Eur. Phys. J. E*. **2004**, *14*, 299–308.

104 May, S. A Molecular Model for the Line Tension of Lipid Membranes. *Eur. Phys. J. E*. **2000**, *3*, 37–44.

105 Lee, W. B.; Mezzenga, R.; Fredrickson, G. H. Self-consistent Field Theory for Lipid-based Liquid Crystals: Hydrogen Bonding Effect. *J. Chem. Phys.* **2008**, *128*, 074504–074510.

106 Ginzburg, V.V.; Balijepalli, S. Modelling the Thermodynamics of the Interaction of Nanoparticles with Cell Membranes. *Nano Lett.* **2007**, *7*, 3716–3722.

107 Ayton, G.; Voth, G. A. Bridging Microscopic and Mesoscopic Simulations of Lipid Bilayers. *Biophys. J.* **2002**, *83*, 3357-3370.

108 Wang, Z.-J.; Deserno, M. A Systematically Coarse-grained Solvent-free Model for Quantitative Phospholipid Bilayer Simulations. *J. Phys. Chem. B* **2010**, *114*, 11207.

109 Wang, Z.-J.; Deserno, M. Systematic Implicit Solvent Coarse-graining of Bilayer Membranes: Lipid and Phase Transferability of the Force Field. *New J. Phys.* **2010**, *12*, 095004.

110 Kumar, P.B.S.; Rao, M. Kinetics of Phase Ordering in a Two Component Fluid Membrane. *Mol. Cryst. Liq. Cryst.* **1996**, *288*, 105.

111 Laradji, M.; Kumar, P.B.S. Anomalously Slow Domain Growth in Fluid Membranes with Asymmetric Transbilayer Lipid Distribution. *Phys. Rev. E: Stat., Nonlinear, Soft Matter Phys*. **2006**, *73*, 040910.

112 Illya, G.; Lipowsky, R.; Shillcock, J. C. Two-component Membrane Material Properties and Domain Formation from Dissipative Particle Dynamics. *J. Chem. Phys.* **2006**, *125*, 114710.

113 Groot, R. D.; Warren, P. B. Dissipative Particle Dynamics: Bridging the Gap between Atomistic and Mesoscopic Simulation. *J. Chem. Phys.* **1997**, *107*, 4423–4435.

114 Hoogerbrugge, P. J.; Koelman, J. M. V. A. Simulating Microscopic Hydrodynamic Phenomena with Dissipative Particle Dynamics. *Europhys. Lett.* **1992**, *19*, 155.

115 Alexeev, A.; Upsal W. E.; Balazs, A. C. Harnessing Janus Nanoparticles to Create Controllable Pores in Membranes. *ACS Nano*. **2008**, *2*, 1117–1122.

116 Rekvig, L.; Kranenburg, M.; Vreede, J.; Hafskjold, B.; Smit, B. Investigation of Surfactant Efficiency Using Dissipative Particle Dynamics. *Langmuir*. **2003**, *19*, 8195.

117 Spangler, E. J.; Laradji, M.; Kumar, P.B.S. Anomalous Freezing Behavior of Nanoscale Liposomes. *Soft Matter* **2012**, *8*, 10896-10904.

118 Revalee, J.D.; Laradji, M.; Kumar, P.B.S. Implicit-solvent Mesocale Model based on Soft-core Potentials for Self-assembled Lipid Membranes. *J. Chem. Phys.* **2008**, *128*, 035102.

119 Brown, F. L. H. Continuum Simulations of Biomembrane Dynamics and the Importance of Hydrodynamic Effects. *Q. Rev. Biophys.* **2011**, *44,* 391–432.

120 Wu, S. H. W.; McConnell, H.M. Phase Separations in Phospholipid Membranes. *Biochemistry*. **1975**, *14*, 847-854.

121 Bagatolli, L.A.; Gratton, E. A Correlation between Lipid Domain Shape and Binary Phospholipid Mixture Composition in Free Standing Bilayers: A Two-Photon Fluorescence Microscopy Study. *Biophys J.* **2000**, *79*, 434-447.

122 Bagatolli, L.A.; Gratton, E. Two Photon Fluorescence Microscopy of Coexisting Lipid Domains in Giant Unilamellar Vesicles of Binary Phospholipid Mixtures. *Biophys J.* **2000**, *78*, 290-305.

123 Leidy, C.; Kaasgaard, T.; Crowe, J. H.; Mouritsen, O. G.; Jorgensen, K. Ripples and the Formation of Anisotropic Lipid Domains: Imaging Two-Component Double Bilayers by Atomic Force Microscopy. *Biophys. J.* **2002**, *83*, 2625–2633.

124 Kraft, M. L.; Weber, P. K.; Longo, M. L.; Hutcheon, I. D.; Boxer, S. G. Phase Separation of Lipid Membranes Analyzed with High-Resolution Secondary Ion Mass Spectrometry. *Science*. **2006**, *313*, 1948–1951.

125 Lin, W. C.; Blanchette, C. D.; Ratto, T. V.; Longo, M. L. Lipid Asymmetry in DLPC/DSPC-Supported Lipid Bilayers: A Combined AFM and Fluorescence Microscopy Study. *Biophys. J.* **2006**, *90*, 228–237.

126 Longo, G. S.; Schick, M.; Szleifer, I. Stability and Liquid-Liquid Phase Separation in Mixed Saturated Lipid Bilayers. *Biophys J.* **2009**, *96*, 3977–3986.

127 Honerkamp-Smith, A.R.; Cicuta, P.; Collins, M.D. ; Veatch, S.L.; den Nijs, M.; Schick, M.; Keller, S.L. Line Tensions, Correlation Lengths, and Critical Exponents in Lipid Membranes Near Critical Points. *Biophys. J.* **2008**, *95*, 236-246.

128 Honerkamp-Smith, A. R.; Veatch, S. L.; Keller, S. L. An Introduction to Critical Points for Biophysicists; Observations of Compositional Heterogeneity in Lipid Membranes. *Biochim. Biophys. Acta* **2009**, *1788,* 53-63.

129 Dutt, M.; Kuksenok, O.; Balazs, A.C. Nano-pipette Directed Transport of Nanotube Transmembrane Channels and Hybrid Vesicles. *Nanoscale* **2013**, *5*, 9773-9784.

130 Allen, M.P.; Tildesley, D.J. Computer Simulations of Liquids. *Clarendon Press*, Oxford, 2001.

131 Kumar, P.B.S.; Gommper, G.; Lipowsky, R. Budding Dynamics of Multicomponent Membranes. *Phys. Rev. Lett.* **2000**, *86*, 3911-3914.

132 Imparato, A.; Shillcock, J. C.; Lipowsky, R. Lateral and Transverse Diffusion in Two-component Bilayer Membranes. *Eur. Phys. J. E* **2003**, *11*, 21–28.

133 Hu, J.; Weikl, T.; Lipowsky, R. Vesicles with Multiple Membrane Domains. *Soft Matter* **2011**, *7*, 6092.

134 Nagle, J. F.; Tristram-Nagle, S. Structure of Lipid Bilayers. *Biochim. Biophys. Acta* **2000**, *1469*, 159.

135 Frenkel, D.; Smit, B. Understanding Molecular Simulations: From Algorithms to Applications. *Academic Press*, San Diego, 2002.

136 Campbell, M.K.; Shawn, O.F. Biochemistry, *Brooks/Cole Cengage Learning*, Belmont, CA, 2012.

137 Liang, X.; Li, L.; Qiu, F.; Yang, Y. Domain Growth Dynamics in Multicomponent Vesicles Composed of BSM/DOPC/cholesterol. *Physica A* **2010**, *389*, 3965-3971.

138 Saeki, D.; Hamada, T.; Yoshikawa, K. Domain-Growth Kinetics in a Cell-Sized Liposome. *J. Phys. Soc. Jpn.* **2006**, *75*, 013602.

139 Yanagisawa, M.; Imai, M.; Masui, T.; Komura, S.; Ohta, T. Growth Dynamics of Domains in Ternary fFuid Vesicles. *Biophys. J.* **2007**, *92*, 115-125.

140 Lifshitz, I. M.; Slyozov, V. V. The Kinetics of Precipitation from Supersaturated Solid Solutions. *J. Phys. Chem. Solids* **1961**, *19*, 35-50.

141 Weijs, J. H.; Marchand, A.; Andreotti, B.; Lohse, D.; Snoeijer, J. H. Origin of Line Tension for a Lennard-Jones Nanodroplet. *Phys. Fluids* **2011**, *23*, 022001.

142 Lipowsky, R.; Dimova, R. Domains in Membranes and Vesicles. *J. Phys.: Condens. Matter,* **2003**, *15*, 31–45.

143 Putzel, G. G.; Schick, M. Phenomenological Model and Phase Behavior of Saturated and Unsaturated Lipids and Cholesterol. *Biophys. J.* **2008**, *95*, 4756–4762.

144 Glaser, R. Biophysics, *Springer*, Berlin, 1996.

145 Tanford, C. Hydrostatic Pressure in Small Phospholipid Vesicles. *Proc. Nati. Acad. Sci. USA* **1979**, *76*, 3318-3319.

146 White, S. H. Small Phospholipid Vesicles: Internal Pressure, Surface Tension, and Surface Free Energy. *Proc. Nati. Acad. Sci. USA* **1980**, *77*, 4048-4050.

147 Schofield, P.; Henderson, J. R. Statistical Mechanics of Inhomogeneous Fluids. *Proc. R. Soc. London Ser. A* **1982**, *379*, 231.

148 Uline, M. J.; Schick, M.; Szleifer, I. Phase Behavior of Lipid Bilayers under Tension. *Biophys. J.* **2012,** *102*, 517–522.

149 Hamada, T.; Kishimoto, Y.; Nagasaki, T.; Takagi, M. Lateral Phase Separation in Tense Membranes. *Soft Matter* **2011**, *7*, 9061.

150 Kondo, T.; Hayashi, S.   Mitotic Cell Rounding Accelerates Epithelial Invagination. *Nature* **2013**, *494*, 125–129.

151 Leach, A.R. *Molecular Modeling Principles and Applications*. Addison Wesley Longman: Essex, England, 1996.

152 Chan, E.R.; Ho, L.C.; Glotzer, S.C. Computer Simulations of Block Copolymer Tethered Nanoparticle Self-Assembly. *J. Chem. Phys.* **2006**, *125*, 064905.

153 Kremer, K.; Grest, G.S. Dynamics of Entangled Linear Polymer Melts: A Molecular-dynamics Simulation. *J. Chem. Phys.* **1990**, *92*, 5057.

154 Kučerka, N.; Nieh, M.P.; Katsaras, J. Fluid Phase Lipid Areas and Bilayer Thicknesses of Commonly Used Phosphatidylcholines as a Function of Temperature. *J. Biochim. Biophys. Acta.* **2011**, *1808*, 2761– 2771.

155 Gonnella, G.; Orlandini, E.; Yeomans, J. M. Phase Separation in Two-dimensional Fluids: The Role of Noise. *Phys. Rev. E.* **1999**, *59*, 4741.

156 Binder, K.; Stauffer, D. Theory for the Slowing Down of the Relaxation and Spinodal Decomposition of Binary Mixtures. *Phys. Rev. Lett.* **1974**, *33*, 1006.

157 Ossadnik, P.; Gyure, M. F.; Stanley, H. E.; Glotzer, S. C. Molecular Dynamics Simulation of Spinodal Decomposition in a Two-dimensional Binary Fluid Mixture. *Phys. Rev. Lett.* **1994**, *72, 2498.

158 Satulovsky, J.; Carignano, M. A.; Szleifer, I. Kinetic and Thermodynamic Control of Protein Adsorption. *Proc. Natl. Acad. Sci*. **2000**, *97*, 9037–9041.

159 Prime, K. L.; Whitesides, G. M. Self-assembled Organic Monolayers: Model Systems for Studying Adsorption of Proteins at Surfaces. *Science*. **1991**, *252*, 1164–1167.

160 Prime, K. L.; Whitesides, G. M. Adsorption of Proteins onto Surfaces Containing End-Attached Oligo (ethylene oxide): A Model System Using Self-Assembled Monolayers. *J. Am. Chem. Soc.* **1993**, *115*, 10714–10721.

161 Kim, P.; Lee, S. E.; Jung, H. S.; Lee, H. Y.; Kawai, T. Suh, K. Y. Soft Lithographic Patterning of Supported Lipid Bilayers onto a Surface and inside Microfluidic Channels. *Lab Chip*. **2006**, *6*, 54–59.

162 Duffy, D. C.; McDonald, J. C.; Schueller, O. J.; Whitesides, G. M. Rapid Prototyping of Microfluidic Systems in Poly(dimethylsiloxane). *Anal Chem.* **1998,** *70*, 4974–4984.

163 Richter, R.; Mukhopadhyay, A.; Brisson, A. Pathways of Lipid Vesicle Deposition on Solid Surfaces: A Combined QCM-D and AFM Study. *Biophys J.* **2003**, *85*, 3035–3047.

164 Li, Y.; Zhang, X.; Cao, D. The Role of Shape Complementarity in the Protein-Protein Interactions. *Sci. Rep.* **2013**, *3*, 3271.

165 Yang, K.; Vishnyakov, A.; Neimark, A. V. Polymer Translocation through a Nanopore: DPD Study. *J. Phys. Chem. B* **2013**, 117, 3648–3658.

166 Somani, S.; Shaqfeh, E. S. G.; Prakash, J. R. The Effect of Solvent Quality on the Coil-stretch Transition. *Macromolecules* **2010**, *43*, 10679–10691.

167 Seifert, U.; Berndl, K.; Lipowsky, R. Shape Transformations of Vesicles: Phase Diagram for Spontaneous-curvature and Bilayer-coupling Models. *Phys. Rev. A.* **1991**, *44*, 1182.

168 Shinoda, W.; Discher, D. E.; Klein, M. L.; Loverde, S. M. Probing the Structure of PEGylated-lipid Assemblies by Coarse-grained Molecular Dynamics. *Soft Matter* **2013**, *9*, 11549.

169 Helal, K.; Biben, T.; Hansen, J. -P. Influence of Capillary Confinement on the Equilibrium Shape of Vesicles. *J. Phys.: Condens. Matter.* **1999**, *11*, 51–58.

170 Hood, R. R.; Kendall, E. L.; Junqueira, M.; Vreeland, W. N.; Quezado, Z.; Finkel, J. C.; DeVoe, D. L. Microfluidic-Enabled Liposomes Elucidate Size-Dependent Transdermal Transport. *PLoS ONE* **2014**, *9*, 92978.

171 Jahn, A.; Stavis, S. M.; Hong, J. S.; Vreeland, W. N.; DeVoe, D. L.; Gaitan, M. Microfluidic Mixing and the Formation of Nanoscale Lipid Vesicles. *ACS Nano*. **2010**, *4*, 2077–2087.

172 Banerjee, I.; Pangule, R. C.; Kane, R. S. Antifouling Coatings: Recent Developments in the Design of Surfaces That Prevent Fouling by Proteins, Bacteria, and Marine. *Organisms. Adv. Mater.* **2011**, 23, 690–718.

173 Pavithra, D.; Doble, M. Biofilm Formation, Bacterial Adhesion and Host Response on Polymeric Implants—Issues and Prevention. *Biomed. Mater.* **2008**, *3*, 034003.

174 Du, H.; Chandaroy, P.; Hui, S. W. Grafted Poly-(ethylene glycol) on Lipid Surfaces Inhibits Protein and Cell Adhesion. *Biochimica et Biophysica Acta(BBA)-Biomembranes* **1997**, *1326*, 236-248.

175 Horbett, T. A. Principles Underlying the Role of Adsorbed Plasma Proteins in Blood Interactions with Foreign Materials. Cardiovasc. Pathol. **1993**, *2*, 137S-148S.

176	Pozzi, D.; Colapicchioni, V.; Caracciolo, G.; Piovesana, S.; Capriotti, A. L.; Palchetti, S.; de Grossi, S.; Riccioli, A.; Amenitsch, H.; Lagana, A. Effect of polyethyleneglycol (PEG) Chain Length on the Bio-nano-interactions between PEGylated Lipid Nanoparticles and Biological Fluids: from Nanostructure to Uptake in Cancer Cells. *Nanoscale* **2014**, *6*, 2782-2792.

177	Price, M. E.; Cornelius, R. M.; Brash, J. L. Protein Adsorption to Polyethylene Glycol Modified Liposomes from Fibrinogen Solution and from Plasma. *Biochim. Biophys. Acta* **2001***, 1512*, 191-205.

178	Nuytten, N.; Hakimhashemi, M.; Ysenbaert, T.; Defour, L.; Trekker, J.; Soenen, S. J.; van der Meeren, P.; De Cuyper, M. PEGylated Lipids Impede the Lateral Diffusion of Adsorbed Proteins at the Surface of (Magneto) Liposomes. *Colloids Surf. B Biointerfaces* **2010**, *80*, 227-231.

179	Wang, B.; Zhang, L.; Bae, S.C.; Granick, S. Nanoparticle-induced Surface Reconstruction of Phospholipid Membranes. *PNAS* **2008**, *105*, 18171-18175.

180	Ge, Z.; Li, Q.; Wang, Yi. Free Energy Calculation of Nanodiamond-membrane Association-The Effect of Shape and Surface Functionalization. *J. Chem. Theory Comput.* **2014,** *10*, 2751-2758.

181	Van Lehn, R. C.; Ricci, M.; Silva, P. H.; Andreozzi, P.; Reguera, J.; Voitchovsky, K.; Stellacci, F.; Alexander-Katz, A. Lipid Tail Protrusions Mediate the Insertion of Nanoparticles into Model Cell Membranes. *Nat. Commun*. **2014**, 5, 4482.

182	Wong-Ekkabut, J.; Baoukina, S.; Triampo, W.; Tang, I. M.; Tieleman, D. P.; Monticelli, L. Computer Simulation Study of Fullerene Translocation through Lipid Membranes. *Nat. Nanotechnol.* **2008,** *3*, 363-368.

183 Li, Y.; Chen, X.; Gu, N. Computational investigation of interaction between nanoparticles and membranes: hydrophobic/hydrophilic effect. *J. Phys. Chem. B* **2008**, *112*, 16647-16653.

184 Huang, C.; Zhang, Y.; Yuan, H.; Gao, H.; Zhang, S. Role of Nanoparticle Geometry in Endocytosis: Laying Down to Stand Up. *Nano Lett.* **2013**, *13*, 4546-4550.

185 Shi, X.; von dem Bussche, A.; Hurt, R. H.; Kane, A. B.; Gao, H. Cell Entry of One-dimensional Nanomaterials Occurs by Tip Recognition and Rotation. *Nat. Nanotechnol.* **2011**, *6*, 714-719.

186 Song, Y.; Chen, S. Janus Nanoparticles: Preparation, Characterization, and Applications. *Chem. Asian J.* **2014**, *9*, 418-430.

187 Szleifer, I. Protein Adsorption on Surfaces with Grafted Polymers: A Theoretical Approach. *Biophys. J.* **1997**, *72,* 595-612.

188 Kiselev, V. Y.; Marenduzzo, D.; Goryachev, A. B. Lateral Dynamics of Proteins with Polybasic Domain on Anionic Membranes: A Dynamic Monte-Carlo Study. *Biophys. J.* **2011**, *100*, 1261–1270.